Section I
Small Molecule Gels

Soft Fibrillar Materials: Fabrication and Applications, First Edition. Edited by Xiang Yang Liu and Jing-Liang Li.

1
Molecular Gels and their Fibrillar Networks

Kevin L. Caran, Dong-Chan Lee, and Richard G. Weiss

1.1
Introduction

This chapter will review, in a non-comprehensive fashion, the formation and properties of objects with very high aspect ratios [essentially one-dimensional (1D) objects at the micron or larger distance scales] made from organic molecules [topologically zero-dimensional (0D) objects at micron-range distance scales] which are not linked covalently and aggregate upon separation from dilute organic solutions or sols [1]. It will stress those 1D structures which undergo further assembly into 3D networks [self-assembled fibrillar networks (**SAFIN**s)] that entrap the liquid in which they form. It remains largely unknown how and why many small organic molecules with very different shapes and functionalities [2] are able to separate from dilute organic (NB, leading to organogels) or aqueous (NB, leading to hydrogels) solutions or sols in the form of objects with very high aspect ratios [1].

The general name given to such materials is ''molecular gels'', and the molecules that constitute them are referred to as low-molecular-mass organic gelators (**LMOG**s), although many of the materials may not meet the strict rheological definition of a gel as required by their viscoelastic properties [3]. The smallest known **LMOG** is *N,N*′-dimethylurea, 88 DA [4], and the largest are limited arbitrarily at < 2000 Da (although with some ''poetic license''). The range of small molecules that can lead to gels via fiber and **SAFIN** formation is now in the hundreds, if not more than one thousand [1]. Because the molecules are aggregated but not linked covalently, the disassembly of the 1D objects (and their 3D networks) can be accomplished by application of heat, dilution, shear, or other perturbations which will be discussed.

The history of gels made from **LMOG**s may go back as far as the fourteenth century, although this example remains unsubstantiated and controversial [5]. The first formal description of a hydrogel of which we are aware, employing lithium urate, was reported by Lipowitz in 1841 [6]. A description of gels with the well-known and widely used **LMOG**, 1,3:2,4-di-O-benzylidene-D-sorbitol (**1**), was published in 1891 [7]. However, it was not until the middle of the twentieth century that scientists began to confront the intricacies of **SAFIN**s and different forms of

Soft Fibrillar Materials: Fabrication and Applications, First Edition. Edited by Xiang Yang Liu and Jing-Liang Li.

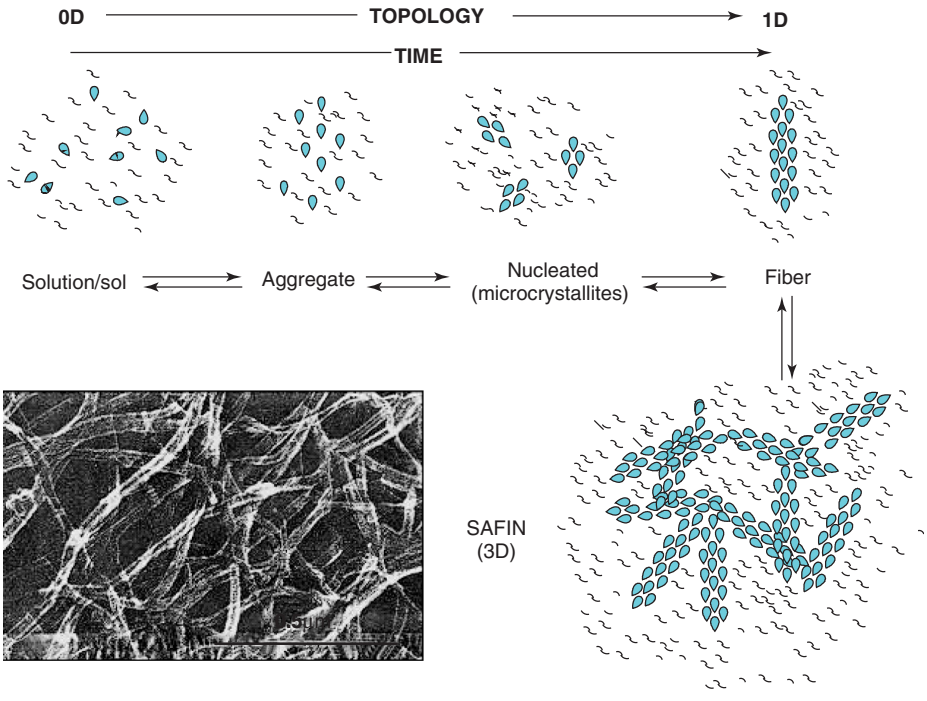

Figure 1.1 Cartoon representation of the steps in the evolution of **LMOG**s (0D objects; tear drops) to fibers (1D objects) and, in some cases, to **SAFIN**s (3-D objects) in liquids (wavy lines). Lower left is a freeze-fracture electron micrograph of a **SAFIN**. Reprinted with permission from Ref. [11]. Copyright 1989 American Chemical Society.

gels. In his ''structural classification of gels,'' Flory included those starting with 0D molecules as an afterthought, naming them ''particulate, disordered structures''! [8] Although much has been learned during the last decade about the supramolecular assembly of polymeric chains (topologically 1D objects) into a variety of 2D and 3D objects [9, 10], much less is known about the *initial* steps that take 0D molecules to 1D objects, such as fibers, rods, tapes, and nanotubes (Figure 1.1); for the purposes of this chapter, all of these high-aspect-ratio objects will be designated as ''fibers'', regardless of the details of their shape, unless specified otherwise for purposes of differentiation.

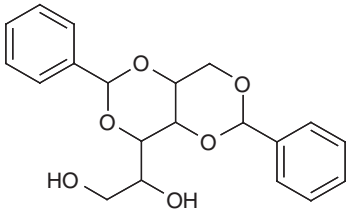

1

This type of 1D aggregation is distinguished from other types of self-assembly [12] that do not lead to fibrous networks and may involve plates, multilayered objects [13], and even bulk crystals as the basic units [14]. In many cases, the micro-phase separation of the 1D objects leads to organogels when the liquid is organic or hydrogels when it is aqueous. In both cases, there is an evolution of the aggregate structures which is controlled by very complex dynamics.

To date, the vast majority of studies of molecular gels has concentrated on structural and rheological aspects of their properties. In fact, the number of detailed studies treating both structure and kinetics of fiber formation in **SAFIN**s is relatively small [15–19]. As a result, many questions remain about how small aggregates of **LMOG**s (still topologically 0-D objects at submicron length scales) form and then become (topologically) 1D objects. There are many important gaps in our knowledge as well about how 1D fibers transform into 2D or 3D objects, how 1D fibers of a **SAFIN** revert to 3D (microcrystalline) objects [20–23], how they undergo Ostwald ripening [21], and what controls their thixotropic behavior [24]. **SAFIN**s may form as depicted in Figure 1.1 or by a completely different series of events, depending on the structure of the gelator, its concentration, the liquid component, and the protocol to transform the solution/sol to the gel. For example, in an alternative mode, new grains may develop on the sides of fibers or by tip-splitting (i.e., branching at the ends of growing fibers), giving rise to branched structures that lead to branched networks or spherulites [19]. Most of the systems discussed here undergo microphase separation by nucleation phenomena rather than by spinodal decomposition mechanisms [25].

Because the **LMOG** molecules in fibers are not attached covalently, the relevant intermolecular interactions include H-bonding, π-π-stacking, dipolar interactions, and London dispersion forces [1, 26]. In fact, the manner in which 1D objects, especially those composed of unbranched polymeric chains (i.e., objects in which one dimension of aggregation is due to covalent bonds) [27], convert to 2D and 3D objects [28] has received much more attention than the 0D → 1D transformations (i.e. those involving **LMOG**s) because experimental observations become much easier as the objects under scrutiny increase in size. Many of the polymeric gel networks are not disassembled by the same stimuli mentioned above; instead, they undergo conformational changes or separate otherwise physically from other polymer chains without losing their 1D status. For both 1D objects composed of **LMOG**s and polymer chains, additional interactions are needed to make them into 3D networks. Those interactions can be chain entanglements, branching, or inter-object associations involving ''junction zones'' of various types. Branching of the 1D objects made from **LMOG**s can be thought of as a consequence of defective growth during the 0D → 1D process [19c]. Junction zones occur at points of intersection between two 1D objects, and the participating molecules are frequently more disordered than within the ''undisturbed'' parts along the object. Alternatively, a junction zone may consist of abutting segments of two objects.

In some of the 1D objects, the constituent molecules are packed in a crystalline fashion whereas others, such as giant worm-like micelles, are not. The amount of detailed packing information potentially available about the crystalline objects is

greater than about the amorphous (non-crystalline) ones. Yet, the ability of gels made with the amorphous (non-crystalline) 1D objects to recover their viscoelastic properties after cessation of severe shearing [24b] is much greater because many of them are in dynamic equilibria which allows self-annealing with time.

The study of 1D objects, especially those composed of **LMOG**s, and their gels requires multidisciplinary approaches among chemists, physicists, chemical engineers, biologists, and theoreticians. Research in this area, a branch of supramolecular chemistry, is important because systems based upon 1D objects and their assemblies, especially if the keys to designing them *de novo* can be discovered, can yield fundamental understanding of complex and highly selective catalytic processes, useful devices, and new ways to exploit systems available in nature. It can also shed light on the evolution and function (or malfunction) of systems of important biomolecular fibers that are involved with blood clotting and neurodegenerative diseases such as Alzheimer's, mad cow disease, and sickle cell anemia [29]. Also, fiber aggregates of small molecules are used to modify the mechanical properties of polymers [30] and food-related oils [31]. Ingenious manipulation of gelators in sols can lead to monodomains of 1D viscoelastic objects which are centimeters long [32] and may be useful in biological applications.

The questions of ''How'' and ''Why'' molecules with such diverse structures organize into 1D objects – fibers, tapes, nanotubes, and so on, with very high aspect ratios – remain largely unanswered. Although there are several theoretical [33–36] and experimental approaches [9, 15–17b, 19c,d,e, 37–40] to explain such aggregation and growth and even some predictive models for molecules with specific structures [19a,b, 35, 41–43], a generally applicable set of rules for when 1D objects will form is not available. It is likely that more than one basic mechanism controls the aggregation of molecules into the 1D objects, and the specific mechanism depends on the structure of the molecules, the nature of the solvent in which aggregation occurs [44], and the mode by which the sol phase is transformed into a gel [45]. Besides the need for strong attractive interactions along the long axis of the objects [46], there seem to be no real unifying principles. Although this chapter cannot present solutions to the parts of this science that remain unresolved, it can, is intended to, and hopefully will present a current picture of the state of the art in ways that allow the reader to discern where fruitful approaches to solutions may lie.

1.2
Advances and Perspectives for Design of Gelators

1.2.1
Analyses of Structure Packing via X-Ray, Synchrotron, and Other Techniques, Including Spectroscopic Tools

Elucidation of the molecular packing within the fibers formed during organogelation remains a challenging task. However, this information can provide key

insights into the design of better gelators. Typically, fibers are characterized in the gel state (native gel, henceforth) or the dried gel state (xerogel). Microscopic characterization techniques such as polarized optical microscopy (POM), scanning electron microscopy (SEM), transmission electron microscopy (TEM), and atomic force microscopy (AFM) have provided pictures of fiber morphologies in xerogels. Various characterization methods, as described in this section, can yield detailed information on the structures of **SAFIN**s of gels at different length scales. However, information from a single characterization method is usually insufficient to reveal all aspects of a gel structure. Complementary tools should be employed and data from them used to build a cohesive picture of gel structure, including fiber morphology, molecular packing, intermolecular interactions, and so on.

A caveat noted by many others is reiterated here: the morphology of a xerogel does not represent necessarily that of the native gel because fiber damage or secondary assembly may occur during the drying process [47]. To minimize the possibility of such complications, freeze-fracture/etching SEM, and cryo-TEM techniques have been employed to visualize **SAFIN** structures of native gels. For example, the 3D network of 1D fibers of a steroid **LMOG** (**2**) in cyclohexane gel was revealed by

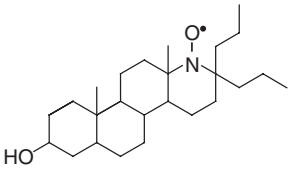

2

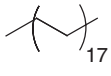

3

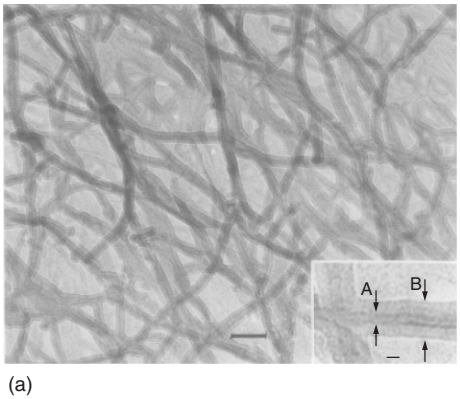

(a)

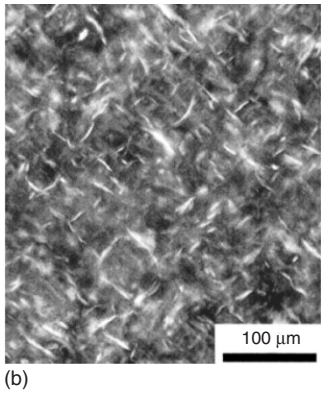

(b)

Figure 1.2 (a) Electron micrograph of a gel (**2**) replica with a carbon film overlay showing the filament gel network protected (Scale bars are 100 nm for the main image and 10 nm for the inset); each filament is imaged as three layers and consists of a core (region A) sandwiched between a more electron-transparent coating, the outer edges of which are marked with arrows at B. Reprinted with permission from Ref. [48]. Copyright 1986 Elsevier.) (b) Optical micrographs of a 0.01 M **3**/silicone oil gel at room temperature viewed through crossed polars; sample thickness = 0.8 mm. (Reprinted with permission from Ref. [49]. Copyright 2000 American Chemical Society.

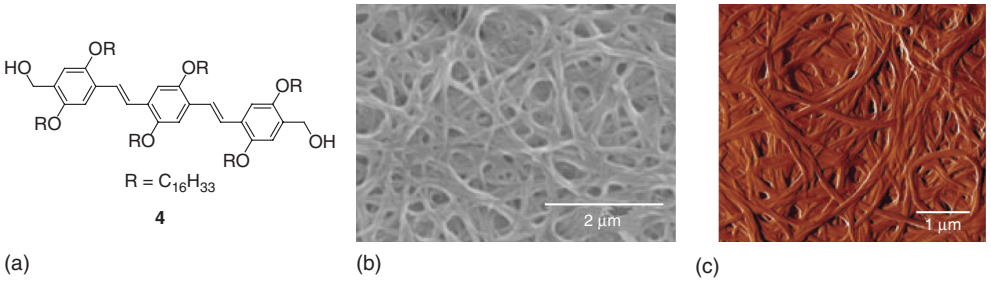

Figure 1.3 Structure of gelator **4** (a), SEM (b) and AFM (c) images from xerogels of **4**. Reprinted with permission from Ref. [50]. Copyright 2005 Wiley.

a freeze-etching replication, electron-microscopy method (Figure 1.2a) [48]. Albeit less well resolved, POM can also provide the **SAFIN** structure of an organogel. Figure 1.2b demonstrates the POM image of a native gel of *n*-hexatriacontane (**3**) in silicone oil prepared in a flattened, sealed glass capillary [49].

Fibrillar structures can be clearly visualized from xerogels by SEM and AFM techniques, as shown in Figure 1.3 with gelator **4** [50]. However, as mentioned above, a correlation between such images and those of the gel itself should be made only if supported by additional characterization techniques, such as small angle scattering (SAS) [51], which relate the **SAFIN** structure and xerogels.

SAS, including X-rays (SAXS) and neutrons (SANS), is a powerful technique to provide structure information about native gels. It has been used to provide insights into many gel structures [52]. As a result of their high intensity, synchrotron sources can enable characterization of native gels better than conventional X-ray sources. To perform SANS experiments, either deuterated gelators or deuterated solvents (or other contrasting liquids) are required. The difficulty to deuterate significant portions of most gelator structures has resulted, as expected, in the vast majority of studies being conducted with deuterated liquid components.

SAS is a model-based approach involving extensive mathematical operations; fortunately, many fitting programs are available. When SAS profiles of a native gel are obtained, an appropriate model needs to be chosen (e.g., rigid-rod, tubule, ribbon, or cylinder). Then, comparison is made between the simulated and experimental SAS profiles to validate the chosen model after the fitting parameters for size, persistence length, and so on, have been optimized. Terech and co-workers have reported many SAS investigations on gels, revealing the morphology of fibers as well as their junction zones [53]. For example, gelator **5** [53c] in decane formed hexagonally packed bundles (from structure factor analysis at large-angle scattering) of cylinders (from form factor analysis at low-angle scattering) (Figure 1.4). In addition, a solvent-dependent morphology change to more rectangular ribbon-shaped objects was observed in 1-alkanols.

Sakurai *et al.* have employed synchrotron SAXS to support a previously proposed model [54] for molecular arrangement in a helical fiber of an azobenzene–cholesterol-based gelator (**6**) [52a]. A hollow cylinder model exhibited better agreement with the experimental SAXS profile than a solid cylinder model,

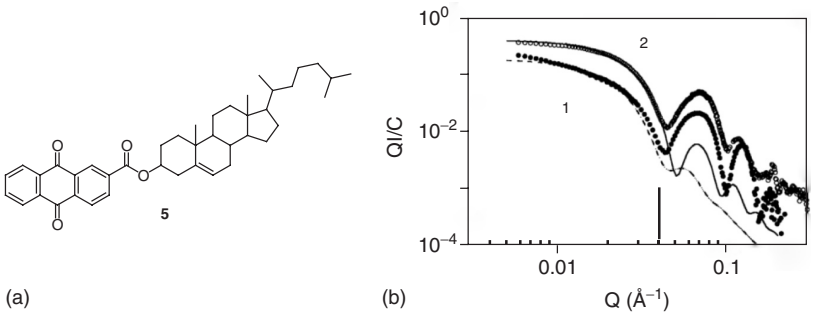

Figure 1.4 (a) Structure of gelator **5**. (b) SAXS cross-sectional intensity *(QI/C)* versus *Q* for organogels of **5** in 1-octanol (1 (●), $C = 0.0017$ g cm^{-3}) and in decane (2 (○), $C = 0.0043$ g cm^{-3}); the lines are based on a theoretical fitting: 1, full line, R_0 (the geometric radii) = 72 Å, ε (the cross-sectional radial dispersity) = 0.1; 2, dotted line, $R_0 = 75$ Å, $\varepsilon = 0.2$; the vertical bar is a visual guideline between the low-angle and high-angle parts of the scattering data sets. Reprinted with permission from Ref. [53c]. Copyright 1996 American Chemical Society.

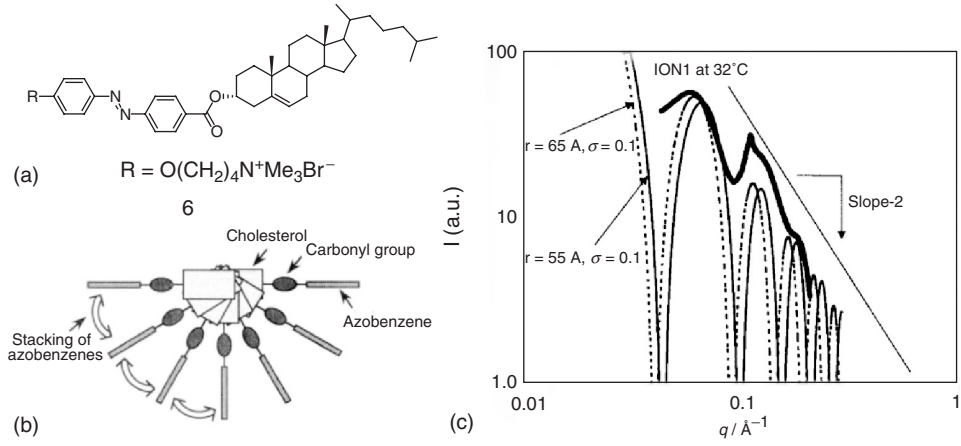

Figure 1.5 (a) Structure of gelator **6**. (b) Proposed molecular packing in the fiber. Reprinted with permission from Ref. [54]. Copyright 1994 American Chemical Society. (c) Comparison of the measured SAXS data and the particle scattering functions of the hollow cylinder model with *r* (radius) = 65 and 55 Å. Reproduced from Ref. [52a] with permission of The Royal Society of Chemistry. *http://dx.doi.org/10.1039/B005470O*

suggesting that higher-electron-density azobenzene moieties are located at the exterior of the fibers while lower-electron-density cholesterol moieties are at the core of the fibers (Figure 1.5).

Wide-angle X-ray diffraction (WAXD) [55] has been utilized to investigate molecular packing within the crystalline fibers of gelators. Solving the crystal structure from single-crystal X-ray crystallography is a desired method to identify molecular packing. However, growing single crystals of **LMOG**s suitable for diffraction has been quite challenging; many form fibers or crystallize in a morph that is different

from the one in the gel fibers. When a single crystal from a gelator is available and the X-ray powder diffraction (XRD) patterns from the crystal (or simulated XRD patterns from the crystal structure) and from the organogel are the same, molecular packing in the fiber can be elucidated [9]. As mentioned, the morphs of gelator fibers and bulk crystals may be either identical [4, 56] or different [57]. Ostuni *et al*. have demonstrated that XRD patterns of gelator fibers in a native gel (**5**/1-octanol) can be isolated by subtracting those of the solvent [57a]. It was found that the fibers had molecular packing closer to that of the neat solid cooled from the melt than to crystals isolated by precipitation from solution. The gelator *(R/S)*-**7** (Figure 1.6a) also exhibited a similar behavior [57b]. The solvent subtracted XRD of its decane gel showed a pattern closer to that of the sublimed solid than to the bulk crystal (Figure 1.6b). Based on the single-crystal data of the sublimed solid, molecular packing in the fibers has been proposed (Figure 1.6c).

Dastidar *et al*. have used molecular packing in gel fibers and in bulk crystals as obtained from XRD data to design effective gelators by identifying supramolecular synthons capable of 1D (and 2D) hydrogen-bonding (HB) networks that promote anisotropic fiber growth [9]. For example, dicyclohexylammonium 4-nitrocinnamate **8** (Figure 1.7a) gelates a few organic liquids such as benzene, toluene, xylene, and even gasoline [58].

A single-crystal packing structure of the organic salt **8** shows that one-dimensional HB is the most important intermolecular interaction responsible for the molecular arrangement. As shown in Figure 1.7b, XRD patterns simulated from the single-crystal data are nearly superimposable with those from the bulk solid, indicating the same molecular packing. Also, xerogels from benzene and *p*-xylene gels of **8** showed XRD patterns nearly identical to that of the pattern simulated from the single-crystal data. This result indicates that fibers in the xerogels adopt the same molecular arrangements found in the single crystal and the bulk solid. However, the molecular packing in the gel state could not be directly correlated with that in

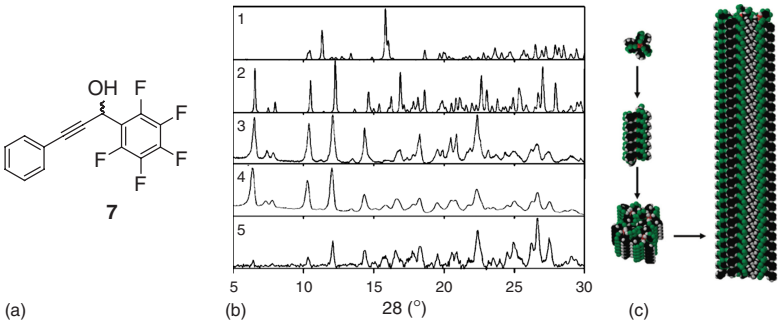

Figure 1.6 (a) Structure of gelator *(R/S)*-**7**. (b) Comparison of simulated XRD patterns of both known solid-state morphologies of (*R/S*)-**7** (1: single-crystal data from solution, 2: single-crystal data from sublimed material) to XRD patterns of (*R/S*)-**7** (3: sublimed solid, 4: solid cooled from neat melt, 5: solvent subtracted decane gel). (c) Aggregation model for (*R/S*)-**7** in gel fibers. Reprinted with permission from Ref. [57b]. Copyright 2008 American Chemical Society.

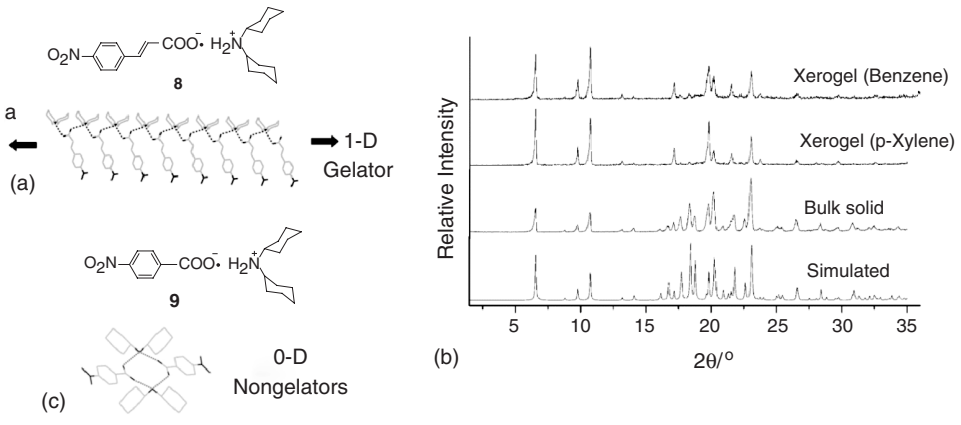

Figure 1.7 (a) The structure of gelator **8** and 1D HB network of ion pairs in the crystal structure of **8**. (b) XRD patterns under various conditions for **8**. (c) The structure of nongelator **9** and 0D HB network of ion pairs in the crystal structure of **9**. Reproduced from Ref. [58] with permission of The Royal Society of Chemistry. *http://dx.doi.org/10.1039/B504969E*

the single crystal since the XRD patterns from the gel was difficult to obtain due to the strong scattering from the solvent. Importantly, salt **9** was unable to form a gel, and only 0D HB networks were identifiable in the single crystal (Figure 1.7c).

Additional spectroscopic tools, including nuclear magnetic resonance (NMR), Fourier-transform infrared (FT-IR), UV–vis absorption, fluorescence (FL), and circular dichroism (CD), are available to monitor the changes in physical properties of aggregates during gelation. These techniques are able to identify different aspects of intermolecular interactions which contribute to gelation. CD spectroscopy, limited to chiral gelators or liquids, is discussed in Section 1.2.2.

A comprehensive description of NMR investigations of gels has been presented in a recent review by Shapiro [59]. Upon transition from a sol to a gel phase, proton resonances in ^{1}H NMR spectra experience significant broadening or disappear completely due to limited molecular motion [53d, 60]. For example, aromatic, vinylic, and some aliphatic protons of compound **10** cannot be observed in gel state spectra, but are clearly seen in the solution/sol phase spectra at high temperature where the system is a solution/sol (Figure 1.8) [60b].

Gels where solvent molecules are incorporated within fibers do allow more proton signals from gelator molecules to be observed, although some line broadening and shifts in proton resonances occur [52b, 61]. For example, a gel of **11** (Figure 1.9a) [61c] in toluene-d_8 exhibited a downfield shift of the N-H protons (H_a and H_b) in the gel state, indicating the presence of HB in the fibers (Figure 1.9b). The aromatic H_c signal appeared as a doublet in the solution/sol state and as two overlapping doublets in the gel state due to their inequivalence as packed in the fibers (Figure 1.9c). The spectra also indicate significant π-π stacking in the gel fibers.

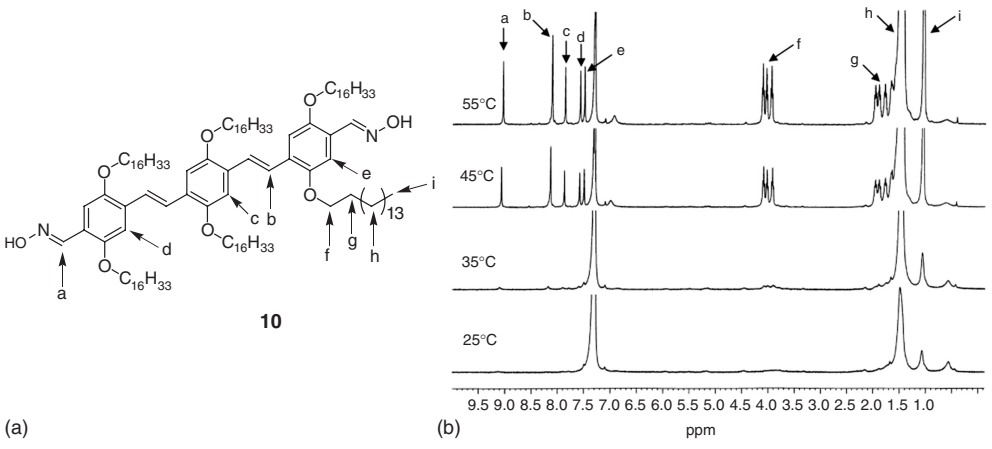

Figure 1.8 (a) Structure of gelator **10**. (b) Variable temperature ^{1}H NMR spectra of 10 mg/ml **10** in C_6D_6 in its gel phase (25 and 35 °C) and its solution/sol phase (45 and 55 °C). Reprinted with permission from Ref. [60b]. Copyright 2009 American Chemical Society.

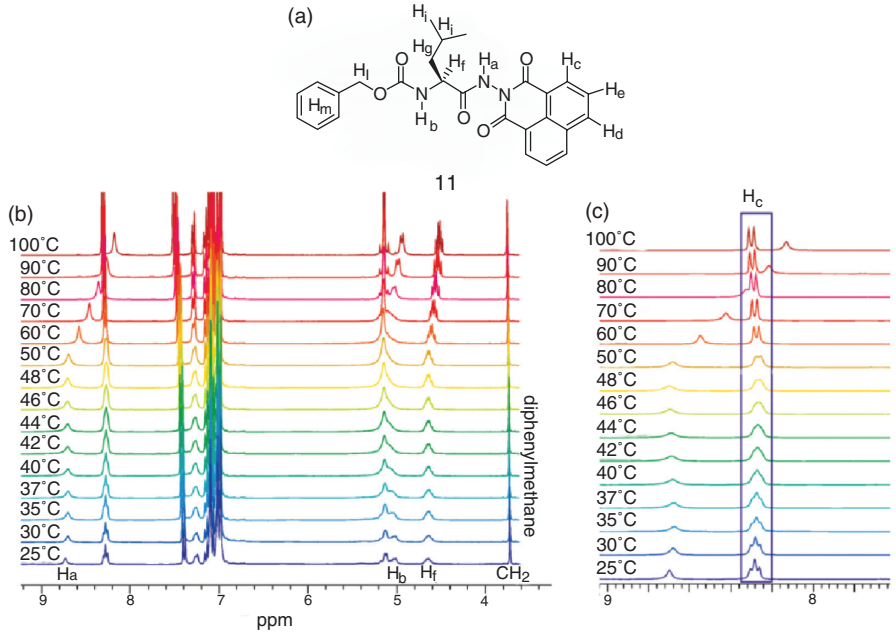

Figure 1.9 (a) Structure of leucine-based gelator **11**. (b) Superimposition of 1 wt% **11** in toluene-d_8 ^{1}H NMR spectra at different temperatures (diphenylmethane as internal standard). (c) Change of signals from the two H_c protons upon heating (in the rectangle). Intensities are normalized. Reprinted with permission from Ref. [61c]. Copyright 2010 American Chemical Society.

Gelators with chromophores or fluorophores typically suffer spectral changes as sol–gel transitions occur [62]. Cofacial (*H*-aggregate) and off-face stacking (*J*-aggregate) of chromophores induce a blue [63] or redshift [64], respectively, in absorption spectra. *J*-aggregate formation is more common and, in many cases, induces enhancement of emission intensities [60,65], whereas *H*-aggregates frequently lead to decreased emission intensities. However, at this point, there are too few examples and inadequate theoretical understanding to conclude that these observations are universal. For example, the xerogel of **12** (Figure 1.10a) has an FL quantum efficiency (Φ_F) nearly two orders of magnitude higher than that of a dilute chloroform solution (Figure 1.10b) [65b]. The redshift in the emission maximum in the gel state (439 nm at 25 °C) from the solution state (402 and 423 nm at 80 °C) indicates *J*-aggregate formation as the cause of the emission enhancement (Figure 1.10c). Aggregation-induced emission enhancement can also be induced by restriction of molecular motion in the gel fibers, which decreases the rates of internal conversion and/or freezes in more planar and conjugated conformations [66].

FT-IR spectroscopy is a valuable tool to identify certain intermolecular interactions in the gel fibers, especially HB [61c, 65c]. Temperature-dependent FT-IR spectra of gelator **11** [61c] clearly shows the existence of intermolecular HB between N–H and C=O groups. In the sol and gel phases, at 90 and 30 °C, respectively, N–H and C=O stretching peaks were shifted to lower frequencies as a result of HB formation (Figure 1.11).

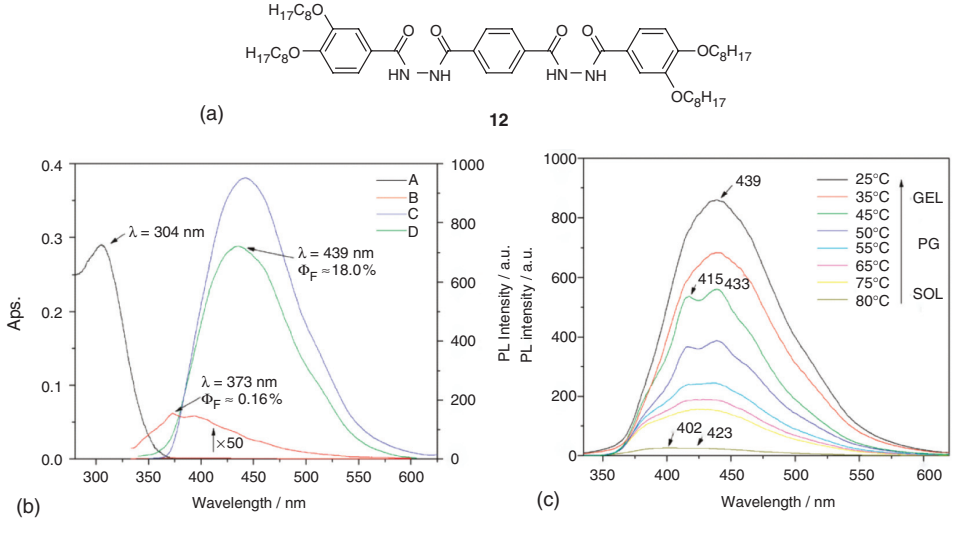

Figure 1.10 (a) Structure of gelator **12**. (b) Absorption (A) and emission (B) spectra of 1.0×10^{-5} mol L^{-1} **12** in chloroform; emission spectra ($\lambda_{ex} = 320$ nm) of a 0.1 wt% **12** gel in chloroform (C) and xerogel from chloroform (D). (c) Photoluminescence spectra ($\lambda_{ex} = 320$ nm) of 1.2 mg mL^{-1} **12** in 1,2-dichloroethane at 80 °C, partial gel from 45 to 75 °C, and gel state below 40 °C. Reprinted with permission from Ref. [65b]. Copyright 2010 American Chemical Society.

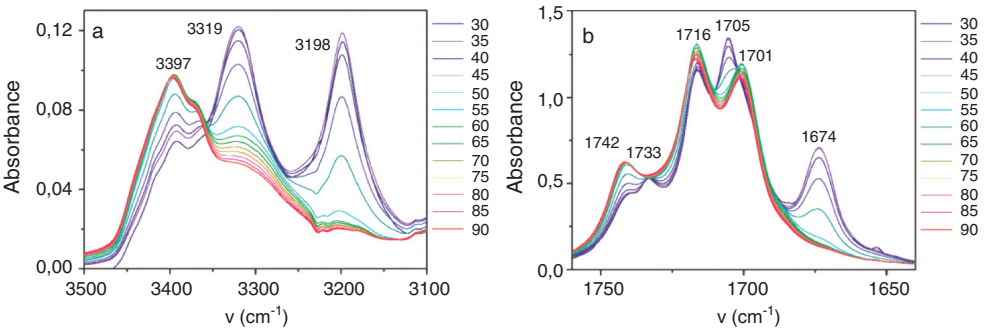

Figure 1.11 Temperature-dependent FT-IR spectra of **11** in toluene-d_8 as gels and solutions/sols (0.8 wt%). Reprinted with permission from Ref. [61c]. Copyright 2010 American Chemical Society.

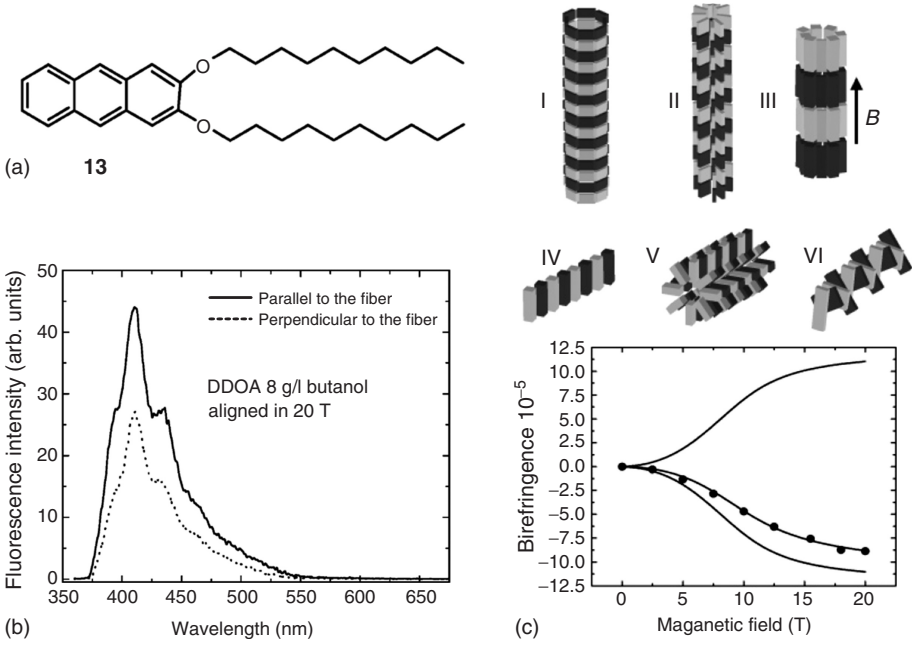

Figure 1.12 (a) Structure of gelator **13**. (b) Polarized fluorescence spectra of a magnetically aligned gel of **13** in butanol; excitation at 340 nm was parallel to the long axis of the fibers and emission was either parallel (solid line) or perpendicular to the fiber long axis (dotted line); no changes in the unpolarized fluorescence spectra were detected before and after application of the magnetic field. (c) Calculated birefringence curves (solid lines) and experimental data points; the different fitting curves correspond to different stacking geometries of the fiber structure shown in (c); see text for explanation. Reprinted with permission from Ref. [67]. Copyright 2005 American Chemical Society.

The investigation of molecular organization in gel fibers by optical properties such as linear birefringence and FL dichroism has received little attention thus far although its potential utility is very high. In one example, fibers of gelator **13** (2,3-*bis*-*n*-decyloxyanthracene, Figure 1.12a) were aligned perpendicular to the direction of a magnetic field of 20 T (due to the diamagnetism of the **LMOG**) that was applied during the gelation process [67].

A higher emission intensity was observed when the detection was parallel to the fiber direction, which is also parallel to the optical transition dipole moment of molecules of **13** (Figure 1.12b); the transition dipole is perpendicular to the long molecular axis and in the plane of the aromatic ring. From this experiment, it was deduced that molecules in the fibers align with an angle ($0 \leq \delta \leq 54.7^\circ$) relative to the original magnetic field. δ is defined as the usual polar angle in polar coordinates which describes the orientation of the long molecular axis with respect to the direction of magnetic field. This result is in good agreement with the birefringence data in which the alignment angle was estimated to be $0 \leq \delta \leq 45^\circ$. Furthermore, possible molecular models were provided, and these agreed well with the calculated birefringence and experimental data (Figure 1.12c). The field-induced birefringence from structures of I and II are positive (curve a), which is inconsistent with the experimental data. Both III and IV produce negative field-induced birefringence: III was inconsistent with fiber alignment direction from SEM; IV overestimates the birefringence (curve c). Only structures V and VI agree well with the experimental birefringence. In addition, the fiber and molecular arrangement directions in these models are consistent with SEM and FL dichroism results.

In another recent and elegant report, FL dichroism of nanofibers in some white-light-emitting multicomponent gels has been utilized to understand fiber structure [68]. The gels consist of 0.012 equiv. of green-emitting (**14**) and red-emitting (**15**) energy transfer (ET) acceptors (Figure 1.13a,b) added to the matrix of blue-emitting gelator **13** (Figure 1.12a for structure and Figure 1.13b for FL in gel) in DMSO (Figure 1.13c). The anisotropy of individual fibers in the white (**W**)-gel was analyzed with confocal FL polarization (***P***, Equation 1.1 where the intensity of linearly polarized emission is measured parallel to the excitation beam and the intensity of polarized emission is measured on the perpendicular axis) imaging under linearly-polarized laser excitation.

$$\boldsymbol{P} = (I_{||} - I_{\perp})/(I_{||} + I_{\perp}) \tag{1.1}$$

Selective absorption of the linearly polarized light occurs when the transition dipole for absorption is aligned parallel to the axis of the excitation beam; the dipoles of **13–15** are along their short molecular axes. ***P*** can range from -1 to $+1$, and the strong variation of ***P*** vs θ (the angle of nanofibers with respect to the orientation of the laser beam polarization) indicates a preferential orientation of the molecules within the nanofibers: in **W**-fibers, component **13** showed a positively polarized emission with $\boldsymbol{P} = 0.25$ for fibers with $\theta = 90 \pm 5^\circ$ relative to the laser polarization (Figure 1.13d, red color code) and a negative polarization for fibers with $\theta = 0 \pm 5^\circ$ ($\boldsymbol{P} = -0.10$, blue color code; $400\,\text{nm} < \lambda_{em} < 450\,\text{nm}$).

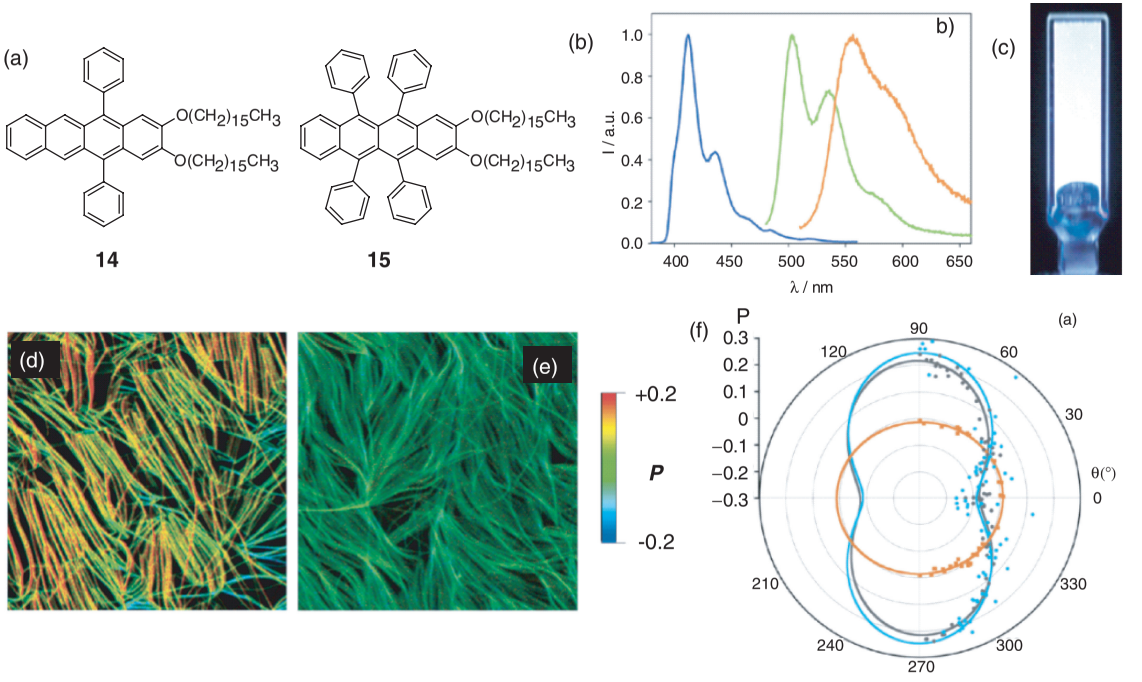

Figure 1.13 (a) Structures of **LMOG** energy transfer (ET) acceptors (**14** and **15**). (b) Fluorescence spectra ($\lambda_{ex} = 365$ nm) of **13** (2 mM gel in dimethylsulfoxide (DMSO), blue), **14** (10 μM solution in tetrahydrofuran (THF), green), and **15** (10 μM solution in THF, red). (c) Cuvette with 2.0 mM **13** and 0.012 equiv. of **14** and **15** in DMSO (**W**-gel) under UV light, $\lambda_{ex} = 365$ nm. (d,e) Fluorescence polarization confocal images (30 × 30 μm) under horizontally polarized excitation (horizontal, $\lambda_{ex} = 385$ nm) of a **W**-gel: (d) 400 nm < λ_{em} < 450 nm and (e) λ_{em} > 500 nm. Color codes correspond to the polarization ***P*** (from negative to positive: blue, green, and red). (f) Polar plots of average ***P*** for individual fiber segments (2–5 μm long) as a function of the angle θ of the fiber axis with respect to the laser polarization (horizontal) with $\lambda_{ex} = 385$ nm: (gray circles) **13**-fibers λ_{em} > 405 nm; (blue circles) **W**-fibers, 400 nm < λ_{em} < 450 nm (orange squares) λ_{em} > 500 nm. Reprinted with permission from Ref. [68]. Copyright 2011 American Chemical Society.

The large change of polarized emission with the angle θ indicates a high degree of molecular order and a preferential average orientation of molecules of **13** within the **W**-fibers. Because this result is very similar to that from fibers of **13** in the absence of the ET acceptors (Figure 1.13e, $-0.08 \leq \boldsymbol{P} \leq +0.22$), it can be concluded that the self-assembly of **13** is not affected by the presence of **14** and **15**. When sensitized by **13** ($\lambda_{ex} = 385$ nm, $\lambda_{em} > 500$ nm; Figure 1.13e,f), the FL from the **14** and **15** components in the **W**-fibers is almost non-polarized. Additional experiments revealed that **13** and **14** have similar preferential orientations, while **15** is more randomly oriented.

1.2.2
Chirality as a Tool – Comparisons between Optically Pure and Racemic Gelators and Optically Pure and Racemic Liquids

LMOGs with stereogenic centers have been studied extensively [69]. Enantio-pure gelators have enhanced our understanding of the gelation process by virtue of their ability to create helical supramolecular assemblies with a single handedness. Upon gelation, these helical assemblies are typically characterized using CD spectroscopy [69a,b] coupled with other microscopic techniques that help visualize fiber morphology [47, 69a]. In the solution state, chiral molecules generally exhibit very weak CD signals. Upon gelation of enantio-pure or enantio-enriched systems, significantly enhanced CD effects are commonly observed as a result of helical structure formation.

Typically, racemic mixtures of chiral gelators either do not form gels or they form unstable ones that degenerate easily into precipitates or bulk-separated crystals [69a, 70]. However, there have been some interesting exceptions in which a racemate produces stronger gels than their enantio-pure counterparts [70, 71].

The gelation of 12-hydroxyoctadecanoic acid (or 12-hydroxystearic acid) **16** has been studied as a model system based upon its structural simplicity. Tachibana, T. *et al*. initially investigated the gelation abilities of (*R*)-**16** (D-**16**) as compared to its racemic mixture (DL-**16**) (Figure 1.14) [72]. The gels of enantio-pure **16** in CCl_4 exhibited CD maxima at 350 nm. Because this **LMOG** possesses no chromophores which absorb in this region, the origin of this band was hypothesized to be from preferential reflection of circularly polarized light of one sense by the gel. Interestingly, this effect is solvent dependent; the CD band shifted to 480 nm in benzene. Also, the racemic mixture, DL-**16**, did not form a gel at comparable concentrations.

Recent work by Grahame *et al*. has demonstrated the relationship between the gelation ability of **16** and its enantio-purity in mineral oil [73]. Thus, the critical gelator concentration (CGC) of enantio-pure **16** was less than 1.0 wt%, while racemic DL-**16** required ~ 2 wt%. The morphologies of the crystalline objects in **SAFIN**s were drastically different as well. The gel of enantio-pure D-**16** produced long, twisted fibers (Figure 1.15a), while the racemic mixture exhibited platelet crystallites (Figure 1.15b). When the ratio of D:L content in **16** was systematically varied, the FT-IR spectra of the resultant gels in mineral oil could be interpreted according to

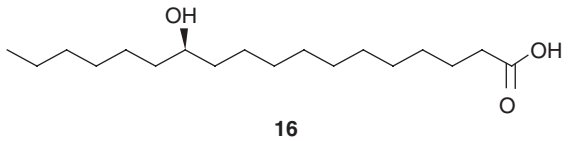

16

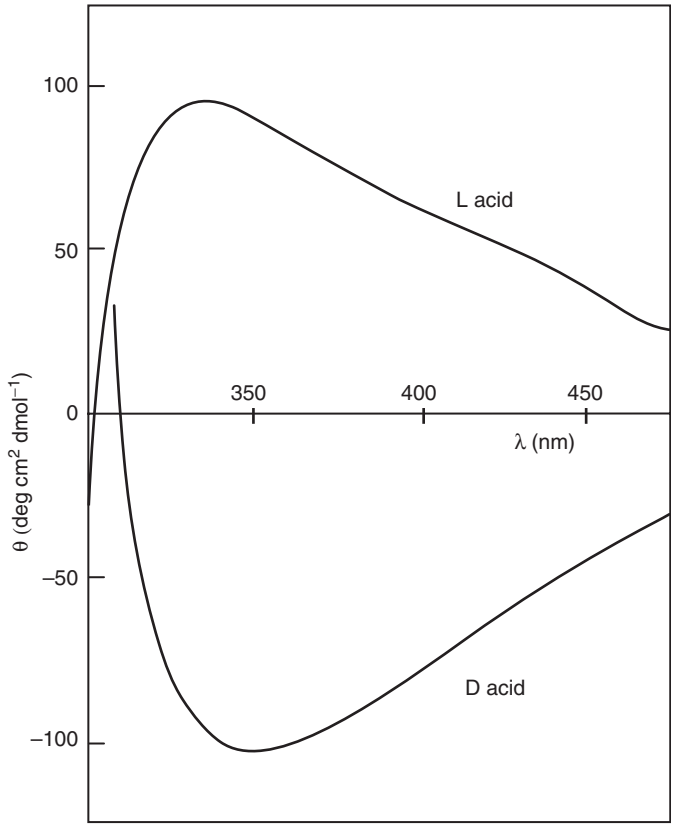

Figure 1.14 CD spectra of enantiomerically pure **16** in CCl_4 gels: 25.7 mmol L^{-1} for the L-acid; 35.7 mmol L^{-1} for the D-acid. Reprinted with permission from Ref. [72]. Copyright 1979 Nature Publishing Group.

two different modes of crystallization. The analyses focused on the hydroxyl and carbonyl stretching regions. Fitting the area of hydroxyl HB peaks to the Avrami model [74] indicated (i) platelet-like crystals and sporadic nucleation (or spherulitic crystals and instantaneous crystallization) at D:L ratios below 80 : 20 and (ii) fiber-like crystal growth and sporadic nucleation at D:L ratios above 80 : 20. From analysis of the carbonyl stretching region, it was found that equal amounts of cyclic and acyclic dimers, formed between carboxylic acids, were present at D:L ratios below 80 : 20. At D:L ratios higher than 80 : 20, significantly more cyclic dimers were present.

Based on this experimental characterization, the authors postulated that hydroxyl groups are positioned on opposite sides of the cyclic dimers in gels of optically

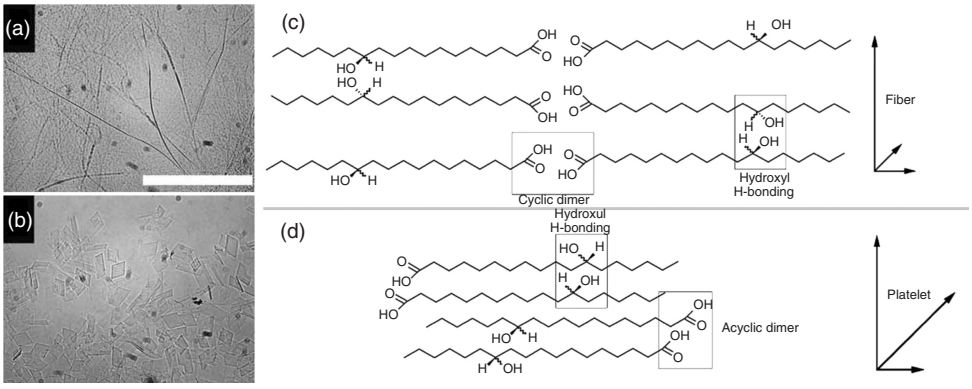

Figure 1.15 Bright-field micrographs of (a) D-**16** and (b) 50 : 50 D:L-**16**. (bar = 20 μm). Schematic representations of D-**16** packing (c) and DL-**16** packing (d) in **SAFIN**s of mineral oil gels. Reproduced from Ref. [73] with permission of The Royal Society of Chemistry. *http://dx.doi.org/10.1039/C1SM05757J*

pure **16** (Figure 1.15c). Because of this alignment, HB along the transverse axis can promote longitudinal growth leading to fibrils. In contrast, single, in-plane acyclic dimers are likely to form in the gels of racemic **16**, which favor platelet growth rather than longitudinal growth along the transverse axis (Figure 1.15d).

The exciton-coupled CD enhancement of choromophoric chiral gelators can be used to study the development of fiber formation and, more importantly, molecular packing within the fibers. An example is the recent chiro-optical studies on gelation by the dicarbamate derivatives of (3*S*,4*S*) and (3*R*,4*R*)-3,4-dihydroxypyrrolidines (Figure 1.16a) [75]. Compound (*S*,*S*)-**18** was a more efficient gelator than (*S*,*S*)-**17**; the CGC of (*S*,*S*)-**18** in cyclohexane was found to be ~1 mg mL^{-1}. Gels of enantio-pure (*R*,*R*)-**18** and (*S*,*S*)-**18** in cyclohexane exhibited CD spectra that were almost perfect mirror images of each other above 250 nm. An AFM study on xerogels (*R*,*R*)-**18** and (*S*,*S*)-**18** revealed the presence of left-handed and right-handed helices, respectively. In this system, racemic **18** also formed organogels in cyclohexane. However, their T_g (gel–sol transition temperatures) were lower than that of gels employing enantio-pure gelators (Figure 1.16b). The CD spectra of (*S*,*S*)-**18** in cyclohexane exhibited an enhanced signal as the temperature was lowered (Figure 1.16c) as a result of helical fiber formation. The CD spectra alone are insufficient to provide detailed molecular packing information, however. By combining crystallographic data from structural analogs of (*S*,*S*)-**18** with Merck Molecular Force Field (MMFF) calculations, it was possible to postulate a molecular packing mode for (*S*,*S*)-**18** in the fibers (Figure 1.16e) [75]. A calculated CD spectrum, based upon a hexamer model using the DeVoe method [76] (Figure 1.16d), was in reasonably good agreement with the experimental CD spectrum.

Cholesterol [77] and sugar moieties [78] have been popular groups used to render chirality in **LMOG**s. For example, sugar-containing terphenyl gelator **19** (Figure 1.17a) self-assembled into helical ribbons upon gelating a cooled H_2O/dioxane mixture [78g]. As shown in Figure 1.17b, **19** in H_2O/dioxane at

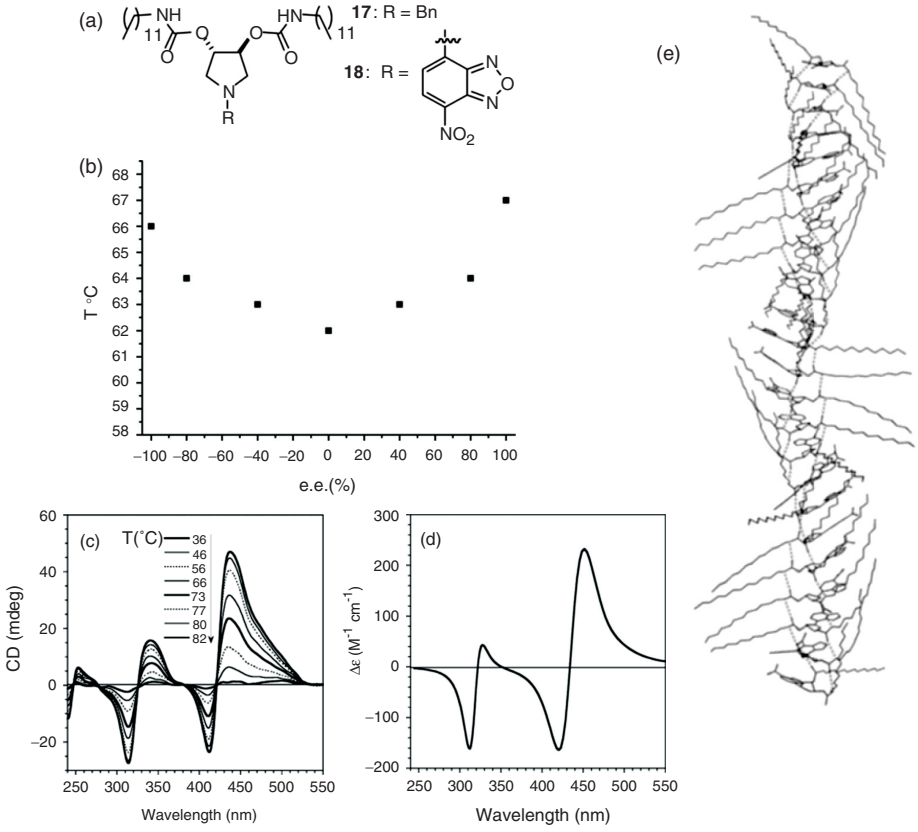

Figure 1.16 (a) Molecular structures of dicarbamate derivatives of 3,4-dihydroxy pyrrolidine. (b) T_g values vs enantiomeric excess of gels of **18** in cyclohexane (overall concentration 6.5 mg mL^{-1}). (c) CD spectra of (*S*,*S*)-**18** in cyclohexane (2.5 mg mL^{-1}) at different temperatures. (d) Calculated CD spectrum for the gel of (*S*,*S*)-**18** using the DeVoe method on a hexamer aggregate. (e) MMFF-optimized structures for the 24-mer of (*S*,*S*)-**18**. Reprinted with permission from Ref. [75c]. Copyright 2011 Wiley.

60 °C exhibited no discernible CD signal (indicative of a molecularly dissolved state). When the solution/sol was cooled, a strong exciton-coupled CD signal was observed. A noteworthy aspect of this system is that the signs of CD signals were reversed when the cooling rate was changed. The authors ascribed this phenomenon to the formation of two possible molecular packing modes: a metastable kinetically-driven molecular arrangement and a thermodynamically stable one. Fast cooling from a hot solution/sol produced ribbons with right-handedness (kinetically controlled), while slow cooling from a hot solution/sol produced ribbons with the opposite handedness (thermodynamically controlled). Electron micrographs of the xerogels supported the hypotheses (Figure 1.17c for slow-cooled and Figure 1.17d for fast-cooled) in which helical ribbons showed opposite handedness.

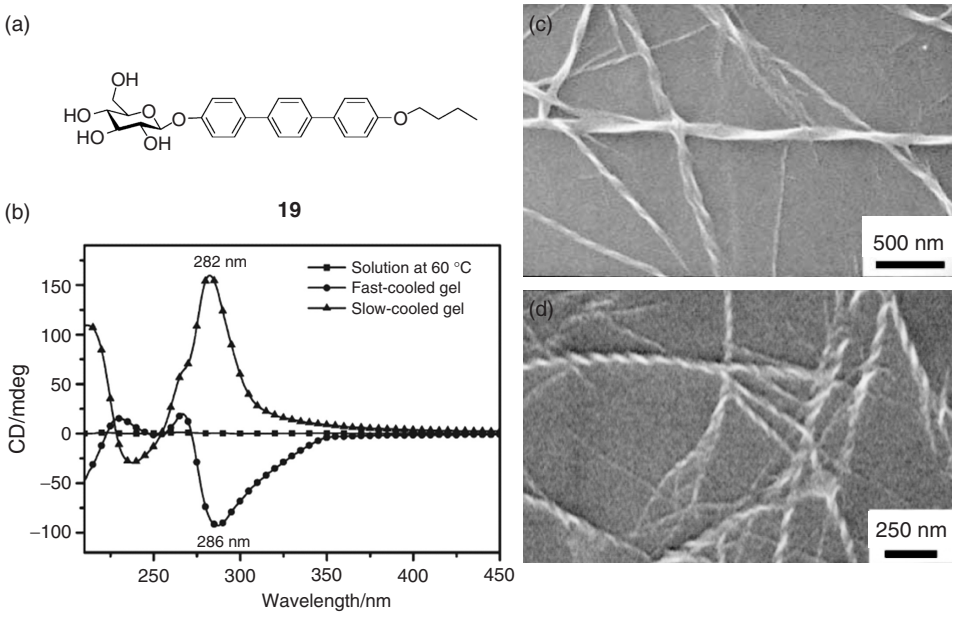

Figure 1.17 (a) Sugar-appended terphenyl gelator **19**. (b) CD spectra of a solution/sol of 2 mg mL^{-1} **19** in H_2O/1,4-dioxane (40/60 v/v) at 60 °C (■), the fast-cooled gel state (●), and the slow-cooled gel state (▲) at 20 °C. SEM micrograph of the slow-cooled (c) and fast-cooled (d) gel of 5 mg mL^{-1} **19** in 40/60 (v/v) H_2O/1,4-dioxane. Reprinted with permission from Ref. [78g]. Copyright 2010 American Chemical Society.

Gelation-induced helix formation can be achieved and strong CD signals can be observed even when the chiral centers are far from a chromophore. Oligo(*p*-phenylenevinylene) (OPV) functionalized with two chiral side groups and four dodecyl side groups [79] (**20**, Figure 1.18a) was found to gelate alkanes such as dodecane, heptane, and cyclohexane (CGC = 6.4×10^{-3} M). Although a chloroform solution of **20** at a concentration of 5.3×10^{-4} M was CD inactive, suggesting a lack of aggregation (Figure 1.18b inset), a strong exciton-coupled CD spectrum was observed in dodecane at the same concentration, indicating the transfer of molecular chiral information to the self-assemblies in a helical sense (Figure 1.18b inset). In sharp contrast, compound **21**, with six chiral side groups, did not form a gel in any of the solvents examined.

The shape of the CD spectrum changed with concentration (Figure 1.18b), exhibiting two transitions: (i) a Cotton effect with zero crossing at 440 nm below 3×10^{-5} M and (ii) a zero crossing at the absorption maximum (400 nm) above 3×10^{-5} M where a true exciton-coupled CD spectrum is observed. Based upon additional data from AFM (Figure 1.18c), this unusual phenomenon was interpreted to arise from two hierarchical supramolecular assemblies that involve the formation of left-handed chiral aggregates (in the low concentration regime) and secondary assembly to coiled-coil ropes (in the high concentration regime).

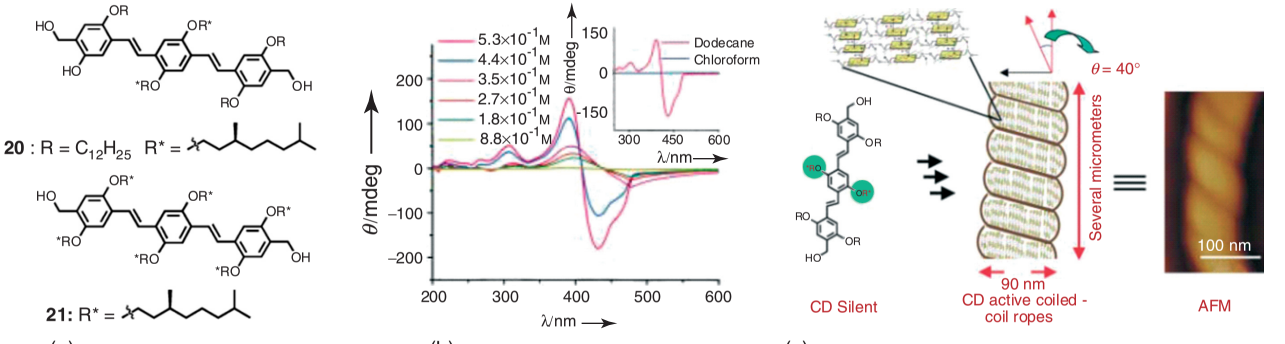

Figure 1.18 (a) Structure of OPV-based chiral molecules. (b) CD spectra of compound **20** in dodecane at different concentrations ($T = 293$ K, $l = 1$ mm); the inset shows the CD spectra of compound **20** in dodecane and chloroform ($c = 5.3 \times 10^{-4}$ M, $l = 1$ mm). (c) Schematic representation of the hierarchical self-assembly of compound **20** into helical coiled-coil gel nanostructures; a magnified AFM image of the coiled-coil rope is shown on the right (scale bar is 100 nm). Reprinted with permission from Ref. [79]. Copyright 2004 Wiley.

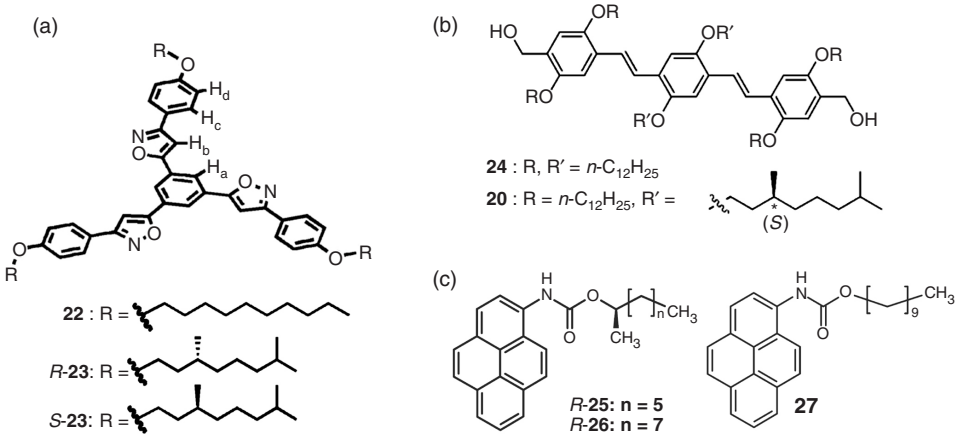

Figure 1.19 (a) Molecular structures of tris(phenylisoxazolyl)benzene-based, (Reproduced from Ref. [81c] with permission of The Royal Society of Chemistry. *http://dx.doi.org/10.1039/B715871H*.) (b) OPV-based,(Reprinted with permission from Ref. [81a]. Copyright 2006 Wiley.) and (c) pyrene-based chiral and achiral gelators for induced CD. (Reprinted with permission from Ref. [81e]. Copyright 2010 American Chemical Society.)

In some systems, a small amount of chiral dopant can be added to an achiral gelator to induce chirality through the so-called ''sergeant-and-soldiers'' effect. This effect was first discovered in poly(alkyl isocyanates) where monomeric units are covalently bonded [80], and was later applied to organogel systems where the building blocks are connected through intermolecular interactions [81].

As an example, the addition of only 0.01 mol% of chiral *R*-**23** or *S*-**23** to achiral **22** (Figure 1.19a) induced a remarkable Cotton effect by forming helical columnar structures; *R*-**23** or *S*-**23**, alone at the same concentration, exhibited a very weak Cotton effect [81c]. Similar chiral amplification effects were also observed from the co-assembly of OPV-based [81a] or pyrene-based [81e] achiral and chiral gelators (Figure 1.19b,c, respectively).

Most sergeant-and-soldiers systems have structurally similar chiral dopant and achiral gelators. If the two components are structurally dissimilar, they will usually remain segregated in the fibers, and no co-assembly will be observed. However, Hong *et al*. have demonstrated that the sergeant-and-soldiers effect can also be achieved from chiral and achiral molecules of very different structures [81d].

An achiral molecule containing an aromatic ring and two alkyl amides (**28**) and chiral molecules containing two D- or L-alanine residues (**29** or **30**, respectively) (Figure 1.20a) formed gels in toluene [81d]. Xerogels from **28** in toluene formed both left- and right-handed helical ribbons. However, no helical structures were observed from the xerogels of **28** and **29**. The addition of 1% of chiral **29** or **30** to achiral **28** induced enantio-pure helices with mirror image Cotton effects (characterized from xerogels), while xerogels of **29** and **30** showed CD spectra corresponding to the intrinsic chirality of the gelators (as opposed to a helical structure) (Figure 1.20b).

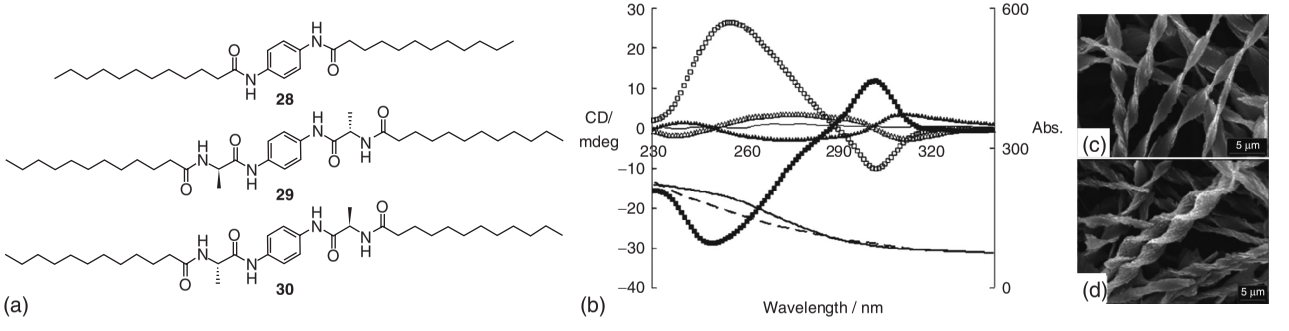

Figure 1.20 (a) Structures of achiral gelator **28** and chiral dopants (**29** and **30**). (b) CD spectra of **28** (—), **29** (▲), **30** (△), **28**:**29** 99:1 (■) and **28**:**30** 99:1 (□); UV–vis absorption spectrum of **28**:**29** 99:1 (– – -) and **28** (—) in its xerogel phase. SEM images of xerogels: (c) 99:1 **28**:**29**, M helices, and (d) 99:1 **28**:**30**, P helices. Reprinted with permission from Ref. [81d]. Copyright 2008 Wiley.

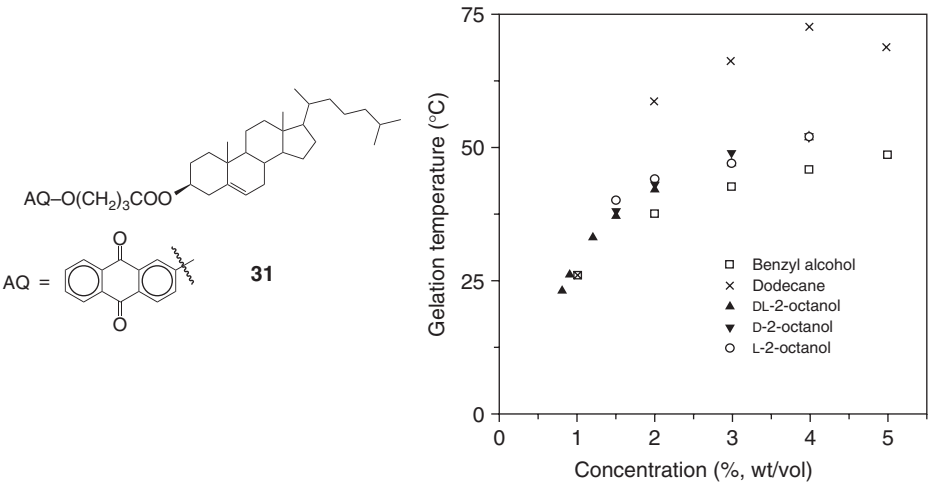

Figure 1.21 Gelator concentration versus gelation temperature for **31** in various liquids. Reprinted with permission from Ref. [43c]. Copyright 1996 American Chemical Society.

The helical ribbons with opposite handedness for xerogels of **28** : **29** (99 : 1) and **28** : **30** (99 : 1) (Figure 1.20c,d) were consistent with the CD results.

The examples described thus far include only achiral liquids (solvents) gelled by chiral gelators. If an enantio-pure liquid is employed, specific diastereomeric liquid-gelator interactions can be expected. Such an interaction may (or may not) influence **SAFIN** formation. That possibility was investigated by Mukkamala *et al.* using a chiral **LMOG** which incorporates an aromatic (A), a linker (L), and a steroidal (S) group ("ALS"), **31** [43c]. Figure 1.21 shows T_g as a function of gelator concentration. As the gelator concentration was increased, T_g increased rapidly followed by a plateau region for all the liquids listed in the figure. Notably, T_g values for the gels in DL-, D-, or L-2-octanol were indistinguishable within experimental error. This result indicates that enantiopurity of the liquid had no apparent influence on the **SAFIN** formation of **31**. On the other hand, liquid polarity affected T_g significantly: higher T_g values were found for the gel in dodecane than in either alcohol. Currently, there is an insufficient number of examples of this sort to form a conclusion about the generality of liquid-induced chiral induction in **SAFIN**s of achiral **LMOG**s.

1.2.3
Liquids and their Influence on Gelator Networks

Attempts to correlate the properties of molecular gels with the nature of their liquid components have been only partially successful. The liquid intervenes at the initial stages of **SAFIN** development, and thus, correlations between the final characteristics of a gel, such as its stability to heat and shear, and the bulk or even molecular properties of a liquid should not be expected in many cases. In addition,

the rate at which a sol is cooled to its gel phase can affect the ultimate gel properties profoundly; both of these effects have been shown in several cases to be linked. In all but a very few cases [52b, 82], the liquid components of (at least) organogels appear to be excluded from **SAFIN** networks; the liquid is in a ''supporting role'' after the gel is formed. That supporting role can be probed more directly in terms of the interactions between a liquid component and a **SAFIN** structure when the gels are thixotropic and their rheological properties are compared with the molecular and bulk properties of the liquid. Unfortunately, few studies of this sort have been conducted for **LMOG**-based gels [83]. Learning how the liquid and the temperature affect the gelation process is as important to understanding molecular gels as is determining the basic design criteria for a gelator. Unfortunately, and as is the case with molecular design of gelators, a satisfactory level of understanding cannot be claimed to date for how temperature or liquid properties affect gelation.

Although several early attempts to derive empirical correlations between liquid composition and gel properties did provide some insights, they were useful with a limited range of gelator structures. In one example, gels containing about 1.5 wt% of cholesteryl 4-(2-anthryloxy)butanoate (**CAB**) and *n*-hexadecane, 1-octanol, or their mixtures as the liquid component were investigated as the sols were cooled at either about 8 (fast) or 0.5 (slow) °C/min to room temperature [84]. The results of spectral and thermal measurements of the **SAFIN**s in gels with different liquid compositions led to the conclusion that bulk solvent properties, especially polarity, are more important than specific solvent–**CAB** intermolecular interactions in determining the nature of the gel phases formed, but even the dependence on bulk polarity is complex. When l-octanol/*n*-hexadecane compositions in the range 80/20 to 85/15 (wt/wt) were employed, two different gel types (with sol → gel transition temperatures of ∼40 and 62 °C and FL emission maxima at 421–422 and 427 nm in the low and high 1-octanol regimes, respectively) could be identified depending upon the protocol for cooling the precursor isotropic phases. At l-octanol/*n*-hexadecane compositions above or below these wt/wt ratios, only one of the two **SAFIN** types was produced, regardless of the cooling protocol used to effect the sol → gel transformation. In addition, sample-holding cells whose wall separations are smaller than the diameters of the colloidal (spherulitic) units in the gels inhibited gel formation. Similar observations of cooling rate-induced and liquid-induced polymorphism within the **SAFIN**s of gels with **32**, a bis-glutamine and aromatic core **LMOG** structure, have been reported as well [85]. In this system, DMSO or mixtures of DMSO and another liquid were employed. The extensive experimental evidence points to molecular packing schemes within the gel fibers, as shown in Figure 1.22.

In another example, it was possible to modulate the concentration of 5α-cholestan-3β-yl *N*-(2-naphthyl)carbamate (**CNC**; see Section 1.4) in *n*-octane and the incubation temperatures of the sols to obtain **SAFIN**s with different morphologies [15]. The sizes of the spherulites could be increased by increasing the incubation temperatures so that they were closer to the sol → gel transition temperatures, T_g (and the thermodynamic driving force for **SAFIN** formation was reduced) or by increasing the **CNC** concentration at constant incubation temperature. At very

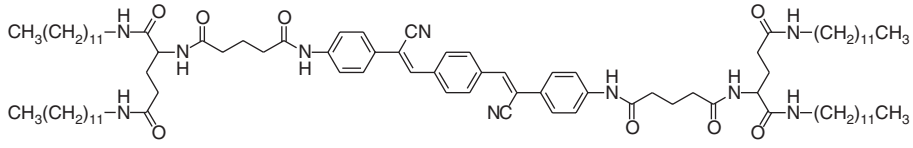

32

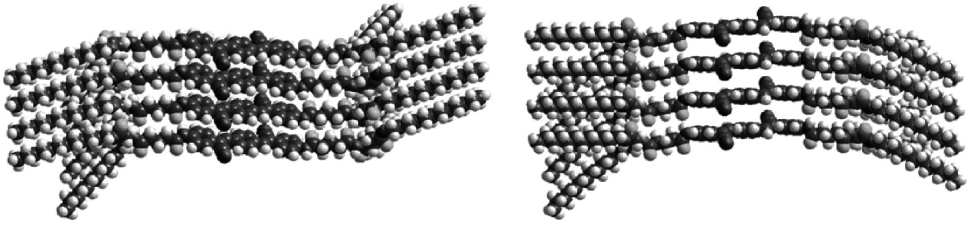

Figure 1.22 Possible molecular packing modes of **LMOG 32** in gels with DMSO/diphenyl ether (1 : 9, v/v, left) and DMSO (right) as the liquid. Reprinted with permission from Ref. [85]. Copyright 2009 Wiley.

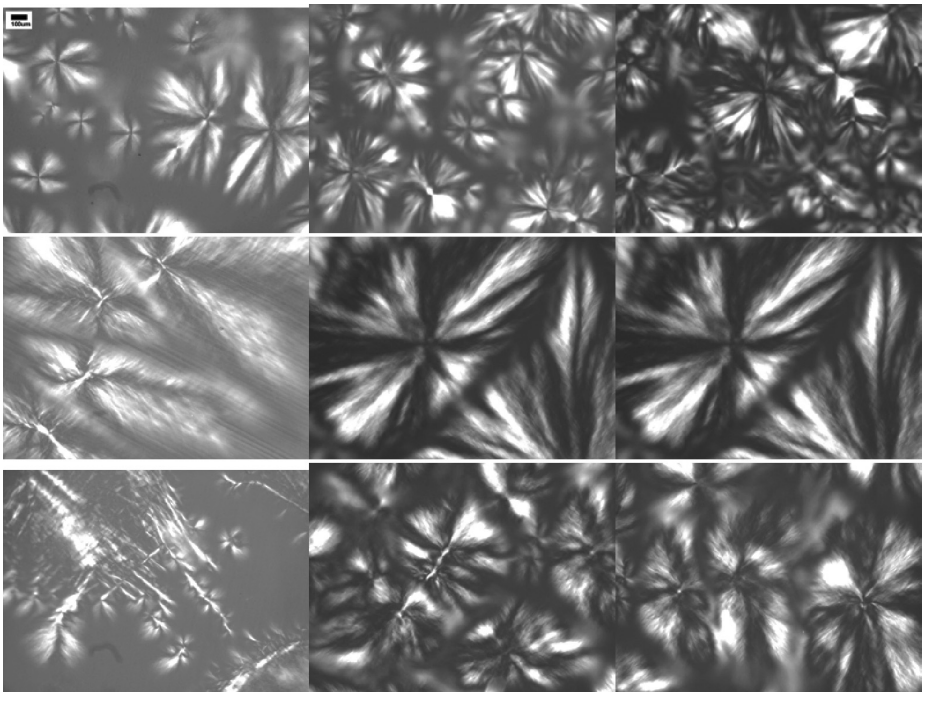

Figure 1.23 Polarized optical micrographs of 0.89, 1.46, and 1.94 wt% **CNC**/*n*-octane organogels (from left to right) prepared by incubating sols at (from top to bottom) 14.5, 32.2, and 36.3 °C after cooling them from well above their T_g. The scale bar, 100 μm, applies to all micrographs. Reprinted with permission from Ref. [15]. Copyright 2005 American Chemical Society.

low gelator concentrations and high incubation temperatures, the morphology is changed completely, from spherulitic to rod-like (NB, lower left panel in Figure 1.23). Transformations from spherulitic to rod-like **SAFIN**s have been observed in other organogel systems, with gelators with much simpler different structures, as well [4].

Even more dramatic changes in the microstructures of the aggregates were observed for the dipeptide **LMOG**, di-phenylalanine (L-**Phe**-L-**Phe**), in different toluene/ethanol mixtures [86]. The fibrillar network of the gels became micro flower-like crystallites as the ethanol content of the liquid increased (Figure 1.24) and the samples were no longer gels at > 40% ethanol.

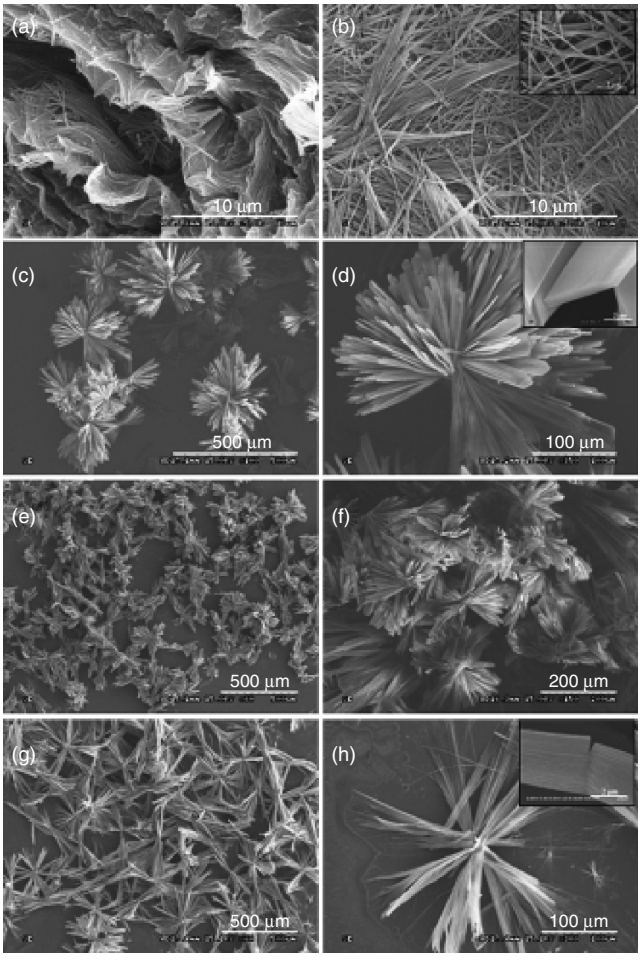

Figure 1.24 Scanning electron micrographs of samples of L-**Phe**-L-**Phe** formed at different toluene/ethanol contents: (a) 100/0; (b) 90/10; (c,d) 75/25; (e) 60/40; (f) 30/70; and (g,h) 0/100. Reprinted with permission from Ref. [86]. Copyright 2010 Wiley.

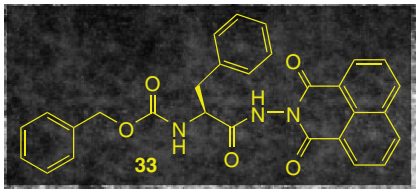

Figure 1.25 Structure of **33 LMOG**. Reproduced from Ref. [87] with permission of The Royal Society of Chemistry.

In addition, CD and FL have been used to investigate the effect of changing the relative volume fractions of toluene/CCl_4 mixtures on the packing of naphthalimide moieties of peptide **LMOG** molecules (**33**) within their **SAFIN**s [87]. One of the naphthalimide gelators is shown in Figure 1.25. The chirality of the packing of the **33** molecules can be altered by small structural changes to the **LMOG** as well. Clearly, the bulk properties of the liquid mixtures (as modulated by the volume fractions of toluene and CCl_4) and the manner in which each liquid type interacts with the **LMOG** molecules as they aggregate in the sol phase upon cooling influence the eventual packing within the **SAFIN**s.

In another approach, NMR measurements of solubilities in toluene of 4 **LMOG**s consisting of alkanes with α- and ε-amino acid groups of L-lysinelysine (Figure 1.26, **34–37**) have been used in a van't Hoff analysis to calculate temperatures at which the **LMOG**s are completely solubilized at various concentrations [88]. These temperatures can be related to the CGCs of the **LMOG**s in the liquid components, and therefore constitute a predictor of several gel properties, such as the so-called "plateau region" where the values of T_g vary little with **LMOG** concentration. Others have employed the van't Hoff equation (Equation 1.2 in which ΔH_{diss} and ΔS_{diss} are the molar enthalpy and entropy for dissolving a solid in a liquid and Sol is the solubility at T_{eq}) and related equations such as the Schröder–van Laar equation [55] to describe the thermodynamic properties of sol–gel transitions in other systems, but without the same level of detailed analysis. A problem endemic to the use of such treatments is that they suppose that the sol phases are "ideal" solutions; because aggregation frequently persists above T_g, they are not. Nevertheless, in some systems, such as the one mentioned here, interesting and useful information can be obtained.

$$\ln (S) = -\Delta H_{diss}/RT_{eq} + \Delta S_{diss}/R \tag{1.2}$$

Several attempts to correlate the bulk properties of solvents with the ability to be gelated by specific gelators have appeared recently. These physical-organic approaches will be very useful if they can be shown to apply to several structurally diverse classes of gelators. In addition to permitting researchers to make *a priori* assessments of which liquids probably will and will not be gelated by a specific molecule, they will broaden the scope of the anti-solvent approach to making gels [44a, 89]. In it, gelation is induced at room temperature by adding a miscible solvent to a solution in which the gelator is insoluble.

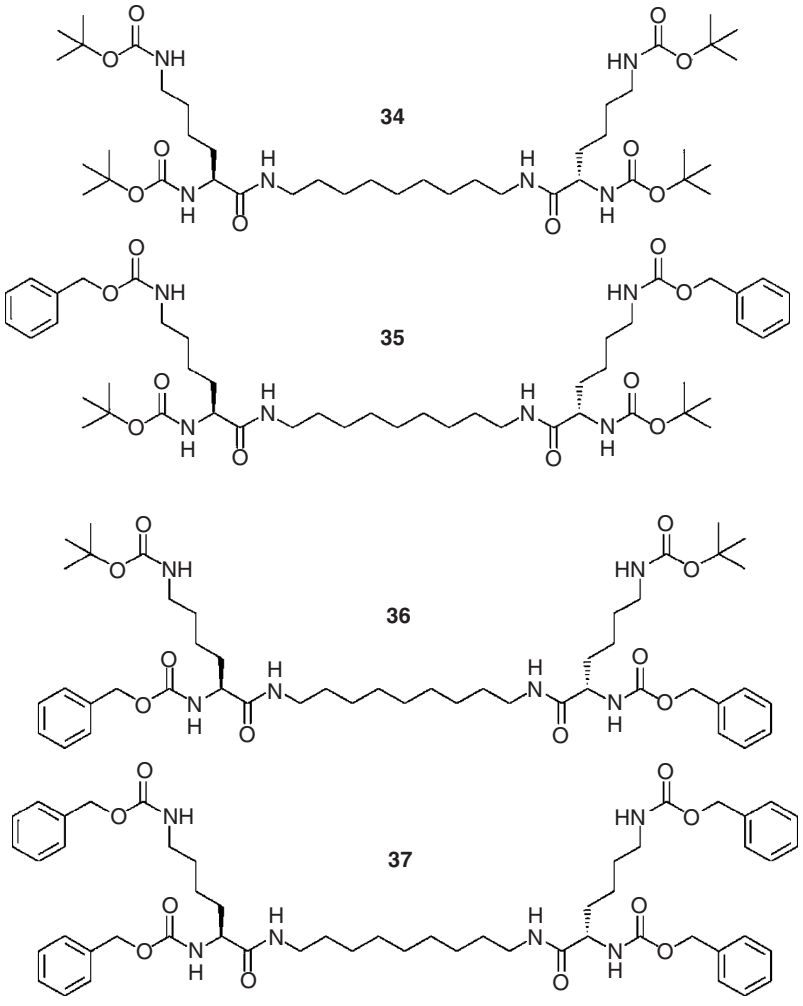

Figure 1.26 **LMOG**s used with the van't Hoff equation to assess toluene gel properties. Reprinted with permission from Ref. [88]. Copyright 2008 American Chemical Society.

Kamlet–Taft parameters [90] have been used to determine the influence of solvent type on the ability of a series of L-lysine *bis*-urea gelators [44]. In this treatment, the H-bond donating and H-bond solvent acceptor parameters of the Hamlet–Taft treatment are used to assess the degree to which the gelator can establish an H-bonding network (because the urea fibers rely on H-bonding networks among the urea gelator molecules), and the polarizability parameter is assumed to be related to the solvation of the *n*-alkyl groups of the gelator near its molecular ends. Thus, the sum of the H-bonding factors is implicated

in intermolecular interactions among the urea gelator molecules within a fiber whereas the polarizability factor relates to the stability of the fibers, including fiber–fiber interactions, because the liquids interact primarily with the external surfaces of the fibers.

A Hansen-type approach [91b], in which the gelator/liquid interaction energy is taken to be the sum of H-bonding, polar, and dispersive interactions, has been used to demonstrate that H-bonding interactions are insufficient to explain the **SAFIN** structures of a sugar-based gelator [92]. This data treatment has been expanded by Wu *et al*. to roughly correlate the properties of gels (e.g., fiber structures, CGCs, and gelation times) made with **38** as gelator [93]. Also, the Hildebrand solubility parameter (which is related to the total of the energetic factors holding liquid molecules together) [94] and $E_T(30)$ solvent scale (which is a measure of the polarity of a liquid) [95] have been employed to correlate the properties of the liquid components with those of gels with 6,6′-diesters of trehalose (**39**) as the gelators [96]. The $E_T(30)$ values were dissected into contributions calculated for polarity/polarizability [97] and solvent acidity/basicity [95]. It was concluded that the most efficient gelation (as measured by the maximum number of liquid molecules gelated by each molecule of gelator at 25 °C) and least bundling of fibers occurs when liquid–gelator interactions are small. The use of Hansen parameters has been advanced further by Raynal and Bouteiller, who have shown that it is possible to correlate the solvent properties and gelation abilities of a fairly broad range of gelators [98] using an approach determining distances in Hansen space to the centers of ''solubility spheres.'' Although not perfect, it is the most exciting and potentially useful method reported to date in the opinion of the authors of this chapter.

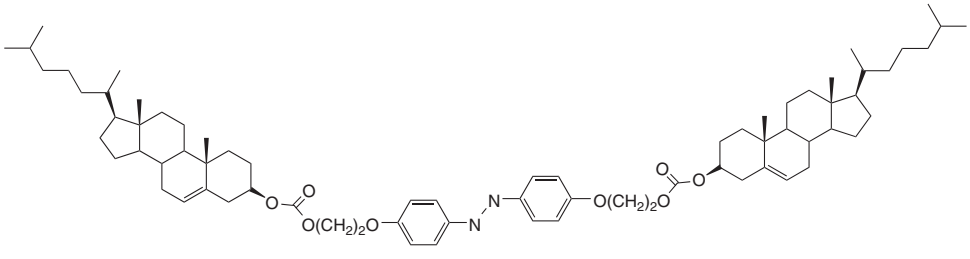

38

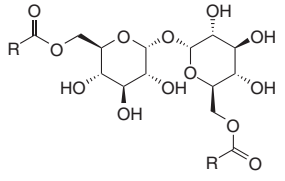

i: R = CH_3
ii: R = $(CH_2)_2CH_3$
iii: R = $(CH_2)_8CH_3$
iv: R = $(CH_2)_{12}CH_3$

39

In a converse sense, the **SAFIN** of a molecular gel can be used to alter the properties of the liquid component. Trivial (but very important) examples of this, endemic to all gels, are the changes in flow characteristics and bulk viscosity experienced by gels compared to their neat liquid components. Although the vast majority of the liquid molecules in a gel are able to diffuse on the micro and sub-micro scales as they do in the bulk, they remain stationary for very long periods when viewed at larger length scales. Such phenomena are related to the mechanical properties of gels (i.e., their rheology) and will not be discussed in this chapter. However, incorporation of ordered liquids, especially nematic liquid crystals, into **SAFIN**s of molecular gelators can result in significant changes to the gels. For example, the nematic phases of such materials have been aligned by magnetic and electrical fields, so that the optical and other properties of the gels become strongly anisotropic on the macro scale. Because the direction of alignment can be switched without physically contacting the gels, they may be useful in a variety of electronic and memory applications. Examples of such systems are shown in Figure 1.27 [99]. As noted, the nature of the phases can be modulated depending on the relative temperatures of the $T_{sol-gel}$ transition of the gelator and the T_{iso-lc} transition of the liquid crystal.

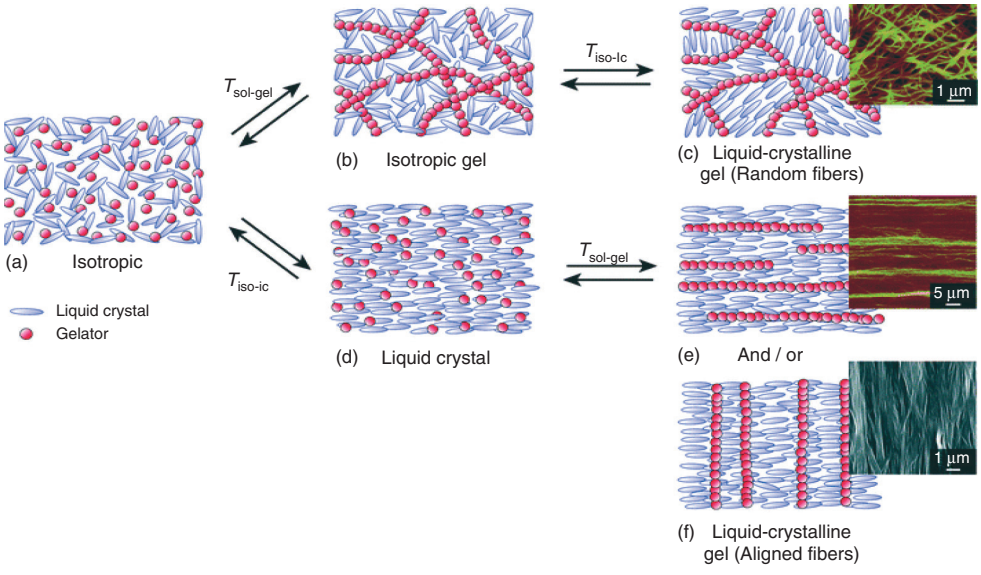

Figure 1.27 Some possible structural changes of molecular gels with nematic liquid-crystal liquid components. The (a) → (b) → (c) changes are possible when $T_{sol-gel} > T_{iso-lc}$. The (a) → (d) → (e, f) changes can be observed when $T_{iso-lc} > T_{sol-gel}$. The insets are AFM images of gels composed of gelator **41** in liquid-crystalline **42** (c) and of gelator **40** in liquid-crystalline **44** (e) and an SEM image of gelator **13** in liquid-crystalline **42** (f). Reproduced from Ref. [99] with permission of The Royal Society of Chemistry.

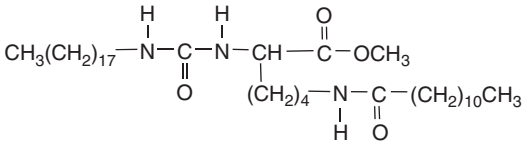

40

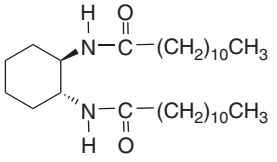

41

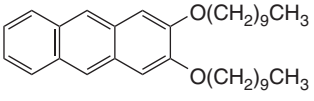

13

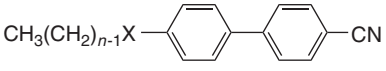

42: n = 4, X = none
43: n = 7, X = O

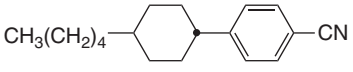

44

1.3
Stimulation of Gelation by Perturbations Other Than Temperature

1.3.1
Enzymatic *In situ* Formation of Gelators and Gels – Potential Biological Applications

A promising and recently expanding method of inducing gel formation utilizes enzyme-mediated biochemical modification to convert non-gelating materials into gels. Such an approach can take advantage of the high degree of selectivity offered by biology that is rarely (if ever) matched by non-biological processes. Many different types of enzymes have been utilized in this arena, including phosphatases, kinases, proteases, β-lactamases, and esterases. The coupling of fiber self-assembly/disassembly to biologically relevant molecules points toward a broad range of potential biomedical applications including targeted drug delivery, wound healing, biosensing, tissue growth, and sequestration of toxins. Several recent reviews on this topic are available [100–102].

Figure 1.28 outlines two general approaches, each converting non-gelling species into gelators, either through enzyme-mediated bond cleavage or bond formation. In the first approach (pioneered by the Xu group [103]), an enzyme is used to cleave a solubilizing group from a pre-gelator, thus converting it into a less soluble derivative and inducing self-assembly. Alternatively, a gelator can be produced *in situ* via enzyme-catalyzed bond formation between two soluble precursors.

The earliest report of *in situ* enzyme-mediated supramolecular gelation was in 2004, when the Xu group reported the use of an alkaline phosphatase to dephosphorylate an Fmoc-protected tyrosine derivative, **45** (Figure 1.29) [103a].

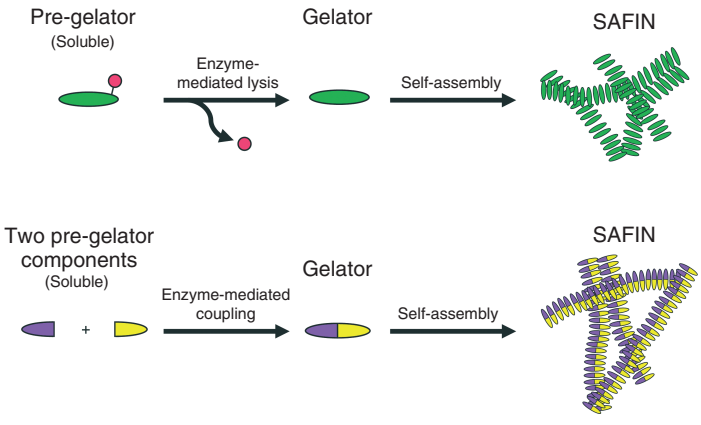

Figure 1.28 Cartoon representation of enzyme-mediated fiber formation. (a) A solubilizing group (red circle) is enzymatically cleaved from a pre-gelator; the resulting decrease in solubility of the product (green oval) results in **SAFIN** formation. (b) Two soluble gelator precursors are linked via an enzyme-catalyzed reaction, yielding an **LMOG**.

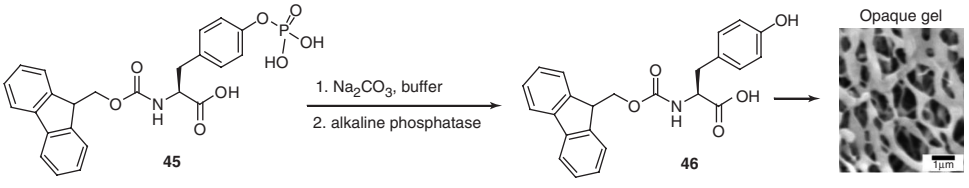

Figure 1.29 Fmoc-(*O*-phospho)-tyrosine (**45**) is converted to the hydrogelator Fmoc-tyrosine (**46**) via an alkaline phosphatase-catalyzed dephosphorylation. The image shows a scanning electron micrograph of the dehydrated gel fibers. Reprinted with permission from Ref. [103a]. Copyright 2004 Wiley.

The phosphate group (which is ionic in the basic conditions of the experiment) renders **45** soluble in water; its removal yields a product with significantly lower solubility (**46**) that subsequently self-assembles into a fibrous aggregate, producing a **SAFIN** as part of an opaque hydrogel. A mixture of **45** and Fmoc-protected lysine (not shown) yields a clear hydrogel under similar conditions. Gels produced by this method are responsive to a range of stimuli, including temperature and pH, allowing several experimental variables to control reversibly the gel–sol transition.

The Xu group has been a *tour de force* in this area over the last decade. A notable development was reported in 2006: reversible gelation of a pentapeptide derivative was controlled by a pair of enzymes that install (**47** → **48**) or remove (**48** → **47**) a phosphate group [104]. Addition of a kinase enzyme to the hydrogel in the presence of ATP converts the tyrosine into a tyrosine phosphate (~46% conversion), thus destroying the gel. The reverse reaction, phosphatase-mediated dephosphorylation (~99% conversion) triggered gel formation (Figure 1.30). Furthermore, subcutaneous injection of the soluble phosphorylated form of the compound into a mouse

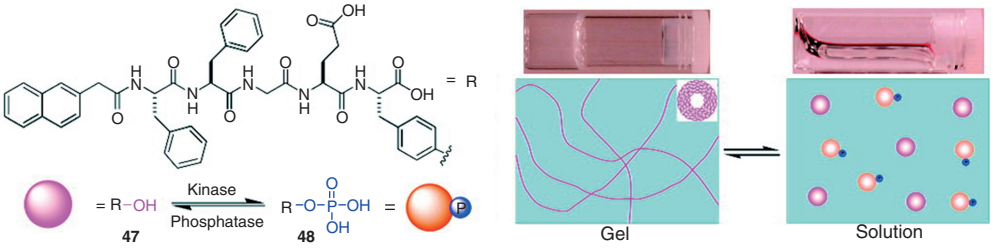

Figure 1.30 The phosphate group of the pentapeptide Nap-FFGEY-P(O)$(OH)_2$ (**47**) is cleaved by a phosphatase enzyme, producing a gelator, **48**. A kinase enzyme (+ATP) catalyzes the reverse reaction, thus converting the gel back to a free-flowing sol. Reprinted with permission from Ref. [104]. Copyright 2006 American Chemical Society.

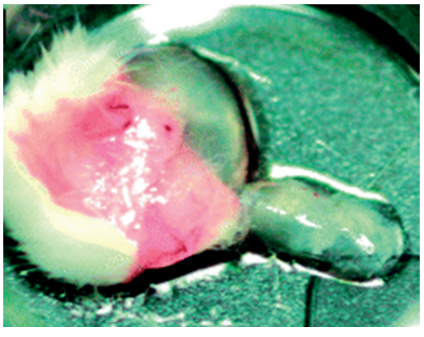

Figure 1.31 Image of a gel formed subcutaneously in a mouse. Reprinted with permission from Ref. [104]. Copyright 2006 American Chemical Society.

led to its dephosphorylation (~80%), thus triggering *in vivo* gel formation within 1 h (Figure 1.31).

Protease enzymes typically hydrolyze peptides, but the reverse reaction can be favored under some conditions (e.g., when the product is thermodynamically stable relative to the reactants). Accordingly, the Uljin group demonstrated that self-assembly can be used as a means of stabilizing the product of a peptide-bond-forming reaction [105]. Fmoc-protected amino acids (**49**) were thus enzymatically coupled with dipeptides (**50**) to yield a self-assembling Fmoc-tripeptide product that afforded stable hydrogels (Figure 1.32). While the peptide-bond-forming reaction would normally be expected to favor hydrolysis in dilute aqueous media ($K_{eq,1} < 1$), favorable self-assembly of the tripeptide product ($K_{eq,2} > K_{eq,1}$) provides a driving force for peptide bond formation. The degree of success of gel formation followed the hydrophobicity of the amino acid side chain of the Fmoc-protected precursor.

For example, while Fmoc-phenylalanine produced a stable gel, Fmoc-glycine did not under the same conditions. The relative amount of product produced (54% for Fmoc-phenylalanine vs < 8% for Fmoc-glycine) is consistent with the decreased driving force for self-assembly of the more soluble derivative. A notable advantage of this approach is the lack of side products (with the exception of water) of the reaction.

Any stimulus-responsive gel can serve potentially as a simple test to detect the presence of a selected perturbation. The outcome of such a test is easily monitored

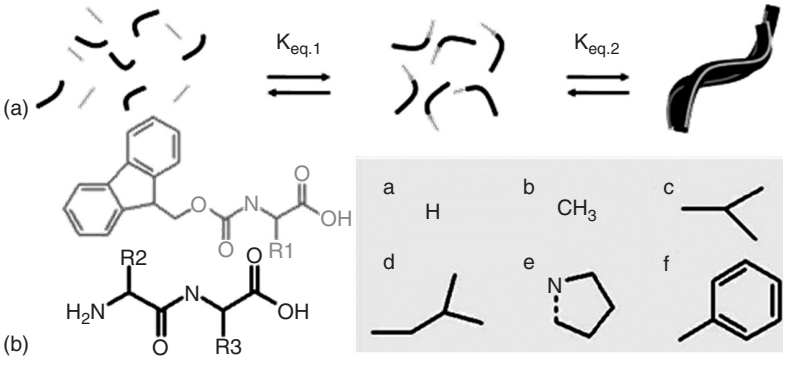

Figure 1.32 (A) Proposed mechanism: Fmoc-amino acids (gray) are enzymatically coupled to dipeptides (black) by a protease to form Fmoc-tripeptides that self-assemble to higher-order aggregates driven by $\pi-\pi$ interactions between fluorenyl groups. $K_{eq,1}$ represents the equilibrium constant for peptide synthesis/hydrolysis, $K_{eq,2}$ for self-assembly. (B) Chemical structures of Fmoc-amino acids (**49**), dipeptide precursors (**50**), and amino acid side chains: (a) Gly, (b) Ala, (c) Val, (d) Leu, (e) Pro, and (f) Phe. Reprinted with permission from Ref. [105]. Copyright 2006 American Chemical Society.

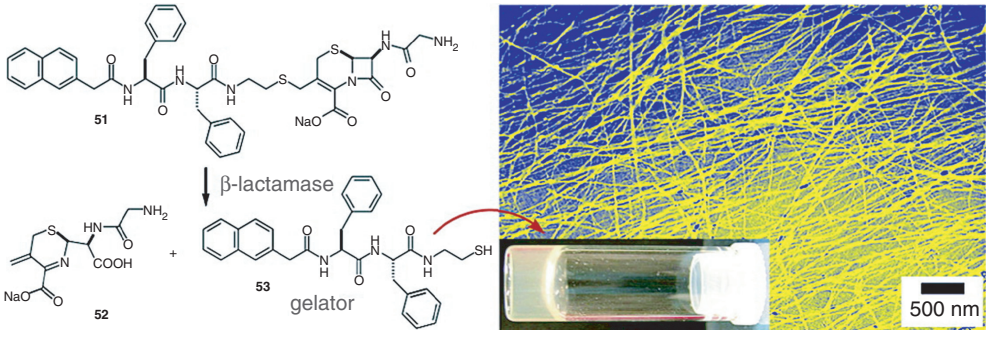

Figure 1.33 β-Lactamase catalyzes the hydrolysis of the β-lactam moiety from an **LMOG** precursor, thus cleaving the solubilizing group and initiating gel formation. Reprinted with permission from Ref. [106]. Copyright 2006 American Chemical Society.

by observing whether a gel has formed. Thus, β-lactamase has been used to catalyze the formation of a hydrogel by catalyzing the hydrolysis of a β-lactam ring (**51** → **52** + **53**, Figure 1.33) [106]. If an enzyme inhibitor is added, the sample fails to form a gel. This offers a simple tool by which enzyme inhibitors may be screened – an approach that is not limited to β-lactamases [107]. Also, when tested against sonicated lysates from several bacterial strains containing different types of β-lactamase, obvious differences were observed in the gelating ability of the resulting samples. As a consequence, this approach provides a selective tool with which to study enzyme activity.

Hydrogels can be utilized for selective and/or controlled release of entrapped drugs in the presence of a specific enzyme. While a number of examples of this

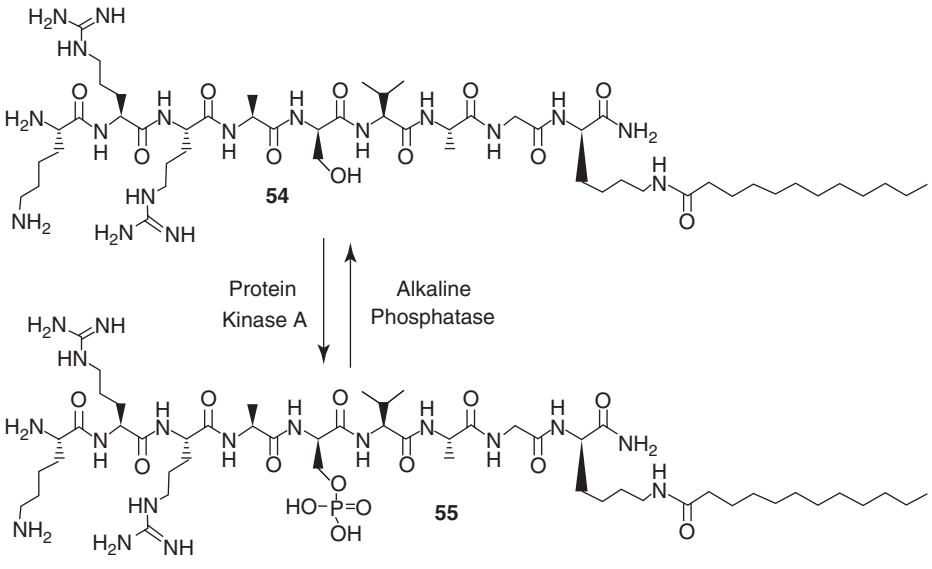

Figure 1.34 Peptide amphiphile (PA **54**) can be converted to its phosphorylated form (PA **55**) with protein kinase A (PKA), and then back to its original form with alkaline phosphatase. Reproduced from Ref. [110] with permission of The Royal Society of Chemistry.

type of approach have been reported [108, 109], here we highlight a recent one aimed at selective targeting of cancer cells. Figure 1.34 shows a peptide amphiphile (PA **54**) containing a serine residue that can be reversibly phosphorylated [installed with alkaline phosphatase; removed with protein kinase A (PKA)] [110]. Akin to similar systems mentioned above, the phosphate-free version is an **LMOG** while the presence of the phosphate group inhibits gel formation. The breast cancer cell line MDA-MB-231 is known to secrete a high concentration of PKA into the extracellular medium. A PA gel was thus loaded with the cancer drug doxorubicin (DOX), and incubated with MDA-MB-231 cells and also with two non-cancerous cell lines (3T3 mouse fibroblasts and human umbilical vein endothelial cells, HUVECs). Examination of the viability of cells demonstrates apparent specificity toward killing the cancer cells, due to phosphorylation of the gelator and subsequent fiber disassembly and drug release (Figure 1.35, center column). Control experiments using only the drug (no gel) resulted in more indiscriminate killing (left), while use of a gel that is stable to PKA (PA **56**, structure not shown) did not release enough drug to kill the cells (right).

Enzyme-initiated self-assembled gels have even been prepared *within* cells by utilizing pre-gelators which are substrates for phosphatases or esterases found in various cell lines. The soluble gelator precursor enters a cell by diffusion, where endogenous enzymes cleave a solubilizing group and, thereby, reveal a gelator. This process is accompanied by cell death, which is presumably induced by intracellular fiber formation as opposed to specific ligand–receptor interactions (Figure 1.36a). One example of this approach utilizes a gelator coupled to a hydrophilic group

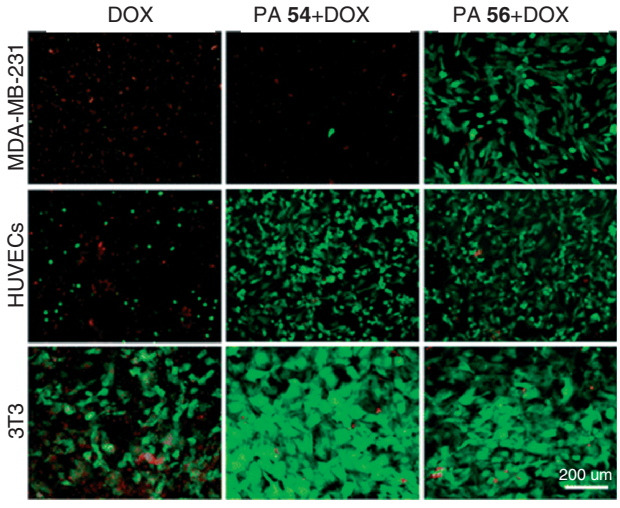

Figure 1.35 Live (Green)/Dead (Red) cell viability imaging of three different cell types (MDA-MB-231, HUVECs, and 3T3) after DOX or either PA **54** or PA **56** mixed with DOX was added to the conditioned media of a confluent cell monolayer. PA **54** is responsive to PKA, while PA **56** is not. Reproduced from Ref. [110] with permission of The Royal Society of Chemistry.

(carboxylic acid) via an enzyme-cleavable ester linkage (Figure 1.36b) [111]. Incubation of **57** with HeLa cancer cells results in an uptake of the compound with subsequent intracellular hydrolysis (**57** → **59** + **60**) and gelation. Dead cancer cells were collected, separated from the culture medium, and broken open. The resulting material was shown to contain the gelator (**59**), which was also capable of forming a hydrogel (with fibrous aggregates as observed in TEM). Cells that survived the treatment were subjected to an analogous preparation, but did not form gels. A derivative in which the ester was replaced with an amide (**58**) was stable to hydrolysis, and thus did not form gels or cause cell death. Incubation of **57** with a non-cancerous mammalian cell line (NIH3T3) did not result in cell death. This result is consistent with a higher level of esterase in the HeLa cells, demonstrating the potential specificity of this type of approach.

A similar study with a phosphatase-sensitive gelator precursor was used to kill bacterial cells that over-expressed phosphatase [112]. Among the controls in this work was a set of experiments that utilized derivatives that differed only in the stereochemistry of the **LMOG**. The stereoisomers (which were also competent gelators) were able to inhibit bacterial growth at comparable concentrations. This demonstrates that the inhibitory effect was not due to a specific ligand-receptor interaction, but rather due to the formation of intracellular aggregates. This finding may lead to new types of therapeutic agents which will be insensitive to drug resistance. In this regard, a simple assay, using the fluorescent stain, Congo red, offers researchers a quick and facile approach to designing new peptide-based gelators aimed at intracellular gelation [113].

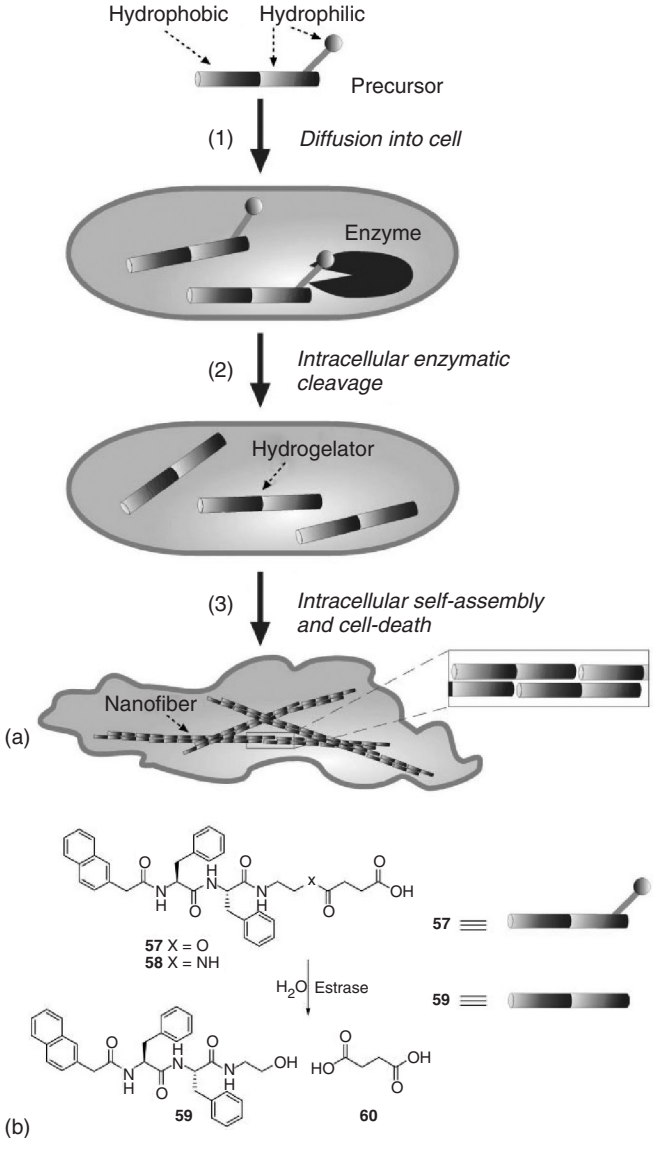

Figure 1.36 (a) Schematic intracellular formation of nanofibers that leads to hydrogelation and cell death. (b) The chemical structures and graphic representations of the precursor (**57**), the control molecule (**58**), and the hydrogelator (**59**). Reprinted with permission from Ref. [111]. Copyright 2004 Wiley.

Intra-cellular gel formation with crystalline **SAFIN** structures is clearly an area of **SAFIN** research with outstanding potential in future biomedical applications. The decade ahead will likely see gelators with increasing complexity that are designed to assemble and disassemble in the presence of specific biomarkers. Facile and divergent synthetic approaches to peptides derivatives make this field even more attractive.

1.3.2
Ultrasound – Conformational and Aggregation/De-Aggregation Effects

Ultrasound has recently emerged as a valuable method to sculpt and control the process of aggregation in molecular gels. It is perhaps not immediately intuitive that ultrasonication (a technique commonly used to break up and disperse molecular aggregates and thus aid in dissolution) would serve as a tool to direct aggregate *formation*. Indeed, many molecular gels (and other materials) are damaged or destroyed by the application of ultrasound [114]. Constructive use of ultrasound was demonstrated in 2005 with two reports of ultrasound-induced gelation (''sonogelation'') [115], the first of which is detailed later in this section.

Here, we present a brief description of ultrasound and its use in gel formation, followed by an account of the discovery of this ''unanticipated'' function of the technique and then several recent examples (from the scores of reports since 2005). Readers interested in exploring the inception of ultrasound in gel formation and supramolecular aggregate manipulation and advances in its use are directed firstly to a highlight by Bardelang describing the paradigm shift of ultrasound from being thought of as solely destructive to being a potentially constructive tool for gelation [116], secondly, to a tutorial review on sound waves and their use in directing gel assemblies, which includes the suggestion that perhaps the 2005 revelation should not have been unexpected based on previous work in other fields [117], and thirdly, to a review of the use of ultrasound in the preparation of a broad range of nanomaterials, including gels [118].

While the relationship between ultrasound and fiber formation is not wholly understood, cavitation (bubble formation, growth, and collapse) and the local changes in temperature and pressure that accompany this process are likely to be important. However, the breadth of experimental observations in sonogelation (see below) suggests that more than one phenomenon which can affect supramolecular aggregation is at work.

Figure 1.37 depicts two general modes of ultrasound-induced fiber formation leading to a sonogel. In the first (a), an **LMOG** that is difficult to dissolve is encouraged to do so by the application of ultrasound. The acoustic energy induces transient dissolution of monomers or small aggregates by breaking intermolecular interactions within the solid, thus allowing recombination, often in a different polymorph. This is represented by arrow (a) by the conversion of an interdigitated lamellar arrangement in a solid to a head-to-tail orientation in the fiber. Changes in molecular conformation may also accompany this process. In many respects, it is akin to more conventional gelation procedures where heating a suspension allows

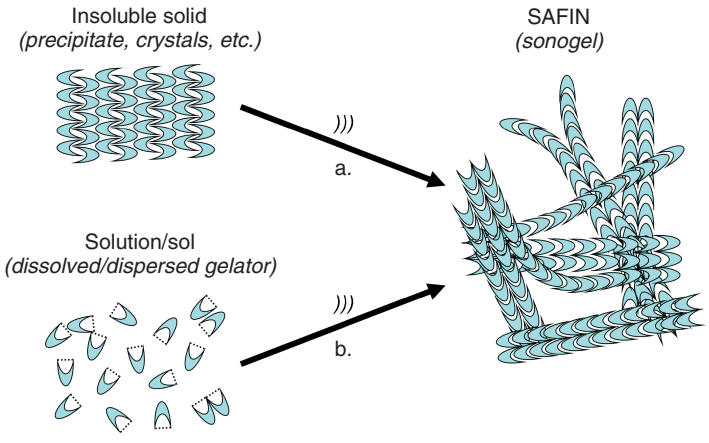

Figure 1.37 Cartoon representation of examples of the process of ultrasound-induced [))))] fiber formation from: (a) insoluble precursors where sonication induces transient dissolution followed by recombination in a different (fiber-forming) polymorph and (b) soluble precursors where sonication provides energy to break intramolecular interactions (represented as dashed lines), thus facilitating intermolecular recombination into fibers.

dissolution, and subsequent cooling induces **SAFIN** formation. However, in many systems ultrasound induces gel formation (often by providing access to otherwise inaccessible polymorphs or nanostructures) where conventional methods fail.

For arrow (b) in Figure 1.37, the initial state of the sample includes soluble monomers/aggregates in which intramolecular or intra-assembly interactions (H-bonding, metal coordination, π-π stacking, etc.) impede long-range self-assembly. Ultrasound breaks interactions within the molecules or discrete aggregates, aiding the attractive supramolecular interactions which lead to fibers. Notably, ultrasound has long been used, principally by industry, to induce crystallization (a process called *sono-crystallization*) [119]. Modification of ultrasound conditions (frequency, intensity, time, and continuous/non-continuous) can be used to fine-tune crystal size and morphology. Many of the dynamic processes associated with this more established (though also not fully understood) technique are likely operating, and are important to sonogelation; interaction between practitioners of these two fields would surely be fruitful.

The earliest report of a molecular sonogel involves bis-palladium complexes solubilized in a variety of organic solvents, as indicated by visual inspection and confirmed by concentration-independent ^{1}H NMR spectra (Figure 1.38) [115a]. Extremely brief (3 s), low-power sonication resulted in ''instant'' formation of opaque or transparent gels, depending on the liquid. Heating restored the system to its fluid state. On the basis of ^{1}H NMR, single-crystal X-ray diffraction, and UV–vis studies, a molecular-level model of gelation was proposed. Soluble **61** exists in a ''clothespin'' conformation with intramolecular aromatic stacking interactions, essentially prohibiting outside access to one side of the complex (in equilibrium

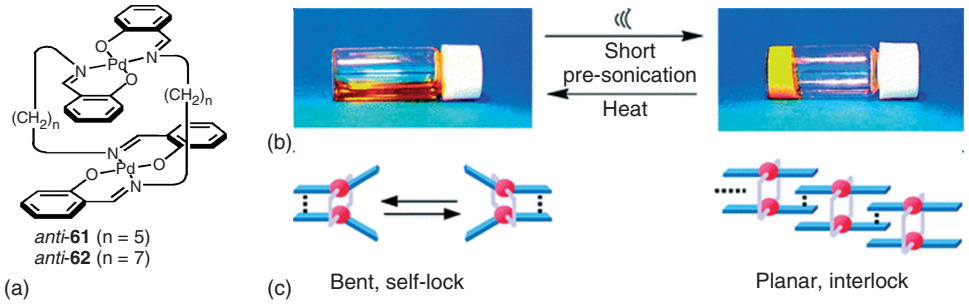

Figure 1.38 (a) Structure of sonogelators **61** and **62**. (b) A stable solution of **61** in acetone instantaneously formed a gel upon brief sonication. (c) Cartoon representations of the conformations of soluble monomers and gelated aggregates. Reprinted with permission from Ref. [115a]. Copyright 2005 American Chemical Society.

between the two equivalent conformations shown in Figure 1.38c). Sonication induces formation of a planar interlocked conformation resulting in an extended supramolecular gel aggregate. Only *anti*-**61** (pictured) forms gels; *syn*-**61** does not. Furthermore, only the racemate of **61** is a gelator; optically pure samples of **61** failed to form gels in analogous preparations. However, optically pure **62** is a more efficient and broadly effective gelator than its racemate. A recent extension of this work demonstrates that phosphorescence is enhanced upon gelation of several derivatives of these homologous bis-palladium complexes, including **61** and **62** [120].

N-(2-Naphthacarbonyl)-1,5-bis-(L-glutamic acid diethyl ester)-L-glutamic diamide (**NBGE**) in Figure 1.39a, is a gelator of both polar (water) and low-polarity liquids (e.g., hexane and toluene) under the influence of ultrasound [121]. Heating and cooling cycles lead to precipitates. However, sonication of a hot solution/sol or of a mixture of the precipitate and liquid at ambient temperature leads to gels (Figure 1.39b). Electron micrographs of the xerogels reveal the fibrous nature of the aggregates (Figure 1.39c). Significant redshifts (compared to $CHCl_3$ solutions) in the IR frequencies of N–H and stretching, C=O (ester) stretching bands of xerogels of **63** from hexane or water were found; they are consistent with the formation of multiple hydrogen bonds in the fibers of the gels. Even more extensive H-bonding was indicated by the FTIR spectra of the precipitate. Based upon these observations, it was suggested that ultrasound aids gel formation by restricting the extent of HB and hindering formation of the precipitate. In addition, UV and CD studies of the gels established the presence of π-π stacking of the naphthyl units and the chirality of its stacks.

Vesicles were formed when water was added to a THF solution of **64** (Figure 1.40) [122]. Subsequent ultrasound treatment (for 10–30 min) led to formation of an opaque fibrous gel. This process was reversible over multiple heating (vesicle formation) and ultrasound (fiber formation) cycles. A more intense X-ray diffraction pattern of the gel sample compared to the vesicles suggests a higher degree of order in the gel fibers. FTIR studies indicate β-sheet-like structures in both types of aggregates. From relative integrations of solid state (CP-MAS) ^{13}C NMR

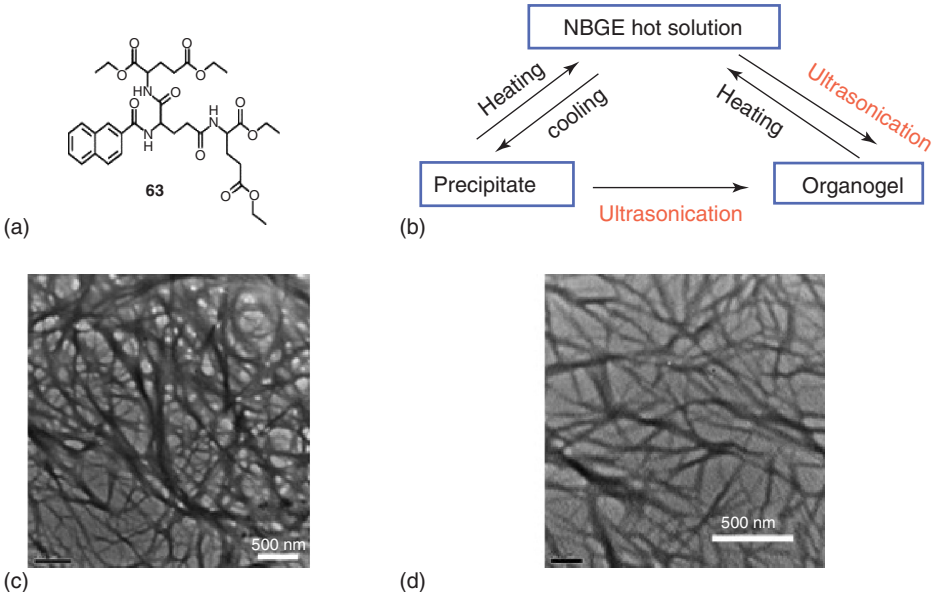

Figure 1.39 (a) Structure of sonogelator (**63**). (b) Stable organogels can be formed by ultrasonic treatment of a hot solution/sol or of the precipitate in a liquid. (c,d) TEM images of the xerogels from hexane (c) and water (d). Reprinted with permission from Ref. [121]. Copyright 2007 Wiley.

spectra of dried samples, it was concluded that a larger percentage of the alanine residues is involved in β-sheets in gel fibers ($\sim$90%) than in the vesicles ($\sim$50%). Because the CD spectra of the two aggregates are very different, there must be significant differences in the orientation of the bipyridine groups and in the packing of the peptide side chains. These data led to the model shown in Figure 1.40b,c. In it, ultrasonication induces conformational changes in the bipyridine linker which lead to changes in the nature of packing of the peptide sections (loose bilayer vs tight bilayer) and the mode of supramolecular aggregation.

An interesting example of ultrasound-induced changes in the aggregate morphology of the zinc coordination polymer of compound **65** is shown in Figure 1.41a. Apparently, ultrasonication here alters the coordination mode of the metal [123]. Non-acoustic processing yields coordination polymer particles (CPPs, Figure 1.41b,c) or single crystals, while sonication enforces gel formation (Figure 1.41d). These gels are very stable thermally – their gel–sol phase transition temperatures exceed the boiling points of the liquid components (MeOH, EtOH, or CH_3CN). The crystal structure (assuming the CPP and single crystals are analogous) shows that the Zn is tetrahedrally coordinated in the CPPs. Also, solid state (CP-MAS) ^{13}C NMR spectral data indicate a difference between the

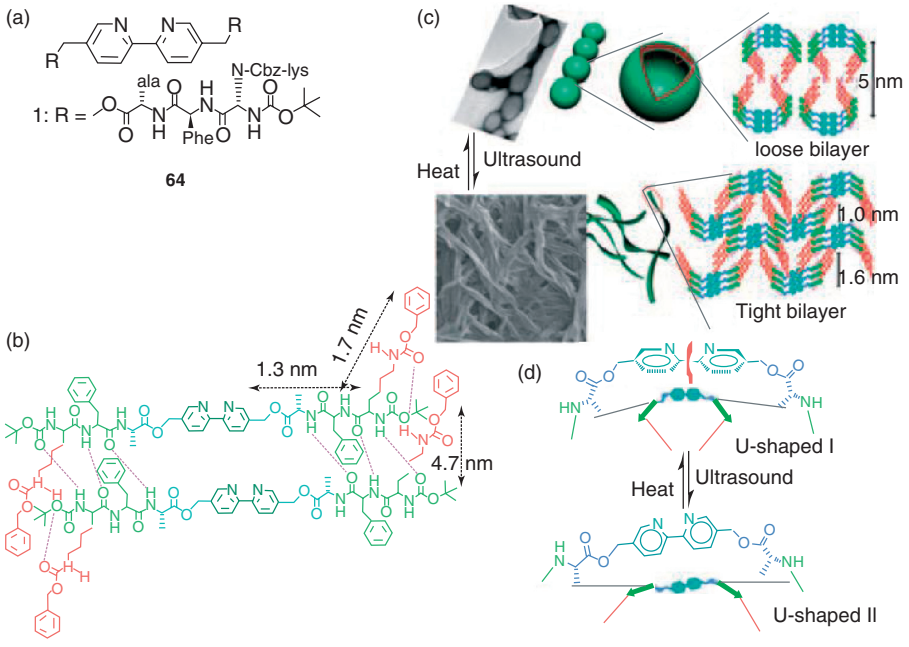

Figure 1.40 (a) Structure of bipyridine tripeptide sonogelator (**64**). (b) Hydrogen bonds and β-sheet-like structures formed from **64**. (c) EM images and proposed models for molecular packing and conformations of **64** in vesicles and in nanofibers. (d) Proposed conformational changes induced by ultrasound and heat. Reprinted with permission from Ref. [122]. Copyright 2011 Wiley.

coordination states of the metal in the CPPs and in the gel fibers. Based upon these data, a gel fiber model (Figure 1.41e) was proposed in which the zinc adopts a see-saw geometry (Figure 1.41f).

A series of bis-alkoxy aryl trihydroxyborate salts (Figure 1.42, **66**) formed gels in benzene when prepared by conventional (heating/cooling) methods [124]. However, this approach was unreliable due to the instability of the **LMOG** upon heating, leading to proto-deboronation. However, ultrasonication for 5 min allowed gel formation without heating.

Organic sonogels of chiral binol derivative (*R*)-**67** (Figure 1.43a) have been shown recently to be visual sensors of chirality [125]. Although addition of an (*S*)-amino alcohol (followed by sonication) induced collapse of the gel, it is stable to addition of the same amount of the (*R*)-aminoalcohol. As expected, gels prepared with the enantiomeric gelator (S)-**67** demonstrated the opposite enantioselectivity. The intensity of FL from the gelator was also enantioselective to additives. In addition, while the metal-free form of the gelator (not shown) has a strong FL signal at 396 nm, this emission is attenuated significantly upon complexation with $Cu^{(II)}$. Figure 1.43b shows that addition of an amino alcohol to the gel results in recovery of the emission intensity as a result of displacement of the $Cu^{(II)}$ ion; the FL enhancement is again enantioselective.

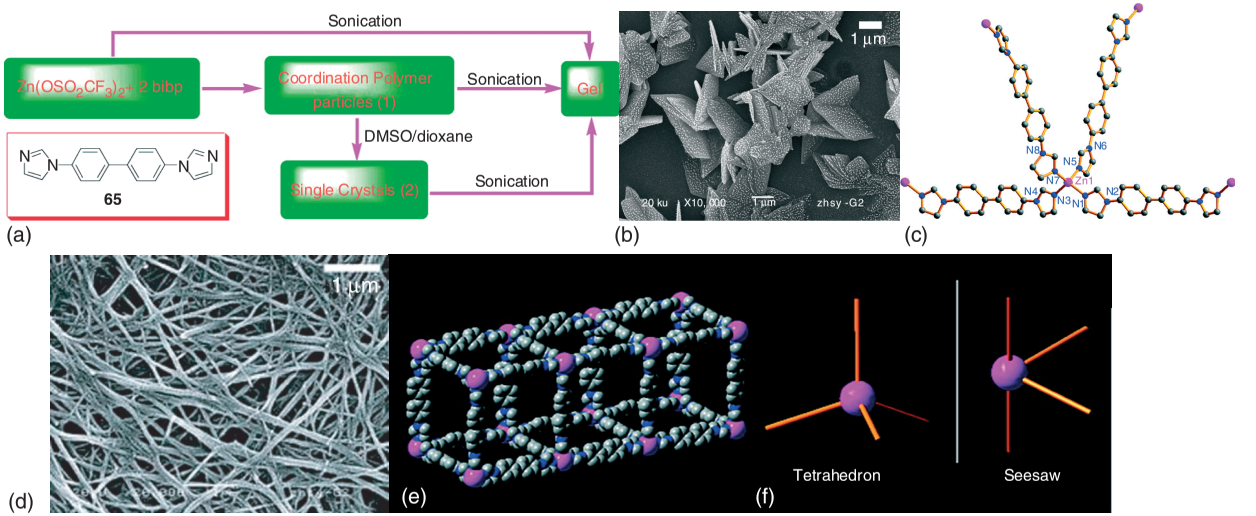

Figure 1.41 (a) Scheme for gel formation of a metal-coordination polymer, and structure of organic component, **65**. (b) SEM of sheet-like coordination polymer microparticles (CPPs). (c) X-ray crystal structure of the Zn complex of **65** showing the tetrahedral coordination mode of zinc. (d) SEM of gel fibers. (e) Proposed model of nanofiber structure. (f) Coordination modes of Zn ions: tetrahedral before sonication and see-saw after sonication. Reprinted with permission from Ref. [123]. Copyright 2009 American Chemical Society.

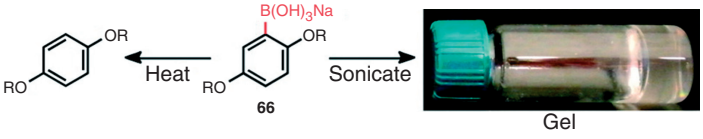

Figure 1.42 Aryl trihydroxyborate salts (**66**) decompose upon heating. Sonication conserves the structure of the gelator and induces gel formation without heating. Reprinted with permission from Ref. [124]. Copyright 2011 American Chemical Society.

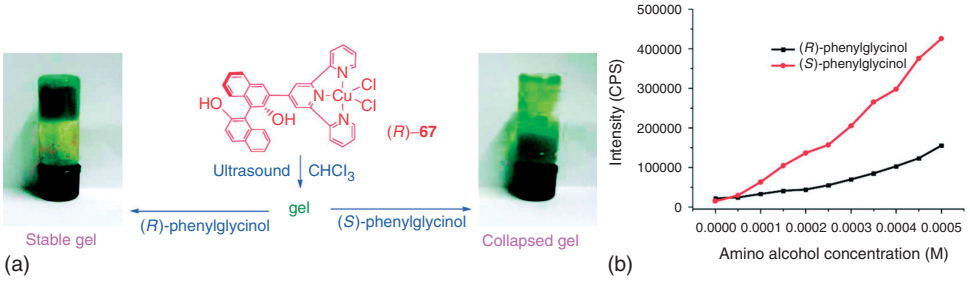

Figure 1.43 (a) Structure of (*R*)-**67**, and enantioselective responses of the gel of (*R*)-**67** toward (*R*)-phenylglycinol and (*S*)-phenylglycinol. (b) Fluorescence responses of (*R*)-**67** (5.0×10^{-7} M) in CH_2Cl_2/*n*-hexane (2/3) toward (*R*)- and (*S*)-phenylglycinol at $\lambda_{em} = 396$ nm. Reprinted with permission from Ref. [125]. Copyright 2010 American Chemical Society.

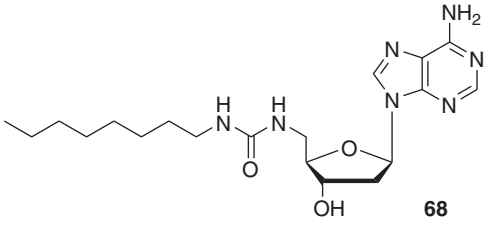

2′-Deoxyadenosine-based gelator **68** formed gels in water when treated with ultrasound, while a simple heating–cooling protocol yielded an opaque sol or unstable aggregate [126]. The sonogel was stable for only 1–2 h after sonication, eventually forming an amorphous precipitate. Subsequent heating followed by ultrasound re-forms the meta-stable gel. The proposed mechanism of action involves modification of the adenine moiety by a hydroxyl radical (HO•, an ultrasound-produced water sonolysis product), which produces a more hydrophilic oxidized product capable of inducing gel formation. Hours after cessation of ultrasound, the original non-oxidized compound **68** is recovered as it precipitates from solution. Evidence for the transient oxidized derivative comes from FT-IR spectra and high resolution mass spectrometry (HRMS) fragments consistent with the presence of a hydroxylated product.

Although not directly germane to the topic of this chapter, it is interesting to note that sonication of a structurally diverse range of proteins has led to the formation

of aggregates which are structurally similar to the amyloid fibrils associated with Alzheimer's, Huntington's, and Parkinson's disease [127]. This observation leads to a fascinating question: Is the process of ultrasound-induced fibrous aggregation in proteins related to that in molecular gels? Results from several other studies suggest that the answer is "Yes!" [128]. Further studies relating these areas would undoubtedly be beneficial.

1.3.3
Radiation-Induced Gelation and Degelation

Ultraviolet and visible radiation can be a powerful tool to induce shape or charge-distribution changes in **LMOG**s and to cause isothermal phase transitions, either from a sol to a gel or a gel to a sol. Only a few of the many examples now in the literature will be highlighted here. A recent example employs the *trans* ⇒ *cis* isomerization of *trans-o*-methoxycinnamic acid (**70**) which binds to the zwitterionic surfactant, erucyl dimethylamidopropyl betaine (**69**), forming short cylindrical micelles in aqueous media [129]. As **70** is isomerized to its *cis* isomer by UV radiation, it is expelled from the micelles of **69**, which grow into long, worm-like micelles and entangle to form a gel-like network (Figure 1.44).

In another example, it was shown that reversible sol ⇔ gel transformations can be induced by irradiation of a cholesteric-azobenzene ether (**71**; R=Me) [54]. Irradiation in the UV region to induce *trans* ⇒ *cis* isomerization of the azobenzene moiety destroyed the fibrillar network of the organogel, leading to a sol phase. Subsequent irradiation of the sol in the visible region allowed reformation of the *trans* isomer and gelation. A similar approach has been demonstrated with gels consisting of aromatic liquids and *N*-glycosylazobenzenes as the **LMOG**s [130]. An

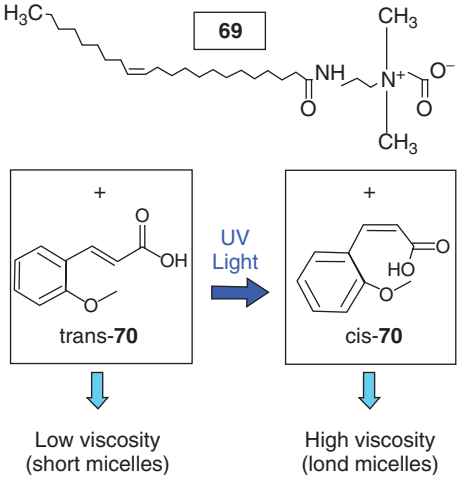

Figure 1.44 Radiation-induced gelation via isomerization of a cinnamic acid derivative. Reproduced from Ref. [129] with permission of The Royal Society of Chemistry.

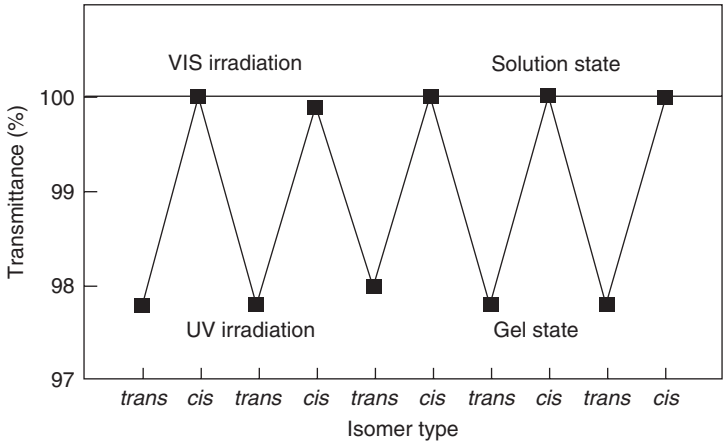

Figure 1.45 Reversible gelation and de-gelation by irradiation of **71**. Reprinted with permission from Ref. [54]. Copyright 1994 American Chemical Society.

example of the reversible gelation of **71** in 1-butanol at 25 °C is shown in Figure 1.45 [54]. Thus, it is possible to effect enormous reversible rheological changes in these samples simply by irradiating them with different wavelengths.

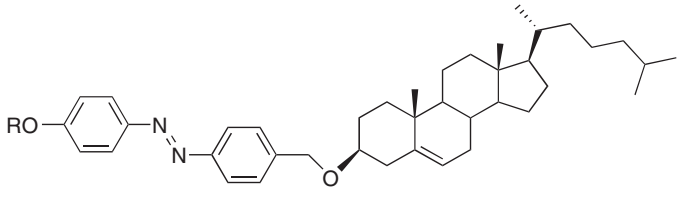

71

Irreversible destruction of the fibrillar networks upon UV irradiation has been reported as well. For example, irradiations of dodecane gels of cholesteryl 4-(2-anthryloxy)butanoate (**CAB**, **72**, see Section 1.2.3) [11], an **LMOG** which contains a photo-active anthryl moiety, were found to lead to loss of the gel phase and formation of 4 photodimers, HH/S, HH/A, HT/S, and HH/A (Figure 1.46), in relative yields similar to those obtained upon irradiation of a toluene solution; the HH/HT dimer ratios were near unity. Protracted irradiation of **72** in its neat solid phase did not lead to detectable dimerization, although irradiation of the liquid crystalline phase [131] did (and in relative photodimer abundances similar to those found from the gel phase). These results highlight the aforementioned fact that many molecular gelators are polymorphous; the molecular packing in the neat solid and even in gels with different liquid components need not be the same.

Ihara and coworkers have used L-glutamic acid-derived lipids (**73–75**) as **LMOG**s. Adding a spiropyran probe (**76**, where R = methyl, butyl, or hexadecyl) and irradiating in the benzene gels created the very polar merocyanine forms (**77**) which closed up back to the **76** form in the dark (Figure 1.47) [132]. It was found

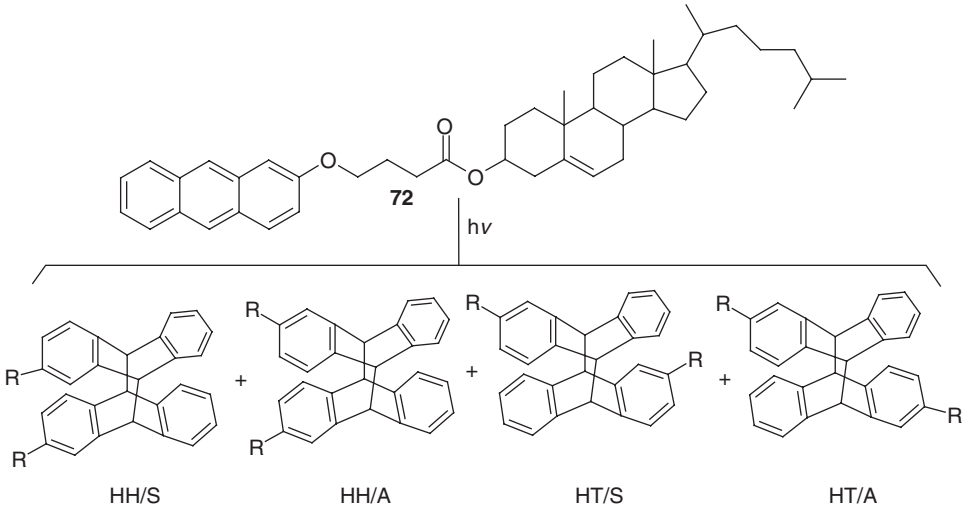

Figure 1.46 Photodimers derived from **72**.

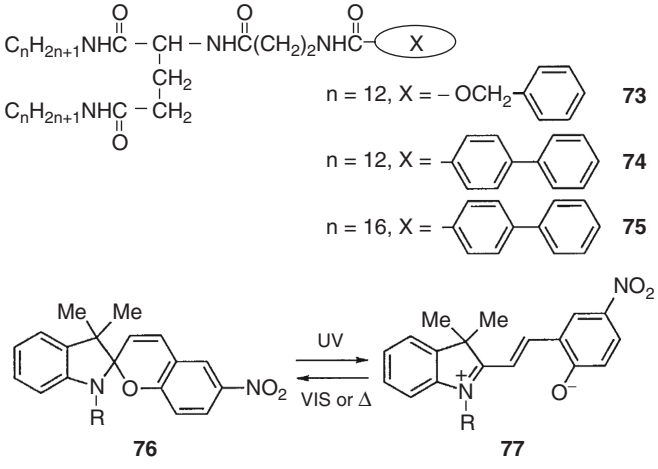

Figure 1.47 Gelation and de-gelation by isomerization of a spriropyran using irradiation and heat.

that the rate of the thermal reversion is accelerated somewhat by aggregation: the rate of isomerization changes when the critical aggregation concentration is reached.

Two *N*-acylamino acids with an attached 2*H*-chromene group, **78** (X = no atom or CH_2O), present another example of exploitation of reversible photochromic behavior to modulate gelation [133]. This system is very interesting because it is sensitive to several stimuli, including UV radiation, temperature, and pH. Thus, the sodium salt of **78** (Na-**78**) is able to gelate DMSO or dimethylformamide (DMF).

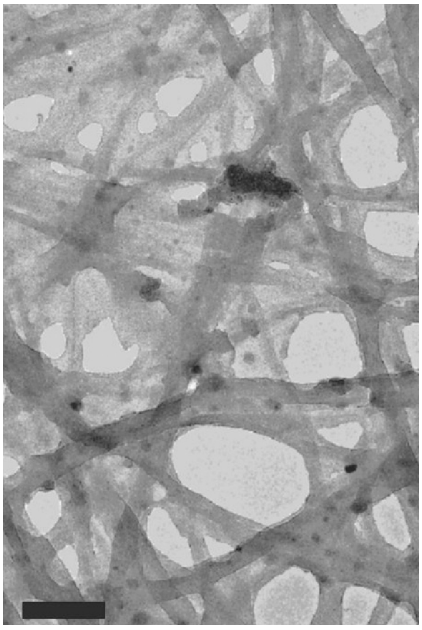

Figure 1.48 Electron micrograph of Na-**78** (x = no atom) in DMF. The scale bar is 400 nm. Reprinted with permission from Ref. [133]. Copyright 2002 American Chemical Society.

An electron micrograph of the fibrous network is shown in Figure 1.48. The narrowest cross-sections for the fibers that could be detected were 50–70 nm across. Irradiation at 366 nm opened the Na-**78** ring, as confirmed by UV–vis and IR spectroscopies, and weakened the gels significantly. Warming the unirradiated or disturbed gel phase led to a sol which could be reconverted to the gel by cooling; in the dark, closure of the opened rings of the Na-**78** occurs. Alternatively, the gel and sol phases could be interconverted by adding acid (to make the sol) or base (to make the gel). These changes are summarized in Scheme 1.1.

1.4
Kinetic Models for Following One-Dimensional Growth and Gelation

To understand how and why **LMOG**s are able to aggregate into 1D objects, it is necessary to follow simultaneously the evolution of the aggregate structures and the dynamics of their formation, and then to use theory to analyze the factors responsible for the aggregate shapes. As mentioned in Section 1.1, the number of detailed studies treating both structure and kinetics of fiber formation in **SAFIN**s is relatively small [10, 15–17, 19]. Yet, understanding the dynamics of fiber formation is critical to understanding the final network structures, and interesting and useful theories for linking crystal shapes to parameters associated with thermodynamic and kinetic driving forces are beginning to emerge [36a, 134–141].

As mentioned, **LMOG**s aggregate through intermolecular interactions which include H-bonding, π-π stacking, dipolar interactions, and London dispersion

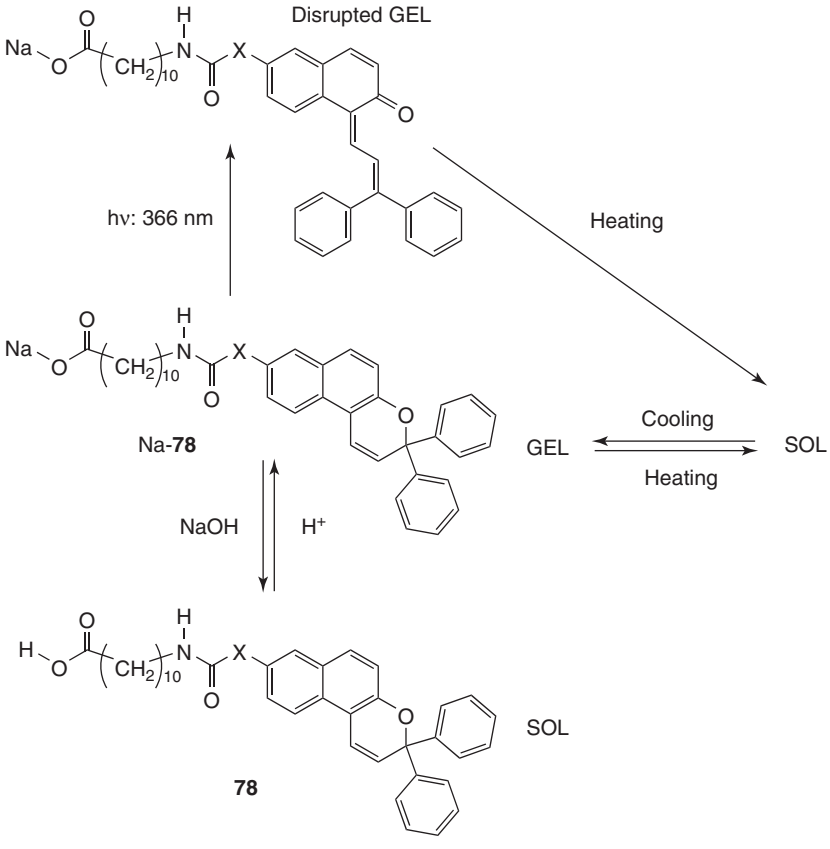

Scheme 1.1 Phase changes initiated in **78** in DMF by irradiation at 366 nm and variations of temperature or pH. Reprinted with permission from Ref. [133]. Copyright 2002 American Chemical Society.

forces [1, 26]. In fact, the methodologies and approaches employed to investigate other types of self-assembly [12] that lead to lamellae, plates, multilayered objects [13], and even bulk crystals [14] are pertinent to the gelation phenomena of **LMOG**s. Among those methodologies are time-dependent SAXS and SANS measurements. Such experiments have become much more feasible as the beam intensities have increased. Even without pulsed sources, neutron and synchrotron radiation can provide intriguing dynamic information about the early events associated with aggregation, nucleation, and growth of 1D objects [142]. However, the data are most difficult to obtain with these techniques in the earliest time regimes (i.e., the periods of greatest interest) because the number of aggregated objects and their ability to scatter/diffract is lowest then. Finally, learning how and why small organic molecules are able to aggregate and grow into objects with very high aspect ratios would be highly useful in designing new materials and the *de novo* design of molecules capable of *arresting* fibrillar growth.

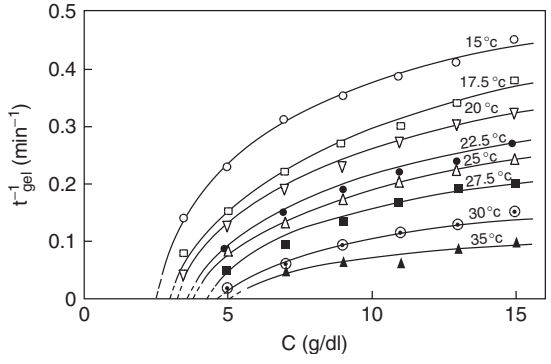

Figure 1.49 t_{gel}^{-1} versus **Boc-AAMe** concentration at different temperatures. Reproduced from Ref. [146] with permission of The Royal Society of Chemistry.

As noted above, relatively few studies have been reported in which the kinetics of **LMOG** aggregation has been combined with structural characteristics of the 1D objects. Perhaps the first in-depth application of a kinetic model to define the dimensionality of growth modes of a gelator from a super-saturated solution was by Terech *et al.* [143, 144] using a form of the Avrami–Mempel law [145]. Of the three equations for growth of 1D, 2D, and 3D objects, the one for 1D growth (Equation 1.3) best fits the evolution of the **SAFIN** of their system, the paramagnetic steroid **2** in cyclohexane, based on infrared, electron spin resonance (ESR), and SANS data sets. Although 1D growth was consistent with the observation of rod-like objects in the gel, the data give a better fit to growth of 2D and/or 3D at early times, where the majority of nucleating events was occurring. In Equation 1.3, $X(t)$ and $X(\infty)$ are the volume fractions of **2** incorporated in the solid phase at time $= t$ and ∞, respectively, and λ and μ are constants of the system which are related to the kinetics of their formation.

$$X(t) = X(\infty)\{1 - \exp[-\lambda(\exp(-\mu t) + \mu t - 1)]\} \tag{1.3}$$

A simple method, tilting samples of a tripeptide, *tert*-butyloxycarbonyl-β-alanyl-α-aminoisobutyryl-β-alanyl methyl ester (**Boc-AAMe**), in dichlorobenzene, has been used to measure the rate of gelation (taken as the inverse of the time needed for the sample not to flow, t_{gel}^{-1}) [146]. Using an expression in which t_{gel}^{-1} is assumed to be directly proportional to the product of two independent terms that are a function of concentration $f(C)$ and of temperature $f(T)$, it was possible to conclude by varying C at constant T that gelation occurs by a 3D percolation mechanism (Figure 1.49) and by varying T at constant C that formation of rod-like crystalline objects and liquid spinodal decomposition proceed in parallel during gelation. The kinetic results are supplemented by data from optical microscopy, FT-IR spectra, wide-angle X-ray scattering (WAXS), and electron diffraction experiments, which provide insights into the nature of the rod-like objects and confirm their crystalline nature (as a three-dimensional lattice).

Another kinetic study has been conducted on the aromatic-linker-steroid gelators, **79** (**CNC**; see Section 1.2.3) and **80** [15, 43a,b], which are known to make spherulites or rod-like fibers (depending on the liquid and the protocol for cooling the sol phase) in the **SAFIN**s of their organogels. The kinetics of formation of these gels has been interpreted according to the Avrami equation (Equation 1.4) [74] and the Dickinson fractal model (Equation 1.5) [147]. In these equations, as modified for gels, X is the volume fraction of the gelator participating in the **SAFIN**, K is a type of rate constant, n is the "Avrami exponent" which is indicative of the type of growth leading to phase separation [148], D_f is the fractal dimension of the **SAFIN**, C is a constant, and t is time. The original articles should be consulted for the conditions under which these equations can and cannot be applied to **LMOG** gel systems. Several interesting modifications of the Avrami equation and re-interpretations of its exponents may make this equation expand its utility to the study of gel formation [149].

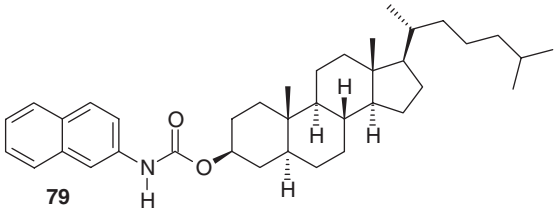

79

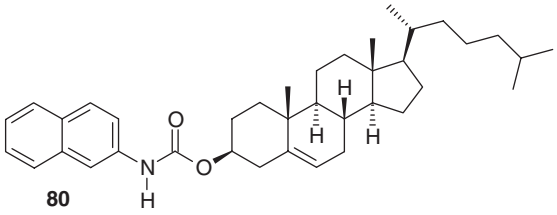

80

Data on gelation of **79** in n-alkanes from four different techniques – CD, FL, rheology, and SANS – are consistent with a process involving 1D growth and "instantaneous nucleation" (i.e., an Avrami exponent, n, close to 1 was always found) [15, 149]. At all temperatures investigated, the D_f values calculated from Equation 1.5 for these gels were between 1 and 2, consistent with the conclusions based on Equation 1.4 of one-dimensional aggregation and growth during gelation. That conclusion is also borne out by the optical micrographs in Figure 1.23 (Section 1.2.3), which show 1D objects being formed at all temperatures of incubation examined.

$$\ln[\ln(1-X)^{-1}] = \ln K + n\ln t \tag{1.4}$$

$$\ln X = C + [(3 - D_f)/D_f]\ \ln t \tag{1.5}$$

However, there are clear changes in the sizes of the spherulites and, very near the gelation temperature, a change to rods rather than spherulites, whose origin can be traced to differing modes of **SAFIN** formation. The inverse of K, from data using three of the experimental techniques versus different incubation

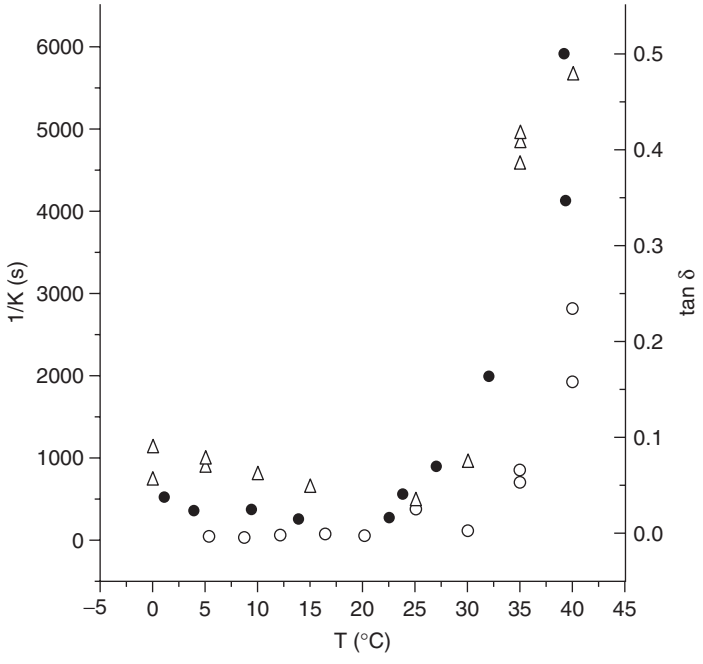

Figure 1.50 $1/K$ values from fluorescence (●) and CD (○) data and tan δ (△, from rheology measurements) versus temperature using 1.0 wt% **79** in *n*-octane or *n*-dodecane. Reprinted with permission from Ref. [15]. Copyright 2005 American Chemical Society.

temperatures of the supersaturated sols (i.e., below the macroscopically measured gelation temperatures) is plotted in Figure 1.50. The values of $1/K$ from the different techniques are consistent, showing one temperature regime in which $1/K$ has a very small temperature dependence and another, approaching the gelation temperature, with a very large temperature dependence. The transition between the two regimes is close to the temperature at which the **SAFIN** morphology changes from spherulites to rods. It suggests that the mode of **SAFIN** formation changes from being dominated by thermodynamic considerations (such as the degree of supersaturation) to kinetic considerations (such as rates of diffusion of **79** molecules to and from growing 1D objects). More detailed descriptions of thermodynamic versus kinetic control of aggregation, nucleation, and growth of 1D objects are described below.

The kinetic data for gelation of **80** in ethyl acetate using Equations 1.4 and 1.5 lead to an even more complicated picture. As seen in Figure 1.51a, the D_f values remain nearly constant ($\sim$1.1–1.3) throughout the temperature range explored. However, the Avrami exponent n undergoes a precipitous jump from ~ 1 to ~ 2 near 2.5 °C! Because there is no discernible differences between the optical micrographs of **SAFIN**s of **80** in the temperature regimes just below and above the point of changing n, a change in the nucleation mechanism (rather than in the growth and structure of the fibers) must be responsible. At incubation temperatures in

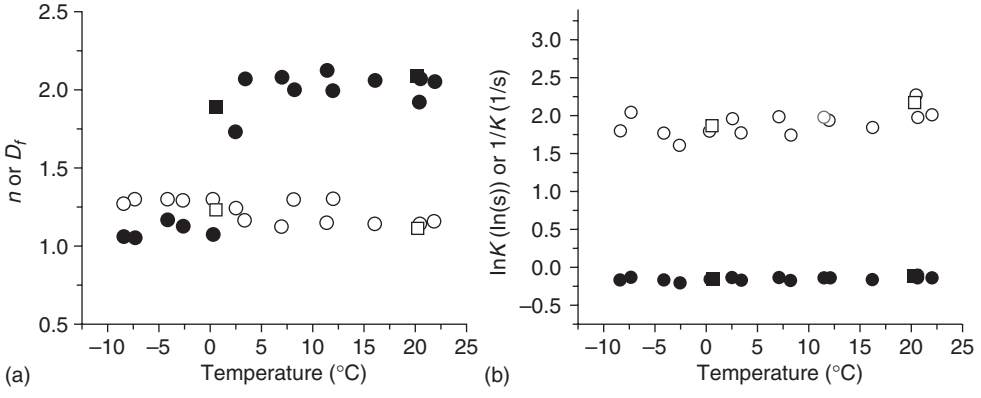

Figure 1.51 Data from 2.0 wt% **80** in ethyl acetate: (a) Avrami component n (●,■) and D_f (○,□) versus temperature from fluorescence (●,○) and CD (■,□) data; (b) $1/K$ (●,■) and ln K (○,□) versus temperature from fluorescence (●,○) and CD (■,□) measurements. Reprinted with permission from Ref. [16]. Copyright 2006 American Chemical Society.

the low temperature regime, *heterogeneous nucleation, interfacial control, and one-dimensional* growth occur; in the high temperature regime, *homogeneous nucleation, interfacial control, and one-dimensional* growth are responsible for **SAFIN** formation [149]. The reason for these changes must involve (as in the case of the spherulite-rod changes found for the **79** in *n*-alkanes) the degree of supersaturation at each incubation temperature. However, it appears that the same fiber growth mechanism is operative in both temperature regimes because the values of K are virtually independent of temperature (Figure 1.51b).

We emphasize that the use of the Avrami and fractal models may not be applicable to gelation by **LMOG**s if the mode of nucleation and growth is different from the ones described by those theories [150].

Rogers and Marangoni have used a non-isothermal variant of the Avrami equation (Equation 1.6) to characterize the kinetics of growth of 1D objects of (*R*)-12-hydroxystearic acid in canola oil, triacylglycerol, methyl oleate, and glycerol as a function of the rate of cooling of the sol phases to below the super-saturation temperatures [39]. Their observable was fiber lengths, Y, from optical microscopic measurements [151]. In Equation 1.6, Y_{max} is the maximum length of the fiber, k_{app} is the rate of growth of the fiber, n is the dimensionality factor (analogous to the one in the Avrami equation), and t and t_g are the time after and the induction time for the observation of a fiber, respectively. The calculated activation energies, 12.1, 39, 2.2, and 15.8 kJ/mol, respectively, as well as $k_{app\,and}$ t_0, were not directly relatable to the polarity of the liquids, and it is difficult to see a correlation with viscosity at one temperature. Abrupt changes in the nature of the nucleating and growth events with cooling rates were observed also and were attributed to regimes controlled by thermodynamics or diffusion (i.e., mass transport).

$$Y = Y_{max}\left\{1 - \exp\left[k_{app}\left(t - t_g\right)\right]^n\right\} \tag{1.6}$$

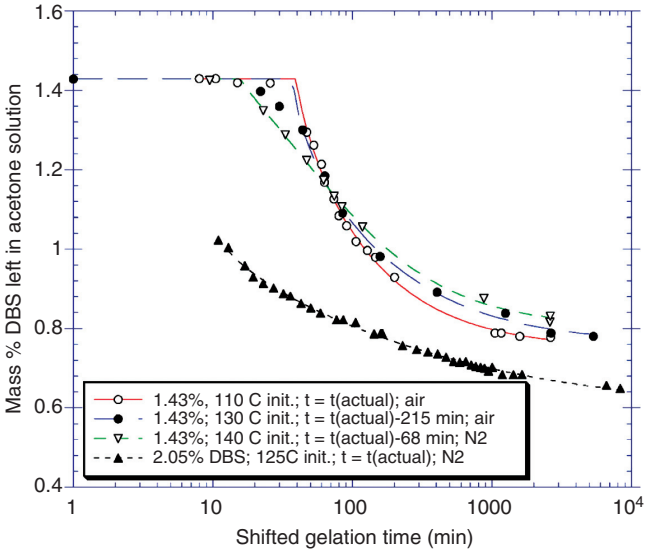

Figure 1.52 Mass % changes of 1 dissolved in acetone as a function of time after solutions/sols are left at 22 °C. The solid lines are best fits to Equation 1.7. Reprinted with permission from Ref. [39b]. Copyright 2009 American Chemical Society.

A detailed study of the gelation and post-gelation changes that occur in the **SAFIN**s of **1** gels in acetone at 22 °C has been conducted using NMR spectroscopic techniques [37]. At 1.43 wt% of 1,3:2,4-di-O-benzylidene sorbitol (**1**), it was possible to observe induction times t^* (that were not reproducible from run-to-run), as well as the time dependence of both initial gelation (as nucleation and growth proceeded) and then the post-gelation changes that they believe do not involve Ostwald ripening [20–22] (although some of their suggested reasons seem related to this phenomenon). The authors have chosen a power-law expression (Equation 1.7) as an initial attempt to fit the data to a mathematical model with physical meaning. Results from those fits to different data sets are shown in Figure 1.52. In the equation, $c(t)$, c_o and c_∞ are the concentrations of **1** in the solution/sol phase, at time $= t$ after the sample has been cooled to 22 °C and at time $= \infty$, respectively; t_{gel} is a "characteristic time" for gelation and ϕ is related to the long-term changes in the amount of **1** in the gel. The data are fitted better at longer times than at shorter ones; the authors note that the same kinetic and thermodynamic processes dominating events at earlier and longer times may be different. Nevertheless, it is remarkable that the single equation is able to fit the data over a very long time period and indicates that it may be valuable in future studies in which different techniques are employed to follow gelation.

$$c(t) - c_\infty = (c_o - c_\infty)/\{1 + [(t - t_{gel})/t*]^\phi\} \tag{1.7}$$

In one of the most detailed studies to date, Aggeli *et al.* examined the stages of aggregation leading to the gelation of water by two oligopeptides, each with 11

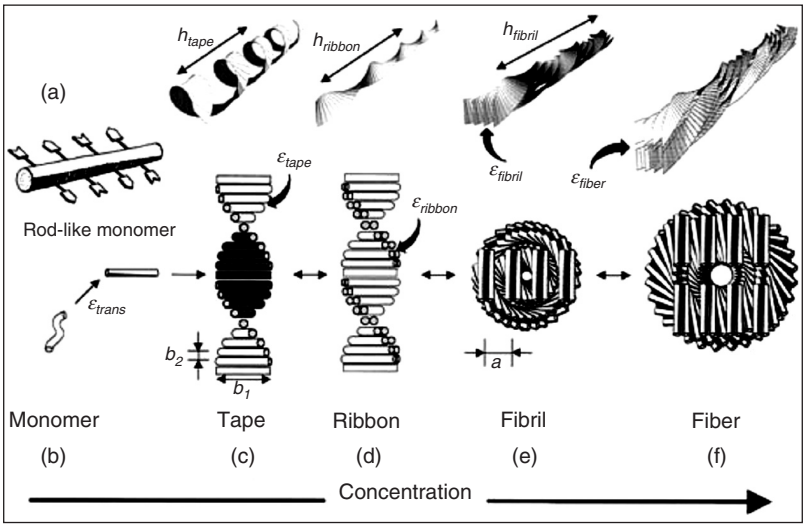

Figure 1.53 Cartoon representation of the progressive steps in the aggregation of the oligopeptides as a consequence of increasing concentration. The arrows protruding from the monomer (a,b) indicate sites of different interaction types with other monomer oligopeptides. Those interactions result in the formation of tapes (c) whose additional twisting as a result of differential surface and edge energies gives ribbons (d), aggregation of the ribbons to form fibrils (e), and bundling of the fibrils to form fibers (f). Reprinted with permission from Ref. [38]. Copyright 2001 National Academy of Sciences.

amino acid units [38]. By increasing concentration, it was possible to observe the chiral rod-like oligopeptides transform progressively from monomeric units into helical tapes, twisted ribbons consisting of double tapes, fibrils consisting of twisted stacks of ribbons, and fibers which are entwined fibrils (Figure 1.53). Although the kinetics of these changes were not investigated, the ability to view the aggregates at various stages of evolution is a notable achievement, and the theoretical framework developed to explain the changing structures has proved valuable to others working with chiral gelators.

The behavior of lithocholic acid (**LCA**) in basic aqueous media is another very important example of the morphological changes in the shapes of 1D objects that can occur over time [152, 153]. When the base was NaOH or ammonium hydroxide, cryo-TEM and SAXS measurements demonstrated that the nanotubules formed had monodisperse outside and inside diameters of 52 and 49 nm, respectively. In addition to single-walled tubules, some multi-walled ones which are from sheets which have rolled onto themselves, could be observed. Some of the cryo-TEM images captured partially rolled sheets. The evolution of these objects was followed with time (and concentration) as shown in Figure 1.54 for tubules with NaOH as the base. Only with ammonium hydroxide as base, the tubules aligned over time into hexagonally packed bundles within domains, and eventually they adopted a single orientation (a monodomain).

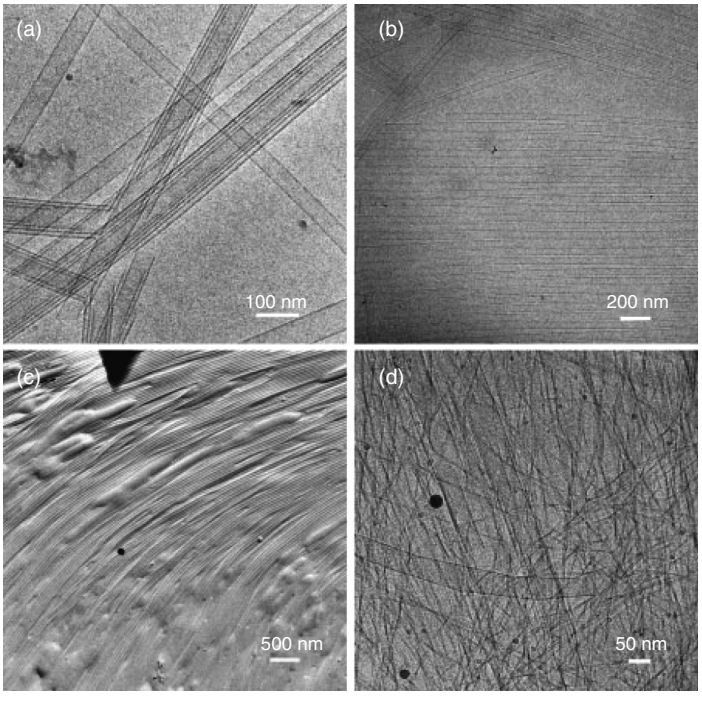

Figure 1.54 Cryo-TEM images of **LCA** nanotubules in aqueous NaOH. (A) 0.25 wt% and 78 s after mixing; (B) 0.1 wt% and 90 000 s after mixing; (C) 5 wt% and about one week after mixing; (D) 0.1 wt% quenched from 62 °C and kept at room temperature for about one week and then heated at 62 °C for 4 h before sample preparation. Reprinted with permission from Ref. [152]. Copyright 2005 Wiley.

Several different approaches to modeling the aggregation, nucleation, and growth of 1D objects have been taken by the group of Liu. For example, they have followed somewhat quantitatively the kinetics of formation of 2D crystalline aggregates of ~1 μm polystyrene spheres in water on a glass surface by modulating particle flow with alternating electric fields [154]. In this way, it was possible to identify the evolution of crystalline structures within amorphous aggregates and to determine the minimum number of spheres needed to form a nucleated species.

In another study, they examined the fractal nature of gels made by incubating super-saturated sol phases of *N*-lauroyl-L-glutamic acid di-*n*-butylamide (**LGAB**; Ajinomoto) in isostearyl alcohol and other viscous liquids at and near room temperature. Their principal experimental measure of the aggregation and **SAFIN** formation, by rheology, was supplemented with scanning electromicrographs [155]. Analyses start with an expression similar in form to Equation 1.6 (i.e., taking into account the incubation time, but replacing Y with X, the fraction of **LGAB** in the crystalline form).

Then, the viscoelasticity of the samples (G^*) is related to X at times after t_0 (Equation 1.8). When the data are plotted according to the modified Avrami

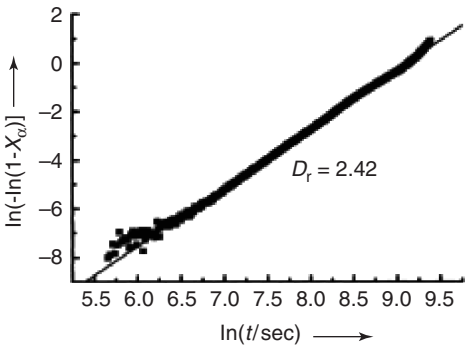

Figure 1.55 Avrami-type plot for the incubation of 6.7 wt% **LGAB** at 40 °C. Reprinted with permission from Ref. [155]. Copyright 2002 Wiley.

equation, the fractal dimension, D_f, can be calculated from the slope (Figure 1.55) and Equation 1.9 (where k^0 is a constant). In the example shown, for 6.7 wt% **LGAB** and 40 °C, $D_f = 2.42$; at 20 and 30 °C, it was found to be 2.10 and 2.40, respectively. These results suggest that the **SAFIN**s from incubation at the lower temperatures are more open structures. Such a change is predicted if the nucleation and growth of the **SAFIN** involves branching caused by epitaxial crystallographic mismatches [156], which are more prevalent as the degree of supersaturation (and the thermodynamic driving force for phase separation) increases [157].

$$X(t) = (G^*_t - G^*_0)/(G^*_{max} - G^*_0) \tag{1.8}$$

$$\ln[1 - X(t)] = -k^0(t - t_g)\exp(D_f) \tag{1.9}$$

This brief and incomplete description of the current state of models to describe kinetics of growth of 1D objects should be sufficient to convince those interested in molecular gels that future progress in the field will depend on our ability to answer two simple questions: ''How and why do some molecules undergo phase separation from liquids to form **SAFIN**s?'' The answers will depend on our ability to look earlier and faster at smaller and smaller aggregates that develop into 1D objects and to understand the mechanisms for their formation. The first part of this recipe for answering the questions will require better experimental methods; the second will depend on more precise theories and models to describe the results from those experiments. Both will be daunting challenges.

1.5
Advances and Perspectives for *a Priori* Design of Gelators

The discovery of new structural classes of **LMOG**s has been serendipitous in many cases. Although there is a growing consensus concerning the structural requirements for a molecule to be a successful **LMOG**, no *a priori* rules have been formulated, and the establishment of such ''rules'' is further complicated by the necessity to include the influence of the liquid component. In fact, we should be thankful that there is no ''universal'' gelator of all liquids and no liquid that can

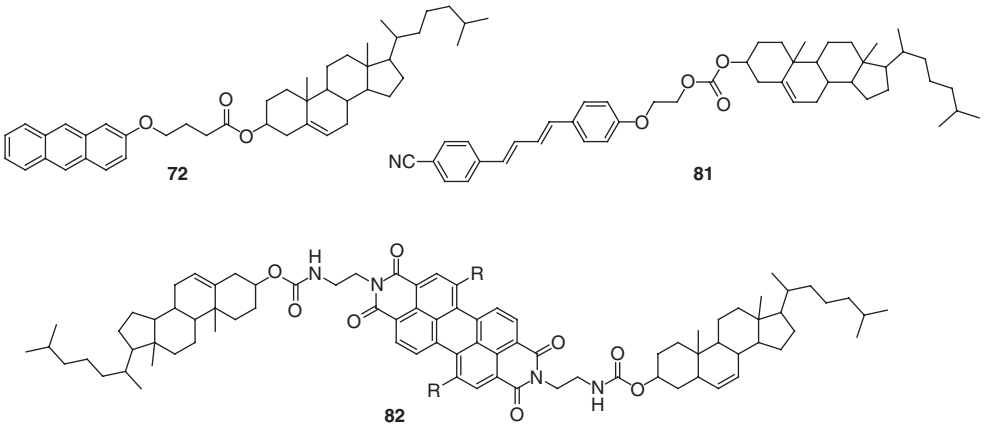

Figure 1.56 Molecular structures of cholesteryl 4-(2-anthryloxy)butanoate (**72**) [11] and two other ALS structures (**81** [63] and **82** [159a]).

gelate all molecules!![1)] However, significant advancements have been made in the development of new types of **LMOG**s and in understanding the gelation process. These advances have been aided by several compendia of gelators according to their structural properties and correlations with liquid properties [9, 26, 77a, 158]. Utilization of the structural databases aids, but does not guarantee, the potential success of a newly designed **LMOG**. Thus, one possible approach to generate new gelators is to combine known structural motifs. Among the structural units which seem empirically to be useful are steroidal, aromatic, and saccharide groups. For example, the serendipitous discovery of cholesteryl 4-(2-anthryloxy)butanoate (**72**) [11] has led to a large number of new "ALS" **LMOG**s (see Section 1.2.2). Three examples are shown in Figure 1.56 [63, 159].

Molecules with aromatic cores and (especially) two attached alkyl groups (i.e., AL_2 molecules) have been examined in detail as **LMOG**s as well. Some examples are shown in Figure 1.57.

2,3-*Bis*-*n*-decyloxyanthracene (**13**), in which two decyloxy side groups are appended to one end of an anthryl core, is an excellent **LMOG** for a limited number of liquids [160]. Several detailed studies have provided very useful insights into how the individual molecules are arranged in its fibers [67, 68, 161]. This asymmetric molecular shape was extended to tetracene-based gelators with hexadecyloxy side groups (**83**) [162] as well as to heteroaromatic phenazine-based gelators (**84**) [163]. Furthermore, it has been demonstrated that the non-alkylated end of phenazine and bisphenazine can be modified by substituents such as halogen atoms or an arylene-ethynylene (R_1-R_4) without compromising gelation ability (**85** [65c, 164]

1) If the latter were possible, we might be confronted with a world like that produced by *Ice Nine*! See Kurt Vonnegut's novel, *Cat's Cradle* for "experimental details."

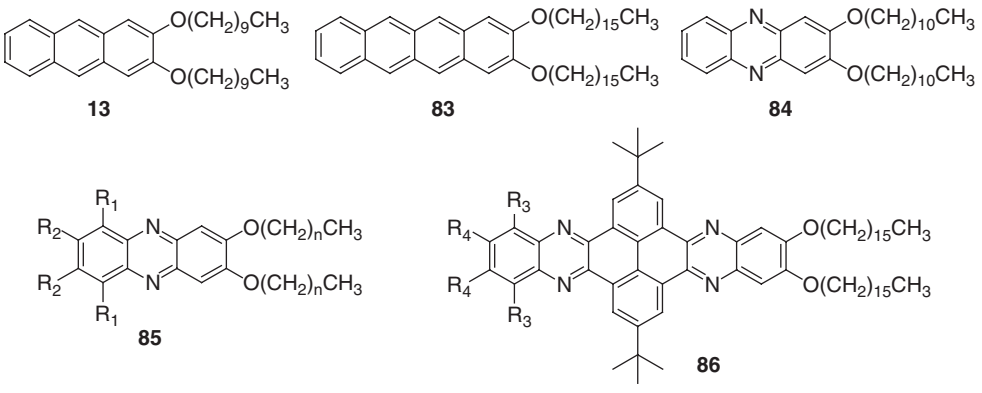

Figure 1.57 Examples of molecular structures of the AL_2 type [160, 162–165].

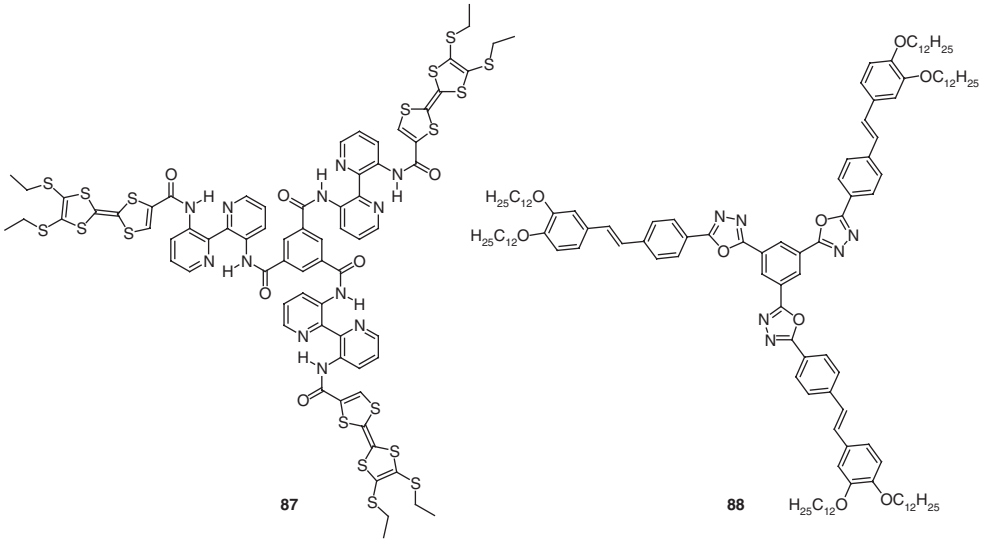

Figure 1.58 Disk-like organogelators **87** [166] and **88** [167].

and **86** [165]). As expected, the gelation ability is affected significantly by the type and length of the alkyl groups.

In addition, disk-like molecular structures have produced **LMOG**s. For example, the C3 symmetric *tris*(tetrathiafulvalene) derivative **87** was shown to gelate *o*-dichlorobenzene [166], and fibers of the oxadiazole containing disk-like molecule **88** were formed through hexagonal columnar stacking with strong core–core interactions [167] (Figure 1.58).

Structurally simple **LMOG**s offer potential advantages for investigating the links between molecular structure and **SAFIN** properties by limiting the number of parameters which must be considered. A step-by-step structural evolution from simple **LMOG**s in a controlled fashion could allow efficient empirical design of

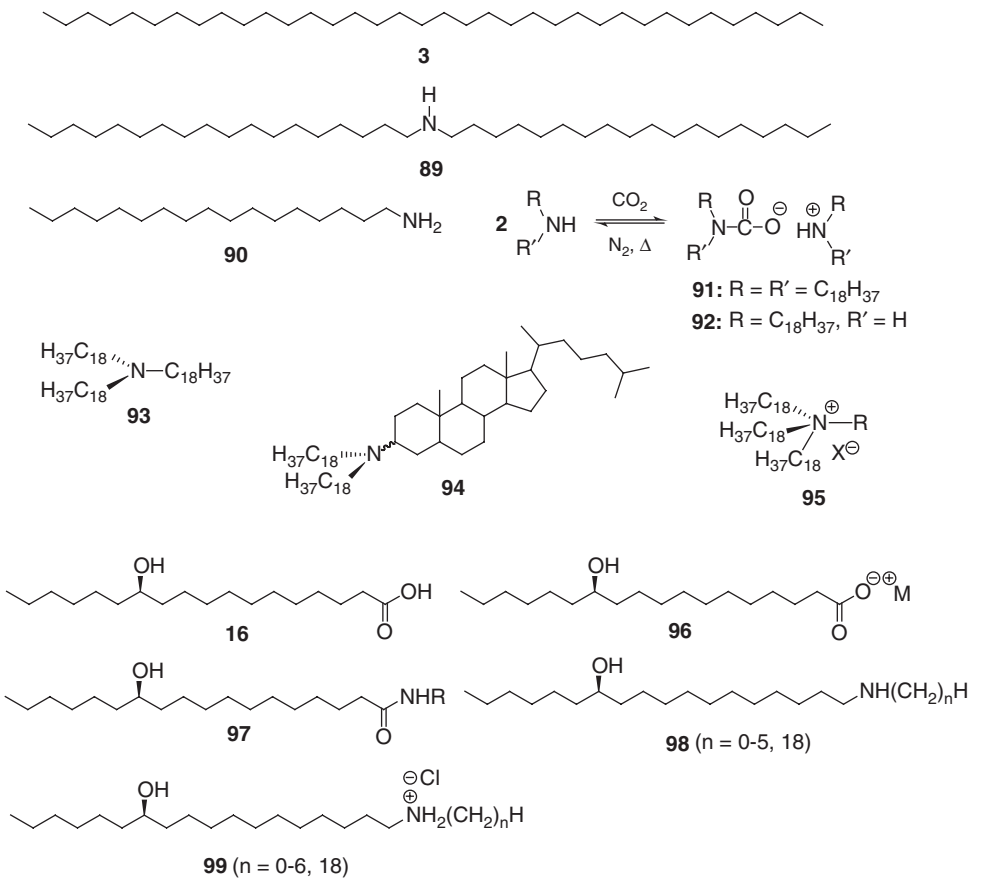

Figure 1.59 **LMOG**s with increasing complexity from their simpler versions [46a, 49, 82b, 168–172].

more complex **LMOG**s [43a, 168]. *n*-Alkanes are structurally the simplest possible **LMOG**s. Those with 24–36 carbon atoms (C36 (**3**) is shown in Figure 1.59) have been shown to gelate shorter *n*-alkanes, 1-alkanols, and silicone oil with London dispersion forces as the only stabilizing intermolecular interaction [49]. However, their **SAFIN**s are composed of interlocking platelets (2D objects) rather than 1D objects. Insertion of an N–H group within an *n*-alkane produces either an internal (**89**) or a terminal aliphatic amine (**90**) which also produces gels with various liquids. Here, the forces responsible for the **SAFIN** stability are HB between amine groups as well as London dispersion forces between alkyl groups and the individual objects are again 1D [169]. Addition of CO_2 converts **89** and **90** to carbamate-ammonium salts (**91** and **92**), much more efficient **LMOG**s than the amines due to the presence of strong electrostatic interactions among molecules in their aggregates [169]. Reconversion of the salts to the amine forms can be achieved by purging the gels with N_2 gas while heating mildly.

More structurally complex **LMOG**s, including tertiary amines, **93** and **94**, and quaternary ammonium salts **95** [170], have been prepared by adding substituents to the nitrogen in **89**. **93** is able to gelate silicone oil and 1-pentanol; only the α-anomer of **94** was able to gelate silicone oil. As expected, the gelating ability of **95** was very dependent on the type of R substituent and counter-ion $X^{\ominus}$.

A diverse system of **LMOG**s is based upon the naturally occurring molecule and known gelator, (*R*)-12-hydroxyoctadecanoic acid ((*R*)-**16**) [40b, 46b, 53a, 171]. It may be viewed as an *n*-alkane with terminal carboxy and internal hydroxy substituents. Several derivatives of **16**, including its salts **96** [46a], *N*-alkylamides **97** [168], *N*-alkylamines **98** [82b, 168], and *N*-alkylammonium chloride salts **99** [172], have been investigated thus far. As a generality, comparing the same homologs, the amines **98** are must less efficient **LMOG**s than the amides **97** which are comparable to or weaker than the ammonium chlorides **99**. The ammonium chlorides are also better gelators than the salts **96** or the parent acid **16**.

Although the properties of gels in which several other substituents have been placed within the *n*-alkane **LMOG** structure have been investigated [43a], the sought for relationship between gelator structure and gel stability has not been achieved. If underlying relationships are to be discovered, they will require additional insights into the **SAFIN** structures and potentially even greater control over changes in **LMOG** structure.

In many respects, polymeric chain growth through covalent bond formation between monomeric units is like 1D fiber growth of molecular gelators. Extracting useful concepts from conventional polymerization processes and extending them to 1D fibrilization may be useful. For example, the degree and type of polymerization is determined in part by the reactivity and steric hindrance of the individual monomeric units. Similarly, 1D fiber formation occurs when **LMOG**s aggregate through anisotropic intermolecular interactions (that are weaker than covalent bonding) which promote growth in one direction. Many molecular gelators rely upon directionally preferential nonbonding interactions, van der Waals forces such as HB, London dispersion interactions, electrostatic interactions, and π-π stacking. However, very few **SAFIN** structures are comprised of only one **LMOG** along the cross-sections of the fibers. Because each of the van der Waals interactions is weaker than a covalent bond in a polymer chain, several **LMOG** molecules must interact along the fiber diameters to attain stabilities that are capable of resisting breakage energies of several kT. HB, being one of the strongest and most directional of the van der Waals interactions, has been employed most frequently to initiate the 1D fiber growth.

With a properly designed gelator, cooperative intermolecular interactions can strengthen and facilitate gelation. As illustrated in Figure 1.60, HB between urea groups supports more effective π-π stacking of perylene *bis*-imide, aiding the gelation process [173].

The necessity of a strong 1D intermolecular interaction (e.g., HB) for fibrilization has been emphasized [174], and Dastidar *et al*. have intensively investigated this concept via crystal engineering [9]. In that regard, prediction of molecular level assembly through crystal engineering using supramolecular synthons is

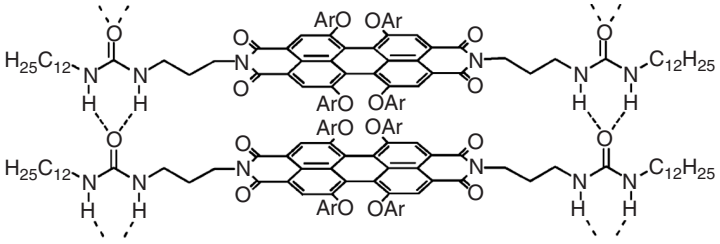

Figure 1.60 A schematic illustration of hydrogen-bonding of a urea substituted perylene *bis*-imide in its fibers [173].

becoming a valuable method to correlate **LMOG** structure and gel properties within select classes of molecules. Based on a working hypothesis that a 1D hydrogen bonding network (HBN) is a prerequisite for anisotropic fiber growth, numerous supramolecular synthons derived from organic salts – including secondary ammonium monocarboxylates (SAMs) [58, 175], secondary ammonium dicarboxylates (SADs) [176], primary ammonium monocarboxylates (PAMs) [177], and primary ammonium dicarboxylates (PADs) [178] – have been developed (Figure 1.61).

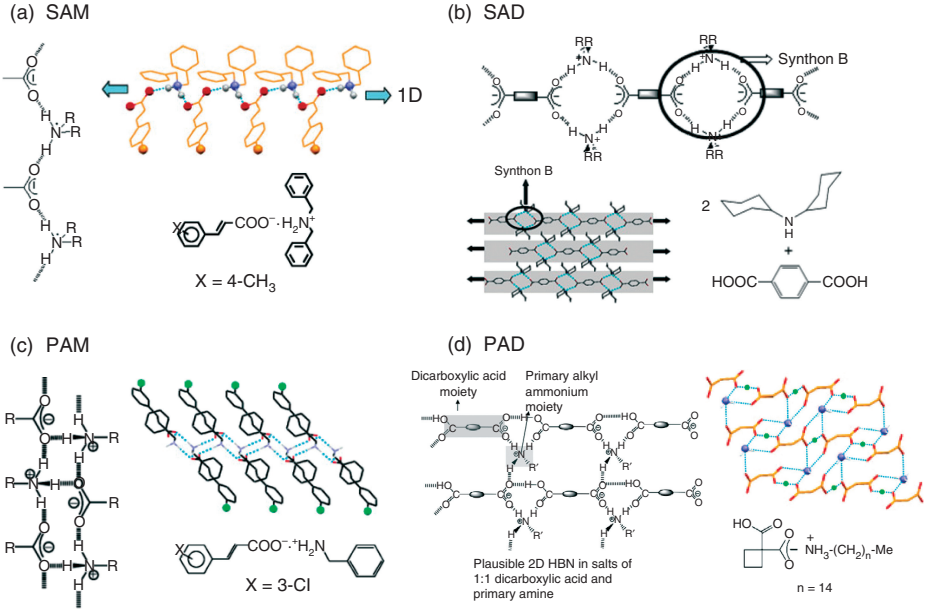

Figure 1.61 Plausible 1D and 2D HBNs in organic salts as postulated from single-crystal structures from organic salt-based supramolecular synthons: (a) SAM (Reprinted with permission from Ref. [175d]. Copyright 2006 American Chemical Society.), (b) SAD (Reprinted with permission from Ref. [176a]. Copyright 2005 American Chemical Society.), (c) PAM (Reprinted with permission from Ref. [177a]. Copyright 2006 American Chemical Society.), and (d) PAD. Reprinted with permission from Ref. [178b]. Copyright 2008 American Chemical Society.

X-ray-derived packing structures of single crystals of many of these two-component-based **LMOG**s have been solved. Salts whose crystal structures revealed a 0D or 3D HBN were not gelators in the liquids investigated. The presence of 1D HBNs in the salts which did lead to gels are consistent with the HBN hypothesis. However, gels were observed from some PAD systems with long primary *n*-alkylamines [178] and SAD systems with 1 : 2 dicarboxylate:secondary amine ratios for which 2D HBNs were present in the crystals [176b]. Although the molecular packing in the single crystals and in the **SAFIN** structures may or may not be the same, the supramolecular synthon strategy seems to be potentially very powerful, and it has been extended successfully to create new metallogels [179].

Molecular modeling, in conjunction with gel characterization data, is a valuable approach to propose structures at the primary (0D), secondary (1D), and even tertiary (3D **SAFIN**) levels of aggregation [42b, 180]. It can also assist the design of new gelators. For example, van Esch *et al.* [181] have demonstrated that molecular modeling can identify appropriate structural moieties of a *bis*-urea gelator to maintain 1D HB (and thus promote 1D growth). As shown in Figure 1.62a, conformational flexibility in the *bis*-urea is necessary to ensure 1D HB network formation. The energy-minimized conformation from the CHARMm 23 forcefield simulation revealed that a cyclohexyl or phenyl would be an appropriate platform to attach the urea groups and attain a 1D HB network. Thus, molecular packing in 1D aggregates of the model compound **100** (*trans*-1,2-bis-(*N*-methylureido)cyclohexane) were calculated (Figures 1.62b, c) and the results were used to gain an understanding of the structures of aggregates of **LMOG 101** (with longer alkyl groups) (Figures 1.62d, e) [181b].

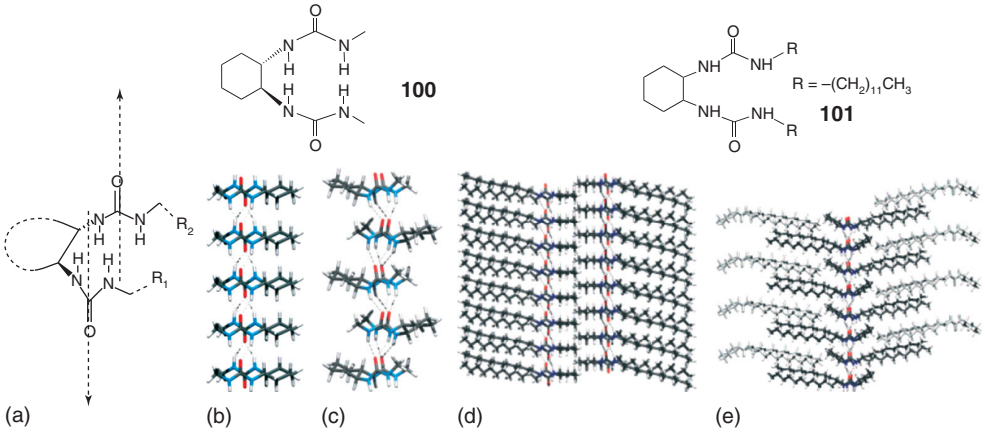

Figure 1.62 (a) Hydrogen bonding directionality of *bis*-urea compounds with conformationally constrained linkers. Two possible hydrogen-bonded aggregates of **100** are shown. (b) Translational aggregate with urea groups antiparallel. (c) Screw axis or glide plane aggregate with urea groups parallel. Tentative arrangement of **101** in a double layer structure, constructed from (d) translational aggregates and (e) an intercalated layer structure constructed from screw axis aggregates. Reprinted with permission from Ref. [181b]. Copyright 2008 Wiley.

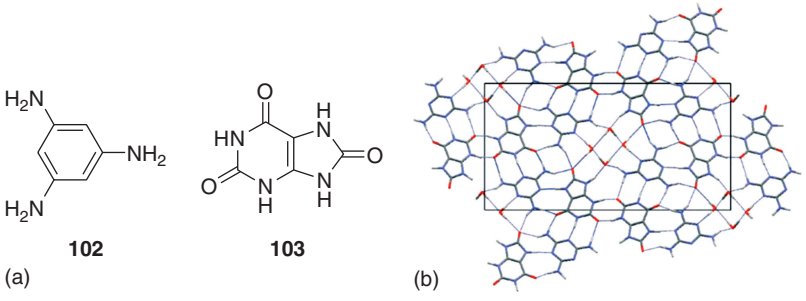

Figure 1.63 (a) Structures of melamine (**102**) and uric acid (**103**). (b) Calculated fourth-lowest-energy crystal structure of **102** · **103** · **2H$_2$O**; monoclinic, P2$_1$/*c*, $a = 3.818$, $b = 25.810$, $c = 14.088$ Å, $\beta = 71.17^\circ$. View down the *a* axis. Reprinted with permission from Ref. [183]. Copyright 2008 Wiley.

Gelation behaviors have also been correlated with the calculated energies of conformations of **LMOG**s and non-**LMOG**s based on a *bis*(amino acid)oxalyl compound [182]. A melamine (**102**) and uric acid (**103**) HB donor/acceptor system forms a gel in water, assisted by sonication. The energy-minimized crystal structure of the two-component **LMOG** predicts inclusion of two molecules of water (Figure 1.63). Furthermore, a 2D anisotropic HB network in the crystal structure was interpreted to contribute to the formation of **SAFIN**s with a tape-like morphology [183].

Despite these successes and although molecular modeling has progressed to the point at which it is becoming possible to predict crystal structures, determination of whether the packing will lead to 1D (e.g., fibers), 2D (platelets), or 3D (i.e., bulk crystalline) objects is still in the future in all except specific cases. Future advances in this area will open important doors to understanding fundamental aspects of gel formation! All facets of gelation, including gelator design, characterization, modeling, and applications have made notable strides in recent years. Nevertheless, continuous efforts need to be made to understand further the fundamentals of gelation. It may be unrealistic to propose a universal rule which encompasses all the variables associated with *a priori* design of **LMOG**s. Even with appropriate structural motifs for proper gelator–gelator and gelator–solvent interactions, incorporating them into one molecular design becomes a critical question for fibrilization. Establishing an extensive database of individual case studies could provide helpful guidelines for more sensible gelator design.

1.6 Some Final Thoughts

Although the amount of knowledge gleaned during the last three decades about **LMOG**s, **SAFIN**s, their gels, and even their modes of formation and disassembly is enormous, each discovery about them seems to add two new questions. The challenges facing scientists studying molecular gels are enormous, and will probably remain so for the foreseeable future. Although some seminal questions can be

formulated, methodologies for answering them are not obvious. For example, a general method for the *a priori* design of **LMOG**s whose structures are not derivatives of existing ones has not been demonstrated. Similarly, viscoelastic properties of gels (a topic not covered here) cannot be predicted. The list of challenges could be increased much more.

However, from what is written in this chapter and elsewhere about molecular gels, it is clear that their potential is enormous for aiding in our understanding of the principles behind self-assembly of materials, for devising new types of materials, for making various types of delivery agents, for constructing new sensors, and for developing many other uses not yet envisioned. For these practical reasons as well as to uncover Mother Nature's secrets, increased study of molecular gels is warranted. The authors hope that this chapter will aid others in those studies.

Acknowledgments

RGW expresses his gratitude to the United States National Science Foundation (Grants CHE-1147353 and CHE-0911089) and to the Gulf of Mexico Research Initiative for their financial support. DCL thanks the United States National Science Foundation for its financial support (Grant DMR-0846479). KLC appreciates and acknowledges support from James Madison University and from The Research Corporation for Scientific Advancement. The authors thank especially their colleagues whose names appear in the references for their efforts to uncover the principles involved in this fascinating and rapidly evolving field. Foremost among those in the professional life of RGW has been Dr. Pierre Terech, a wonderful scientist and collaborator, who has offered insights, inspiration, and especially friendship during many years. All of the authors, recognizing his seminal contributions to the field of molecular gels, dedicate this chapter to him.

References

1. Weiss, R.G. and Terech, P. (eds) (2006) *Molecular Gels: Materials with Self-Assembled Fibrillar Networks*, Springer, Dordrecht.
2. (a) Zubarev, E.R., Sone, E.D., and Stupp, S.I. (2006) *Chem. — Eur. J.*, **12**, 7313–7327. (b) Estroff, L.A. and Hamilton, A.D. (2004) *Chem. Rev.*, **104**, 1201–1217. (c) Shen, W., Kornfield, J.A., and Tirrell, D.A. (2007) *Macromolecules*, **40**, 689–692. (d) Ishi-i, T. and Shinkai, S. (2005) *Supermol. Dye Chem.*, **258**, 119–160. (e) Beginn, U., Möller, M., and Keinath, S. (2005) *Chem. Eng. Commun.*, **192**, 1116–1128. (f) Fujigaya, T., Jiang, D.L., and Aida, T. (2007) *Chem. Asian J.*, **2**, 106–113. (g) Lee, H.-K., Soukasene, S., Jiang, H., Zhang, S., Feng, W., and Stupp, S.I. (2008) *Soft Matter*, **4**, 962–964.
3. Although extremely important to understanding gels and their **SAFIN**s, their rheology will not be discussed in depth here. For an interesting introduction, see: Raghavan, S.R. and Cipriano, B.H. (2006) in *Molecular Gels: Materials with Self-Assembled Fibrillar Networks* (eds R.G. Weiss and P. Terech), Springer, Dordrecht, pp. 233–244.

4. George, M., Tan, G., John, V.T., and Weiss, R.G. (2005) *Chem.—Eur. J.*, **11**, 3243–3254.
5. Garlaschelli, L., Ramaccini, F., and Della Sala, S. (1991) *Nature*, **353**, 507.
6. Von Lipowitz, A. (1841) *Liebigs Ann. Chem. Pharm.*, **38**, 348–355.
7. Meunier, M.J. (1891) *Ann. Chim. Phys.*, **22**, 412.
8. Flory, P.J. (1974) *Discuss. Faraday Soc.*, **57**, 7–18.
9. Dastidar, P. (2008) *Chem. Soc. Rev.*, **37**, 2699–2715.
10. (a) Whitesides, G.M. and Boncheva, M. (2002) *Proc. Natl. Acad. Sci. U.S.A.*, **99**, 4769–4774. (b) Jonkheijm, P., van der Schoot, P., Schenning, A.P.H.J., and Meijer, E.W. (2006) *Science*, **313**, 80–83. (c) Smulders, M.M.J., Schenning, A.P.H.J., and Meijer, E.W. (2008) *J. Am. Chem. Soc.*, **130**, 606–611.
11. Lin, Y.-C., Kachar, B., and Weiss, R.G. (1989) *J. Am. Chem. Soc.*, **111**, 5542–5551.
12. Robinson, B.H. (ed) (2003) *Self-Assembly*, IOS Press, Amsterdam.
13. (a) Ward, M.D. (2005) *MRS Bull.*, **30**, 705–712. (b) Holman, K.T., Pivovar, A.M., and Ward, M.D. (2001) *Science*, **294**, 1907–1911. (c) Holman, K.T., Martin, S.M., Parker, D.P., and Ward, M.D. (2001) *J. Am. Chem. Soc.*, **123**, 4421–4431.
14. (a) Ivan Kuzmenko, I., Rapaport, H., Kjaer, K., Als-Nielsen, J., Weissbuch, I., Lahav, M., and Leiserowitz, L. (2001) *Chem. Rev.*, **101**, 1659–1696. (b) Cox, J.R., Dabros, M., Shaffer, J.A., and Thalladi, V.R. (2007) *Angew. Chem. Int. Ed.*, **46**, 1988–1991. (c) Sun, Y., Xi, H., Ediger, M.D., and Lian Yu, L. (2008) *J. Phys. Chem. B*, **112**, 661–664. (d) Ungar, G., Putra, E.G.R., de Silva, D.S.M., Shcherbina, M.A., and Waddon, A.J. (2005) *Adv. Polym. Sci.*, **180**, 45–87. (e) Desiraju, G.R. (2003) *Crystal Design: Structure and Function*, John Wiley & Sons, Inc., Hoboken, NJ. (f) Atwood, J.L. (2004) *Encyclopedia of Supramolecular Chemistry*, Vol. 1 and 2, Marcel Dekker, New York.
15. Huang, X., Terech, P., Raghavan, S.R., and Weiss, R.G. (2005) *J. Am. Chem. Soc.*, **127**, 4336–4344.
16. Huang, X., Raghavan, S.R., Terech, P., and Weiss, R.G. (2006) *J. Am. Chem. Soc.*, **128**, 15341–15352.
17. Aggeli, A., Boden, N., Carrick, L.M., Mcleish, T.C.B., Nyrkova, I.A., and Semenov, A.N. (2006) in *Molecular Gels: Materials with Self-Assembled Fibrillar Networks* (eds R.G. Weiss and P. Terech) Chapter 3, Springer, Dordrecht.
18. (a) Boettcher, C., Schade, B., and Fuhrhop, J.-H. (2001) *Langmuir*, **17**, 873–877. (b) Fuhrhop, J.-H., Wang, T., Bhosale, S., Bhosale, S., and Lauer, M. (2006) in *Molecular Gels: Materials with Self-Assembled Fibrillar Networks* (eds R.G. Weiss and P. Terech) Chapter 18, Springer, Dordrecht.
19. (a) Wang, R.Y., Liu, X.Y., Narayanan, J., Xiong, J.Y., and Li, J.L. (2006) *J. Phys. Chem. B*, **110**, 25797–25802. (b) Li, J.L., Liu, X.Y., Strom, C.S., and Xiong, J.Y. (2006) *Adv. Mater.*, **18**, 2574–2578. (c) Wang, R.Y., Liu, X.Y., Xiong, J.Y., and Li, J.L. (2006) *J. Phys. Chem. B*, **110**, 7275–7280. (d) Liu, X.Y. (2005) *Top. Curr. Chem.*, **256**, 1–37. (e) Li, J.L., Liu, X.Y., Wang, R.Y., and Xiong, J.Y. (2005) *J. Phys. Chem. B*, **109**, 24231–24235.
20. Voorhees, P.W. and Glicksman, M.E. (1985) *J. Cryst. Growth*, **72**, 599–615.
21. (a) Chou, C.M. and Hong, P.D. (2004) *Macromolecules*, **37**, 5596–5606. (b) Dubinina, E.O. and Lakshtanov, L.Z. (1997) *Geochim. Cosmochim. Acta*, **61**, 2265–2273.
22. Voorhees, P.W. (1985) *J. Stat. Phys.*, **38**, 231–252.
23. Wang, Y.J., Tang, L., and Yu, J. (2008) *Cryst. Growth Des.*, **8**, 884–889.
24. (a) Lu, P.J., Zaccarelli, E., Ciulla, F., Schofield, A.B., Sciortino, F., and Weitz, D.A. (2009) *Nature*, **453**, 499-U4. (b) Barnes, H.A.J. (1997) *J. Non-Newton. Fluid Mech.*, **70**, 1–33.
25. Jones, R.A.L. (2002) *Soft Condensed Matter*, Oxford University Press, New York.
26. Terech, P. and Weiss, R.G. (1997) *Chem. Rev.*, **97**, 3133–3159.

27. Te Nijenhuis, K. (1997) *Thermoreversible Networks*, Advances in Polymer Science, Vol. 130, Springer-Verlag, Berlin.
28. Thompson, D.W. (1961) in *On Growth and Form* (ed J.T. Bonner), Cambridge University Press, Cambridge.
29. (a) Nichols, M.R., Moss, M.A., Reed, D.K., Lin, W.-L., Mukhopadhyay, R., Hoh, J.H., and Rosenberry, T.L. (2002) *Biochemistry*, **41**, 6115–6127. (b) Kumar, S., Mohanty, S.K., and Udgaonkar, J.B. (2007) *J. Mol. Biol.*, **367**, 1186–1204.
30. (a) Wilder, E.A., Hall, C.K., and Spontak, R.J. (2003) *J. Colloid Interface Sci.*, **267**, 509–518. (b) Wilder, E.A., Braunfeld, M.B., Jinnai, H., Hall, C.K., Agard, D.A., and Spontak, R.J. (2003) *J. Phys. Chem. B*, **107**, 11633–11642. (c) Wilder, E.A., Hall, C.K., Khan, S.A., and Spontak, R.J. (2003) *Langmuir*, **19**, 6004–6013. (d) Xu, D.-H., Wang, Z.-G., and Douglas, J.F. (2008) *Macromolecules*, **41**, 815–825. (e) Kashiwagi, T., Du, F.M., Douglas, J.F., Winey, K.I., Harris, R.H., and Shields, J.R. (2005) *Nat. Mater.*, **4**, 928–933. (f) Barnes, K.A., Douglas, J.F., Liu, D.W., and Karim, A. (2001) *Adv. Colloid Interface Sci.*, **94**, 83–104.
31. (a) Rogers, M.A., Wright, A.J., and Marangoni, A.G. (2009) *Curr. Opin. Colloid Interface Sci.*, **14**, 33–42. (b) Toro-Vazquez, J.F., Alonzo-Macias, M., Dibildox-Alvarado, E., and Charo-Alonso, M.A. (2009) *Food Biophys.*, **4**, 199–212. (c) Dibildox-Alvarado, E., Charo-Alonso, M., Alonzo-Macias, M., and Gonzalez-Chavez, M.M. (2007) *J. Am. Oil Chem. Soc.*, **84**, 989–1000. (d) Bot, A. and Agtero, W.G.M. (2006) *J. Am. Oil Chem. Soc.*, **83**, 513–521. (e) Hughes, N.E., Marangoni, A.G., Wright, A.J., Rogers, M.A., and Rush, J.W.E. (2009) *Trends Food Sci. Technol.*, **20**, 470–480. (f) Schaink, H.M., van Malssen, K.F., Morgado-Alves, S., Kalnin, D., and van der Linden, E. (2007) *Food Res. Int.*, **40**, 1185–1193. (g) Toro-Vazquez, J.F., Morales-Rueda, J., Mallia, V.A., and Weiss, R.G. (2010) *Food Biophys.*, **5**, 193–202.
32. (a) Zhang, S., Greenfield, M.A., Mata, A., Palmer, L.C., Bitton, R., Mantei, J.R., Aparicio, C., de la Cruz, M.O., and Stupp, S.I. (2010) *Nat. Mater.*, **9**, 594–601. (b) Matson, J.B., Newcomb, C.J., Bitton, R., and Stupp, S.I. (2012) *Soft Matter*, **8**, 3586–3595.
33. Tanaka, F. (2006) in *Molecular Gels: Materials with Self-Assembled Fibrillar Networks* (eds R.G. Weiss and P. Terech) Chapter 1, Springer, Dordrecht.
34. (a) Gránásy, L., Pusztai, T., Borzsonyi, T., Warren, J.A., and Douglas, J.F. (2004) *Nat. Mater.*, **3**, 645–650. (b) Gránásy, L., Pusztai, T., Tegze, G., Warren, J.A., and Douglas, J.F. (2005) *Phys. Rev. E*, **72**, 011605/1-15. (c) Gránásy, L., Pusztai, T., Warren, J.A., Douglas, J.F., Börzsönyi, T., and Ferreiro, V. (2003) *Nat. Mater.*, **2**, 92–96. (d) Douglas, J.F. (2009) *Langmuir*, **25**, 8386–8391.
35. Selinger, J.V., Spector, M.S., and Schnur, J.M. (2001) *J. Phys. Chem. B*, **105**, 7157–7169.
36. (a) Corezzi, S., Fioretto, D., De Michele, C., Zaccarelli, E., and Sciortino, F. (2010) *J. Phys. Chem. B*, **114**, 3769–3775. (b) Fernandez Toledano, J.C., Sciortino, F., and Zaccarelli, E. (2009) *Soft Matter*, **5**, 2390–2398. (c) Bianchi, E., Tartaglia, P., La Nave, E., and Sciortino, F. (2007) *J. Phys. Chem. B*, **111**, 11765–11769.
37. VanderHart, D.L., Douglas, J.F., Hudson, S.D., Antonucci, J.M., and Wilder, E.A. (2011) *Langmuir*, **27**, 1745–1757.
38. Aggeli, A., Nyrkova, I.A., Bell, M., Harding, R., Carrick, L., McLeish, T.C.B., Semenov, A.N., and Boden, N. (2001) *Proc. Natl. Acad. Sci. U.S.A*, **98**, 11857–11862.
39. (a) Rogers, M.A. and Marangoni, A.G. (2008) *Cryst. Growth Des.*, **8**, 4596–4601. (b) Rogers, M.A. and Marangoni, A.G. (2009) *Langmuir*, **25**, 8556–8566.
40. (a) Lam, R., Rogers, M.A., and Marangoni, A.G. (2009) *J. Therm. Anal. Calorim.*, **98**, 7–12. (b) Grahame, D.A.S., Olauson, C., Lam, R.S.H., Pedersen, T., Borondics, F.,

Abraham, S., Weiss, R.G., and Rogers, M.A. (2009) *Soft Matter*, **7**, 7359–7365.
41. Suzuki, M. and Hanabusa, K. (2009) *Chem. Soc. Rev.*, **38**, 967–975.
42. (a) van Esch, J.H. (2009) *Langmuir*, **25**, 8392–8394. (b) de Loos, M., Feringa, B.L., and van Esch, J.H. (2005) *Eur. J. Org. Chem.*, 3615–3631.
43. (a) George, M. and Weiss, R.G. (2006) *Acc. Chem. Res.*, **39**, 489–497. (b) Lu, L.D., Cocker, T.M., Bachman, R.E., and Weiss, R.G. (2000) *Langmuir*, **16**, 20–34. (c) Mukkamala, R. and Weiss, R.G. (1996) *Langmuir*, **12**, 1474–1482.
44. (a) Sahoo, P., Kumar, D.K., Raghavan, S.R., and Dastidar, P. (2011) *Chem. Asian J.*, **6**, 1038–1047. (b) Edwards, W., Lagadec, C.A., and Smith, D.K. (2011) *Soft Matter*, **7**, 110–117. (c) George, M., Snyder, S.L., Terech, P., and Weiss, R.G. (2005) *Langmuir*, **21**, 9970–9977.
45. Ruzicka, B., Zaccarelli, E., Zulian, L., Angelini, R., Sztucki, M., Moussaid, A., Narayanan, T., and Sciortino, F. (2011) *Nat. Mater.*, **10**, 56–60.
46. (a) Tachibana, T. and Kambara, H. (1968) *J. Colloid Interface Sci.*, **28**, 173–174. (b) Tachibana, T., Mori, T., and Hori, K. (1980) *Bull. Chem. Soc. Jpn.*, **53**, 1714–1719. (c) Tachibana, T., Yamagishi, A., and Hiro, K. (1979) *Bull. Chem. Soc. Jpn.*, **52**, 346–350.
47. Terech, P. and Wade, R.H. (1988) *J. Colloid Interface Sci.*, **125**, 542–551.
48. Wade, R.H., Terech, P., Hewat, E.A., Ramasseul, R., and Volino, F. (1986) *J. Colloid Interface Sci.*, **114**, 442–451.
49. Abdallah, D. and Weiss, R.G. (2000) *Langmuir*, **16**, 352–355.
50. George, S.J. and Ajayaghosh, A. (2005) *Chem.—Eur. J.*, **11**, 3217–3227.
51. Térech, P. (2006) in *Molecular Gels: Materials with Self-Assembled Fibrillar Networks* (eds R.G. Weiss and P. Terech), Springer, Dordrecht, pp. 275–324.
52. (a) Sakurai, K., Ono, Y., Jung, J.H., Okamoto, S., Sakurai, S., and Shinkai, S. (2001) *J. Chem. Soc., Perkin Trans. 2*, 108–112. (b) Sakurai, K., Jeong, Y., Koumoto, K., Friggeri, A., Gronwald, O., Sakurai, S., Okamoto, S., Inoue, K., and Shinkai, S. (2003) *Langmuir*, **19**, 8211–8217. (c) Jeong, Y., Hananbusa, K., Masunaga, H., Akiba, I., Miyoshi, K., Sakurai, S., and Sakurai, K. (2005) *Langmuir*, **21**, 586–594. (d) Takeno, H., Mochizuki, T., Yoshiba, K., Kondo, S., and Dobashi, T. (2009) *Prog. Colloid Polym. Sci.*, **136**, 47–54.
53. (a) Terech, P., Rodriquez, V., Barnes, J.D., and McKenna, G.B. (1994) *Langmuir*, **10**, 3406–3418. (b) Terech, P., Furman, I., and Weiss, R.G. (1995) *J. Phys. Chem.*, **99**, 9558–9566. (c) Terech, P., Ostuni, E., and Weiss, R.G. (1996) *J. Phys. Chem.*, **100**, 3759–3766. (d) Terech, P., Coutin, A., and Giroud-Godquin, A.M. (1997) *J. Phys. Chem. B*, **101**, 6810–6818. (e) Terech, P., Allegraud, J.J., and Garner, C.M. (1998) *Langmuir*, **14**, 3991–3998. (f) Terech, P. and Coutin, A. (1999) *Langmuir*, **15**, 5513–5525.
54. Murata, K., Aoki, M., Suzuki, T., Harada, T., Kawabata, H., Komori, T., Ohseto, F., Ueda, K., and Shinkai, S. (1994) *J. Am. Chem. Soc.*, **116**, 6664–6676.
55. Anne, M. (2006) in *Molecular Gels: Materials with Self-Assembled Fibrillar Networks* (eds R.G. Weiss and P. Terech), Springer, Dordrecht, pp. 325–361.
56. Liu, X.Y. and Swant, P.D. (2002) *Adv. Mater.*, **14**, 421–426.
57. (a) Ostuni, E., Kamaras, P., and Weiss, R.G. (1996) *Angew. Chem. Int. Ed. Engl.*, **35**, 1324–1326. (b) Borges, A.R., Hyacinth, M., Lum, M., Dingle, C.M., Hamilton, P.L., Chruszcz, M., Pu, L., Sabat, M., and Caran, K.L. (2008) *Langmuir*, **24**, 7421–7431.
58. Trivedi, D.R., Ballabh, A., and Dastidar, P. (2005) *J. Mater. Chem.*, **15**, 2606–2614.
59. Shapiro, Y.E. (2011) *Prog. Polym. Sci.*, **36**, 1184–1253.
60. (a) Xue, P., Lu, R., Chen, G., Zhang, Y., Nomoto, H., Takafuji, M., and Ihara, H. (2007) *Chem.—Eur. J.*, **13**, 8231–8239. (b) Samanta, S.K., Pal, A., and Bhattacharya, S. (2009) *Langmuir*, **25**, 8567–8578.
61. (a) Chen, Y., Lv, Y., Han, Y., Zhu, B., Zhang, F., Bo, Z., and Liu, C.-Y. (2009) *Langmuir*, **25**, 8458–8555. (b) Dou, C.,

Wang, C., Zhang, H., Gao, H., and Wang, Y. (2010) *Chem.—Eur. J.*, **16**, 10744–10751. (c) Allix, F., Curcio, P., Pham, Q.N., Pickaert, G., and Jamart-Grégoire, B. (2010) *Langmuir*, **26**, 16818–16827.

62. Bhattacharya, S. and Samanta, S.K. (2009) *Langmuir*, **25**, 8378–8381.
63. Abraham, S., Vijayaraghavan, R.K., and Das, S. (2009) *Langmuir*, **25**, 8507–8513.
64. Kaiser, T.E., Stepanenko, V., and Würthner, F. (2009) *J. Am. Chem. Soc.*, **131**, 6719–6732.
65. (a) Chen, P., Lu, R., Xue, P., Xu, T., Chen, G., and Zhao, Y. (2009) *Langmuir*, **25**, 8395–8399. (b) Zhang, P., Wang, H., Liu, H., and Li, M. (2010) *Langmuir*, **26**, 10183–10190. (c) Jang, K., Brownell, L.V., Forster, P.M., and Lee, D.-C. (2011) *Langmuir*, **27**, 14615–14620.
66. An, B.-K., Lee, D.-S., Lee, J.-S., Park, Y.-S., Song, H.-S., and Park, S.Y. (2004) *J. Am. Chem. Soc.*, **126**, 10232–10233.
67. Shklyarevskiy, I.O., Jonkheijm, P., Christianen, P.C.M., Schenning, A.P.H.J., Del Guerzo, A., Desvergn, J.-P., Meijer, E.W., and Maan, J.C. (2005) *Langmuir*, **21**, 2108–2112.
68. Giansante, C., Raffy, G., Schäfer, C., Rahma, H., Kao, M.-T., Olive, A.G.L., and Del Guerzo, A. (2011) *J. Am. Chem. Soc.*, **133**, 316–325.
69. (a) Brizard, A., Oda, R., and Huc, I. (2005) *Top. Curr. Chem.*, **256**, 167–218. (b) Gottrarelli, G., Spada, S.P., and Castiglioni, E. (2006) in *Molecular Gels: Materials with Self-Assembled Fibrillar Networks* (eds R.G. Weiss and P. Terech), Springer, Dordrecht, pp. 431–446. (c) Oda, R. (2006) in *Molecular Gels: Materials with Self-Assembled Fibrillar Networks* (eds R.G. Weiss and P. Terech), Springer, Dordrecht, pp. 588–591.
70. (a) Makarević, J., Jokić, M., Raza, Z., Štefanić, Z., Kojić-Prodić, B., and Žinić, M. (2003) *Chem.—Eur. J.*, **9**, 5567–5580. (b) Čaplar, V., Žinić, M., Pozzo, J.-L., Fages, F., Mieden-Gundert, G., and Vögtle, F. (2004) *Eur. J. Org. Chem.*, 4048–4059.
71. Watanable, Y., Miyasou, T., and Hayashi, M. (2004) *Org. Lett.*, **6**, 1547–1550.
72. Tachibana, T., Mori, T., and Hori, K. (1979) *Nature*, **278**, 578–579.
73. Grahame, D.A.S., Olauson, C., Lam, R.S.H., Pedersen, T., Borondics, F., Abraham, S., Weiss, R.G., and Rogers, M.A. (2011) *Soft Matter*, **7**, 7359–7365.
74. (a) Avrami, M. (1939) *J. Chem. Phys.*, **7**, 1103–1112. (b) Avrami, M. (1940) *J. Chem. Phys.*, **8**, 212–224. (c) Avrami, M. (1941) *J. Chem. Phys.*, **9**, 177–184.
75. (a) Cicchi, S., Ghini, G., Lascialfari, L., Brandi, A., Betti, F., Berti, D., Ferrati, S., and Baglioni, P. (2007) *Chem. Commun.*, 1424–1426. (b) Cicchi, S., Ghini, G., Lascialfari, L., Brandi, A., Betti, F., Berti, D., Baglioni, P., Bari, L.D., Pescitelli, G., Mannini, M., and Caneschi, A. (2010) *Soft Matter*, **6**, 1655–1661. (c) Cicchi, S., Pescitelli, G., Lascialfari, L., Ghini, G., Bari, L.D., Brandi, A., Bussotti, L., Atsbeha, T., Marcelli, A., Foggi, P., Berti, D., and Mannini, M. (2011) *Chirality*, **23**, 833–840.
76. (a) DeVoe, H. (1964) *J. Chem. Phys.*, **41**, 393–400. (b) DeVoe, H. (1965) *J. Chem. Phys.*, **43**, 3199–3208.
77. (a) Žinčić, M., Vögtle, F., and Fages, F. (2005) *Top. Curr. Chem.*, **256**, 39–76. (b) Ajayaghosh, A., Vijayakumar, C., Varghese, R., and George, S. (2006) *Angew. Chem. Int. Ed.*, **45**, 456–460.
78. (a) Yoza, K., Amanokura, N., Ono, Y., Akao, T., Shinmori, H., Takeuchi, M., Shinkai, S., and Reinhoudt, D.N. (1999) *Chem.—Eur. J.*, **5**, 2722–2729. (b) Gronwald, O. and Shinkai, S. (2001) *Chem.—Eur. J.*, **7**, 4329–4334. (c) Tamaru, S., Nakamura, M., Takeuchi, M., and Shinkai, S. (2001) *Org. Lett.*, **3**, 3631–3634. (d) Friggeri, A., Gronwald, O., van Bommel, K.J.C., Shinkai, S., and Reinhoudt, D.N. (2002) *J. Am. Chem. Soc.*, **124**, 10754–10758. (e) Ghosh, R., Chakraborty, A., Maiti, D.K., and Puranik, V.G. (2006) *Org. Lett.*, **8**, 1061–1064. (f) Zheng, J., Qiao, W., Wan, X., Gao, J.P., and Wang, Z.Y. (2008) *Chem. Mater.*, **20**, 6163–6168. (g) Cui, J., Liu, A., Guan, Y., Zheng,

J., Shen, Z., and Wan, X. (2010) *Langmuir*, **26**, 3615–3622. (h) Cui, J., Shen, Z., and Wan, X. (2010) *Langmuir*, **26**, 97–103. (i) Cui, J., Zheng, Z., and Wan, X. (2010) *Langmuir*, **26**, 15508–15515.

79. George, S.J., Ajayaghosh, A., Jonkheijm, P., Schenning, A.P.H.J., and Meijer, E.W. (2004) *Angew. Chem. Int. Ed.*, **43**, 3422–3425.
80. Green, M.M. and Reidy, M.P. (1989) *J. Am. Chem. Soc.*, **111**, 6452–6454.
81. (a) Ajayaghosh, A., Varghese, R., George, S.J., and Vijayakumar, C. (2006) *Angew. Chem. Int. Ed.*, **45**, 1141–1144. (b) Ajayaghosh, A., Varghese, R., Mahesh, S., and Praveen, V.K. (2006) *Angew. Chem. Int. Ed.*, **45**, 7729–7732. (c) Haino, T., Tanaka, M., and Fukazawa, Y. (2008) *Chem. Commun.*, 468–470. (d) Nam, S.R., Lee, H.Y., and Hong, J.-I. (2008) *Chem.—Eur. J.*, **14**, 6040–6043. (e) Das, R.K., Kandanelli, R., Linnanto, J., Bose, K., and Maitra, U. (2010) *Langmuir*, **26**, 16141–16149.
82. (a) Geiger, C., Stanescu, M., Chen, L., and Whitten, D.G. (1999) *Langmuir*, **15**, 2241–2245. (b) Mallia, V.A., Butler, P.D., Sarkar, B., Holman, K.T., and Weiss, R.G. (2011) *J. Am. Chem. Soc.*, **133**, 15045–15054.
83. See, for example: Brinksma, J., Feringa, B.L., Kellogg, R.M., Vreeker, R., and van Esch, J. (2000) *Langmuir*, **16**, 9249–9255.
84. Furman, I. and Weiss, R.G. (1993) *Langmuir*, **9**, 2084–2088.
85. Xue, P.C., Lu, R., Yang, X.C., Zhao, L., Xu, D.F., Liu, Y., Zhang, H., Nomoto, H., Takafuji, M., and Ihara, H. (2009) *Chem.—Eur. J.*, **15**, 9824–9835.
86. Zhu, P.L., Yan, X.H., Su, Y., Yang, Y., and Li, J.B. (2010) *Chem.—Eur. J.*, **16**, 3176–3183.
87. Pham, Q.N., Brosse, N., Frochot, C., Dumas, D., Hocquet, A., and Jamart-Gregoire, B. (2008) *New J. Chem.*, **32**, 1131–1139.
88. Hirst, A.R., Coates, I.A., Boucheteau, T.R., Miravet, J.F., Escuder, B., Castelletto, V., Hamley, I.W., and Smith, D.K. (2008) *J. Am. Chem. Soc.*, **130**, 9113–9121.
89. Matteucci, M.E., Hotze, M.A., Johnston, K.P., and Williams, R.O. III, (2006) *Langmuir*, **22**, 8951–8959.
90. Kamlet, M.J., Abboud, J.L.M., Abraham, M.H., and Taft, R.W. (1983) *J. Org. Chem.*, **48**, 2877–2887.
91. Barton, A.F.M. (1975) *Chem. Rev.*, **75**, 731–753.
92. Bielejewski, M., Lapinski, A., Luboradzki, R., and Tritt-Goc, J. (2009) *Langmuir*, **25**, 8274–8279.
93. Wu, Y.-P., Wu, S., Zou, G., and Zhang, Q.-J. (2011) *Soft Matter*, **7**, 9177–9183.
94. Barton, A.F.M. (1991) *CRC Handbook of Solubility Parameters and Other Cohesion Parameters*, 2nd edn, CRC Press, Boca Raton, FL.
95. Reichardt, C. (2003) *Solvents and Solvent Effects in Organic Chemistry*, 3rd edn, Wiley-VCH Verlag GmbH, Weinheim.
96. Zhu, G.-Y. and Dordick, J.S. (2006) *Chem. Mater.*, **18**, 5988–5995.
97. Wypych, G. (2001) *Handbook of Solvents*, ChemTec Publishing, Toronto.
98. Raynal, M. and Bouteiller, L. (2011) *Chem. Commun.*, **47**, 8271–8273.
99. Kato, T., Hirai, Y., Nakaso, S., and Moriyama, M. (2007) *Chem. Soc. Rev.*, **36**, 1857–1867.
100. Yang, Z., Liang, G., and Xu, B. (2008) *Acc. Chem. Res.*, **41**, 315–326.
101. Gao, Y., Yang, Z., Kuang, Y., Ma, M.-L., Li, J., Zhao, F., and Xu, B. (2010) *Biopolymers (Pep. Sci.)*, **94**, 19–31.
102. Hahn, M.E. and Gianneschi, N.C. (2011) *Chem. Commun.*, **47**, 11814–11821.
103. (a) Yang, Z., Gu, H., Fu, D., Gao, P., Lam, J.K., and Xu, B. (2004) *Adv. Mater.*, **16**, 1440–1444. (b) Yang, Z., Gu, H., Fu, D., Gao, P., Lam, J.K., and Xu, B. (2006) *Adv. Mater.*, **18**, 545–555.
104. Yang, Z., Liang, G., Wang, L., and Xu, B. (2006) *J. Am. Chem. Soc.*, **128**, 3038–3043.
105. Toledano, S., Williams, R.J., Jayawarna, V., and Uljin, R.V. (2006) *J. Am. Chem. Soc.*, **128**, 1070–1071.
106. Yang, Z., Ho, P.-L., Liang, G., Chow, K.H., Wang, Q., Cao, Y., Guo, Z., and Xu, B. (2007) *J. Am. Chem. Soc.*, **129**, 266–267.

107. Yang, Z. and Xu, B. (2004) *Chem. Commun.*, 2424–2425.

108. Vemula, P.K., Li, J., and John, G. (2006) *J. Am. Chem. Soc.*, **128**, 8932–8938.

109. Liang, G., Yang, Z., Zhang, R., Li, L., Fan, Y., Kuang, Y., Gao, Y., Wang, T., Lu, W.W., and Xu, B. (2009) *Langmuir*, **25**, 8419–8422.

110. Webber, M.J., Newcomb, C.J., Bitton, R., and Stupp, S.I. (2011) *Soft Matter*, **7**, 9665–9672.

111. Yang, Z., Xu, K., Guo, Z., Guo, Z., and Xu, B. (2007) *Adv. Mater.*, **19**, 3152–3156.

112. Yang, Z., Gaolin, L., Guo, Z., Guo, Z., and Xu, B. (2007) *Angew. Chem. Int. Ed.*, **46**, 8216–8219.

113. Liang, G., Xu, K., Li, L., Wang, L., Kuang, Y., Yang, Z., and Xu, B. (2007) *Chem. Commun.*, 4096–4098.

114. For a recent example, see: Liu, J., He, P., Yan, J., Fang, X., Peng, J., Liu, K., and Fang, Y. (2008) *Adv. Mater.*, **20**, 2509–2511.

115. (a) Naota, T. and Koori, H. (2005) *J. Am. Chem. Soc.*, **127**, 9324–9325. (b) Wang, C., Zhang, D., and Zhu, D. (2005) *J. Am. Chem. Soc.*, **127**, 16372–16373.

116. Bardelang, D. (2009) *Soft Matter*, **5**, 1969–1971.

117. Cravotto, G. and Cintas, P. (2009) *Chem. Soc. Rev.*, **38**, 2684–2697.

118. Kharissova, O.V., Kharisov, B.I., Valdés, J.J.R., and Méndez, U.O. (2011) *Synth. React. Inorg. Metal-Org. Nano-Metal Chem.*, **41**, 429–448.

119. Ruecroft, G., Hipkiss, D., Ly, T., Maxted, N., and Cains, P.W. (2005) *Org. Proc. Res. Dev.*, **9**, 923–932.

120. Komiya, N., Murakowa, T., Iida, M., Miyanaga, M., Takahashi, K., and Naota, T. (2011) *J. Am. Chem. Soc.*, **133**, 16054–16061.

121. Li, Y., Wang, T., and Liu, M. (2007) *Tetrahedron*, **63**, 7468–7473.

122. Ke, D., Zhan, C., Li, A.D.Q., and Yao, J. (2011) *Angew. Chem. Int. Ed.*, **50**, 3715–3719.

123. Zhang, S., Yang, S., Lan, J., Tang, Y., Xue, Y., and You, J. (2009) *J. Am. Chem. Soc.*, **131**, 1689–1691.

124. Moy, C.L., Kaliappan, R., and McNeil, A.J. (2011) *J. Org. Chem.*, **76**, 8501–8507.

125. Chen, X., Huang, Z., Chen, S.-Y., Li, K., Yu, X.-Q., and Pu, L. (2010) *J. Am. Chem. Soc.*, **132**, 7297–7299.

126. Park, S.M. and Kim, B.H. (2008) *Soft Matter*, **4**, 1995–1997.

127. Stathopulos, P.B., Scholz, G.A., Hwang, Y.-M., Rumfeldt, J.A.O., Lepock, J.R., and Meiering, E.M. (2004) *Prot. Sci.*, **13**, 3017–3027.

128. Maity, S., Kumar, P., and Haldar, D. (2011) *Soft Matter*, **7**, 5239–5245.

129. Kumar, R. and Raghavan, S.R. (2009) *Soft Matter*, **5**, 797–803.

130. Rajaganesh, R., Gopal, A., Das, T.M., and Ajayaghosh, A. (2012) *Org. Lett.*, **14**, 748–751.

131. Lin, Y.-C. and Weiss, R.G. (1989) *Liq. Cryst.*, **4**, 367–384.

132. Hachisako, H., Nakayama, H., and Ihara, H. (1999) *Chem. Lett.*, 1165–1166.

133. Ahmed, S.A., Sallenave, X., Fages, F., Mieden-Gundert, G., Müller, W.M., Müller, U., Vögtle, F., and Pozzo, J.-L. (2002) *Langmuir*, **18**, 7096–7101.

134. Keith, H.D. and Padden, F.J. Jr., (1963) *J. Appl. Phys.*, **34**, 2409–2421.

135. See for instance: Tegze, G., Granasy, L., Toth, G.I., Douglas, J.F., and Pusztai, T. (2011) *Soft Matter*, **7**, 1789–1799.

136. Lescanne, M., Colin, A., Mondain-Monval, O., Fages, F., and Pozzo, J.-L. (2003) *Langmuir*, **19**, 2013–2020.

137. Spector, M.S., Selinger, J.V., and Schnur, J.M. (2003) in *Materials-Chirality*, Topics in Stereochemistry, Vol. 24 (eds M.M. Green, R.J.M. Nolte, and E.W. Meijer), Wiley-Interscience, Hoboken, NJ, pp. 281–372.

138. Filobelo, L.F., Galkin, O., and Velikov, P.G. (2005) *J. Chem. Phys.*, **123**, 014904.

139. Diao, Y.Y. and Liu, X.Y. (2012) *Adv. Funct. Mater.*, **22**, 1354–1375.

140. Xiang, J.-Y., Liu, X.-Y., Li, J.-L., and Vallon, M.W. (2007) *J. Phys. Chem. B*, **111**, 5558–5563.

141. Erdemir, D., Lee, A.A., and Myerson, A.S. (2009) *Acc. Chem. Res.*, **42**, 621–629.

142. See for example: Grigoriew, H., Luboradzki, R., and Cunis, S. (2004) *Langmuir*, **20**, 7374–7377.
143. Terech, P., Dianoux, A.-J., Ramasseul, R., and Volino, F.C.R. (1981) *Acad. Sci. Paris II*, **293**, 749–752.
144. Terech, P. (1985) *J. Colloid Interface Sci.*, **107**, 244–255.
145. Harrison, L.G. (1969) in *Chemical Kinetics*, Vol. 2 (eds C.H. Bamford and C.F.H. Tipper), Elsevier, Amsterdam, p. 393.
146. Malik, S., Maji, S.K., Banerjee, A., and Nandi, A.K. (2002) *J. Chem. Soc., Perkin Trans. 2*, 1177–1186.
147. Dickinson, E. (1997) *J. Chem. Soc., Faraday Trans.*, **93**, 111–114.
148. (a) Schultz, J.M. (1974) *Polymer Materials Science*, Prentice Hall, Englewood Cliffs, NJ, p. 385. (b) Wunderlich, B. (1976) *Macromolecular Physics*, Vol. 2, Academic Press, New York, pp. 16–52147.
149. See for example: Pradell, T., Crespot, D., Clavaguera, N., and Clavaguera-Mora, M.T. (1998) *J. Phys.: Condens. Matter*, **10**, 3833–3843.
150. Weinberg, M.C. (1991) *J. Non-Cryst. Solids*, **134**, 116–122.
151. A similar, less quantitative approach has been used to follow the kinetics of fiber in a 2-component gelator system: Tan, G., John, V.T., and McPherson, G.L. (2006) *Langmuir*, **22**, 7416–7420.
152. Jean, B., Oss-Ronen, L., Terech, P., and Talmon, Y. (2005) *Adv. Mater.*, **17**, 728–731.
153. Terech, P., Jean, B., and Ne, F. (2006) *Adv. Mater.*, **18**, 1571–1574.
154. (a) Zhang, T.H. and Liu, X.Y. (2007) *J. Am. Chem. Soc.*, **129**, 13520–13526. (b) Zhang, T.H. and Liu, X.Y. (2009) *Angew. Chem. Int. Ed.*, **48**, 1308–1312.
155. Liu, X.-Y. and Sawant, P.D. (2002) *ChemPhysChem*, 374–377.
156. Li, J.-L. and Liu, X.-Y. (2010) *Adv. Funct. Mater.*, **20**, 3196–3216.
157. Li, J.-L., Yuan, B., Liu, X.-Y., and Xu, H.-Y. (2010) *Cryst. Growth Des.*, **10**, 2699–2706.
158. (a) Fages, F., Vögtle, F., and Žinić, M. (2005) *Top. Curr. Chem.*, **256**, 77–131. (b) George, M. and Weiss, R.G. (2006) in *Molecular Gels: Materials with Self-Assembled Fibrillar Networks* (eds R.G. Weiss and P. Terech), Springer, Dordrecht, pp. 449–551.
159. (a) Sugiyasu, K., Fujita, N., and Shinkai, S. (2004) *Angew. Chem. Int. Ed.*, **43**, 1229–1233. (b) Chen, P., Lu, R., Xue, P., Xu, T., Chen, G., and Zhao, Y. (2009) *Langmuir*, **25**, 8395–8399. (c) Wang, G.-T., Lin, J.-B., Jiang, X.-K., and Li, Z.-T. (2009) *Langmuir*, **25**, 8414–8418.
160. Brotin, T., Utermöhlen, R., Fages, F., Bouas-Laurent, H., and Desvergne, J.P. (1991) *J. Chem. Soc., Chem. Commun.*, 416–418.
161. (a) Desvergne, J.-P., Del Guerzo, A., Bouas-Laurent, H., Belin, C., Reichwagen, J., and Hopf, H. (2006) *Pure Appl. Chem.*, **4**, 707–719. (b) Olive, A.G.L., Raffy, G., Allouchi, H., Léger, J.-M., Del Guerzo, A., and Desvergne, J.-P. (2009) *Langmuir*, **25**, 8606–8614.
162. Reichwagen, J., Hopf, H., Guerzo, A.D., Belin, C., Bouas-Laurent, H., and Desvergne, J.-P. (2005) *Org. Lett.*, **7**, 971–974.
163. Pozzo, J.-L., Clavier, G.M., and Desvergne, J.-P. (1988) *J. Mater. Chem.*, **8**, 2575–2577.
164. Lee, D.-C., Cao, B., Jang, K., and Forster, P.M. (2010) *J. Mater. Chem.*, **20**, 867–873.
165. (a) Lee, D.-C., McGrath, K.K., and Jang, K. (2008) *Chem. Commun.*, 3636–3638. (b) Jang, K., Ranasinghe, A.D., Heske, C., and Lee, D.-C. (2010) *Langmuir*, **26**, 13630–13636.
166. Danila, I., Riobé, F., Puigmartí-Luis, J., del Pino, Á.P., Wallis, J.D., Amabilino, D.B., and Avarvari, N. (2009) *J. Mater. Chem.*, **19**, 4495–4504.
167. Varghese, S., Kumar, N.S.S., Krishna, A., Rao, D.S.S., Prasad, S.K., and Das, S. (2009) *Adv. Funct. Mater.*, **19**, 2064–2073.
168. Mallia, V.A., George, M., Blair, D.L., and Weiss, R.G. (2009) *Langmuir*, **25**, 8615–8625.
169. George, M. and Weiss, R.G. (2002) *Langmuir*, **18**, 7124–7135.
170. Lu, L. and Weiss, R.G. (1996) *Chem. Commun.*, 2029–2030.

171. Sakurai, T., Masuda, Y., Sato, H., Yamagishi, A., Kawaji, H., Atake, T., and Hori, K. (2010) *Bull. Chem. Soc. Jpn.*, **83**, 145–149.

172. Mallia, V.A., Terech, P., and Weiss, R.G. (2011) *J. Phys. Chem. B*, **115**, 12401–12414.

173. Würtherner, F., Hanke, B., Lysetska, M., Lambright, G., and Harms, G.S. (2005) *Org. Lett.*, **7**, 967–970.

174. (a) Hanabusa, K., Yamada, M., Kimura, M., and Shirai, H. (1996) *Angew. Chem. Int. Ed. Engl.*, **35**, 1949–1951. (b) van Esch, J.H. and Feringa, B.L. (2000) *Angew. Chem. Int. Ed.*, **39**, 2263–2266.

175. (a) Trivedi, D.R., Ballabh, A., and Dastidar, P. (2003) *Chem. Mater.*, **15**, 3971–3973. (b) Trivedi, D., Ballabh, A., Dastidar, P., and Ganguly, B. (2004) *Chem.—Eur. J.*, **10**, 5311–5322. (c) Trivedi, D. and Dastidar, P. (2006) *Cryst. Growth Des.*, **6**, 1022–1026. (d) Trivedi, D.R. and Dastidar, P. (2006) *Cryst. Growth Des.*, **6**, 2114–2121.

176. (a) Ballabh, A., Trivedi, D.R., and Dastidar, P. (2005) *Cryst. Growth Des.*, **5**, 1545–1553. (b) Trivedi, D.R., Ballabh, A., and Dastidar, P. (2006) *Cryst. Growth Des.*, **6**, 763–768.

177. (a) Trivedi, D.R. and Dastidar, P. (2006) *Chem. Mater.*, **18**, 1470–1478. (b) Ballabh, A., Trivedi, D.R., and Dastidar, P. (2006) *Chem. Mater.*, **18**, 3795–3800.

178. (a) Ballabh, A., Trivedi, D.R., and Dastidar, P. (2006) *Org. Lett.*, **8**, 1271–1274. (b) Ballabh, A., Adalder, T.K., and Dastidar, P. (2008) *Cryst. Growth Des.*, **8**, 4144–4149. (c) Sahoo, P., Adarsh, N.N., Chacko, G.E., Raghavan, S.R., Puranik, V.G., and Dastidar, P. (2009) *Langmuir*, **25**, 8742–8750.

179. (a) Adarsh, N.N., Sahoo, P., and Dastidar, P. (2010) *Cryst. Growth Des.*, **10**, 4976–4986. (b) Sahoo, P., Puranik, V.G., Patra, A.K., Sastry, P.U., and Dastidar, P. (2011) *Soft Matter*, **7**, 3634–3641.

180. Estroff, L.A. and Hamilton, A.D. (2006) in *Molecular Gels: Materials with Self-Assembled Fibrillar Networks* (eds R.G. Weiss and P. Terech), Springer, Dordrecht, pp. 721–742.

181. (a) van Esch, J., De Feyter, S., Kellogg, R.M., De Schryver, F., and Feringa, B.L. (1997) *Chem.—Eur. J.*, **3**, 1238–1243. (b) van Esch, J., Schoonbeek, F., de Loos, M., Kooijman, H., Spek, A.L., Kellogg, R.M., and Feringa, B.L. (1999) *Chem.—Eur. J.*, **5**, 937–950. (c) Schoonbeek, F.S., Esch, J.H., Hulst, R., Kellogg, R.M., and Feringa, B.L. (2000) *Chem.—Eur. J.*, **6**, 2633–2643.

182. Makarević, J., Jokić, M., Perić, B., Tomišić, V., Kojić-Prodić, B., and Žinić, M. (2001) *Chem.—Eur. J.*, **7**, 3328–3341.

183. Anderson, K.M., Day, G.M., Paterson, M.J., Byrne, P., Clarke, N., and Steed, J.W. (2008) *Angew. Chem. Int. Ed.*, **47**, 1074–1078.